Evaluation and Improvement of Energy Management in Industrial Baking Ovens

vorgelegt von
M. Sc.
AHMED HAMDY KAMEL JADO
ORCID: 0000-0001-9585-3433

von der Fakultät III – Prozesswissenschaften
der Technischen Universität Berlin
zur Erlangung des akademischen Grades
Doktor der Ingenieurwissenschaften
- Dr. –Ing. -
genehmigte Dissertation

Promotionsausschuss:
Vorsitzende: Prof. Dr.-Ing. Georgios Tsatsaronis
Gutachter: Prof. Dr. Tetyana Morozyuk
Gutachter: Prof. Dr. Predrag Raskovic

Tag der wissenschaftlichen Aussprache: 17.09.2018

Berlin 2019

Acknowledgements

This work was carried out during my stay as a doctoral student at the Institute for Energy Engineering of the Technische Universität Berlin. At facing the finishing time of my dissertation, I have to express my appreciation to all people who helped, supported and accompanied me to complete this work.

First of all, I have to express my sincere appreciation and gratitude to Professor Tetyana Morozyuk who gave me a chance to be under her supervision in my research work. Always, she had an open door and she was passionate, creative, generous, and helpful. I have to appreciate her for her excellent support.

I would like to express my appreciation to Professor Predrag Raskovic, Faculty of Technology, University of Niš, Serbia for his suggestions, and valuable guidance. I am extremely thankful for his support.

Finally, I would like to express my grateful acknowledgement to my family especially my father and my mother for their continuous help.

Abstract

The final step in bread making is the baking process to produce the final attributes of product quality, including texture, color, and flavor, as a result of several thermal reactions. These thermal reactions are dominated by heat and mass transfer mechanisms inside an oven chamber as well as inside the dough pieces.

This research involves studying existing methods of baking bread in a common type of industrial oven. A simulation of the oven operating conditions and the conditions of the food moving through the oven are performed and analyzed using COMSOL, an engineering modeling design and simulation software.

A 2-D axisymmetric mathematical model was developed in order to simulate coupled heat and mass transfer during the bread baking process and to predict bread temperature and water content at different oven temperatures (180, 200, 220, 240 and 260 °C). The thermal physical properties of bread are the functions of local values of temperature and moisture content. The model equations were solved using COMSOL Multiphysics. Transient temperature and moisture distributions inside the product were predicted.

The results showed that the temperature of the crust increased from 132 °C to 179 °C by raising the oven temperature from 180 to 260°C. The results also showed that increasing bread temperature and decreasing moisture content are the functions of time. The temperature increased from 20 °C to 157 °C, and the "moisture loss" increased from 0 % to 43.7 % during a time period of 30 min at an average oven temperature of 220 °C.

A mathematical model for simultaneous heat, water, and vapor diffusion was developed to predict the diffusion of water inside foods during heat processing. The model is based on Fourier's and Fick's Laws. The diffusion of liquid water is separated from the diffusion of water vapor. The dough dried in a conventional oven at 220 °C and the local water content and temperatures were measured during the drying in the center, halfway to the center as well as at the surface. Several critical values in the temperature and moisture profiles were also taken as characteristic values of the process. The first critical value is the time when bread temperature reaches 100 °C. The second critical value is the time when the liquid water content at the center of bread reaches its peak. The third critical value is the level of the peaked liquid water content at the center.

The results showed that the simulated water content at the surface decreases rapidly when the temperature increases. At first, the simulated water content halfway to the center increases a little and then starts to decrease. The simulated temperature remains on a plateau while the water content starts to decrease. In the center, the water content increases in the beginning and then slowly starts to decrease. The mathematical model was highly sensitive to the time step and satisfactory results were only yielded over a range of time steps, between 15 s and 100 s. Smaller time steps produced an erroneous and diverged result, while a bigger time step rendered a useless result.

The efficiency of a bread oven with direct heating was investigated by using energy and exergy methods. Energy efficiency and exergy efficiency values were evaluated for the natural gas-fired furnace and the efficiency improvement was analyzed before and after a new regenerative burner was installed on the oven.

Zusammenfassung

Der letzte Schritt in der Brotherstellung ist der Backprozess, um die endgültigen Attribute der Produktqualität, einschließlich Textur, Farbe und Geschmack, als Folge von mehreren thermischen Reaktionen zu produzieren. Diese thermischen Reaktionen werden von Wärme-und Massentransfermechanismen in einer Ofenkammer sowie innerhalb der Teigstücke dominiert.

Diese Forschung beinhaltet die Untersuchung von bestehenden Brotbackverfahren in einem üblichen industriellen Ofen. Die Simulation der Ofenbetriebsbedingungen und der Bedingungen der Lebensmittel, die sich durch den Ofen bewegen, wird unter Verwendung von COMSOL, einer technischen Modellierungs-, Entwurfs- und Simulationssoftware, durchgeführt und analysiert.

Ein achsensymmetrisches mathematisches 2-D-Modell wurde entwickelt, um den gekoppelten Wärme- und Stofftransport während des Brotbackprozesses zu simulieren und (die) Brottemperatur und (den) Wassergehalt bei verschiedenen Ofentemperaturen (180, 200, 220, 240 und 260 ° C) vorherzusagen. Die thermischen physikalischen Eigenschaften von Brot sind die Funktionen der lokalen Werte von Temperatur und Feuchtigkeitsgehalt. Die Modellgleichungen wurden mit COMSOL Multiphysics gelöst. Vorübergehende Temperatur- und Feuchtigkeitsverteilungen im Produkt wurden vorhergesagt.

Die Ergebnisse zeigten, dass die Temperatur der Kruste von 132 °C auf 179 °C stieg, indem die Ofentemperatur von 180 auf 260 °C erhöht wurde. Die Ergebnisse zeigten auch, dass die Erhöhung der Brottemperatur und die Verringerung des Feuchtigkeitsgehalts die Funktionen der Zeit. sind Die Temperatur stieg von 20 °C auf 157 °C und der "Feuchtigkeitsverlust" erhöhte sich bei einer durchschnittlichen Ofentemperatur von 220 °C innerhalb von 30 Minuten von 0 % auf 43,7 %.

Ein mathematisches Modell für gleichzeitige Wärme-, Wasser- und Dampfdiffusion wurde entwickelt, um die Diffusion von Wasser in Lebensmitteln während der Wärmebehandlung zu prognostizieren. Das Modell basiert auf den Fourierschen und Fickschen Gesetzen. Die Diffusion von flüssigem Wasser ist von der Diffusion von Wasserdampf getrennt. Der in einem herkömmlichen Ofen bei 220ºC getrocknete Teig und der lokale Wassergehalt und die Temperaturen wurden während des Trocknens in der Mitte, auf halber Strecke zur Mitte und an der Oberfläche gemessen. Mehrere kritische Werte in den Temperatur- und Feuchtigkeitsprofilen wurden ebenfalls als charakteristische Werte des Verfahrens verwendet. Der erste kritische Wert ist die Zeit, wenn die Brottemperatur 100 ° C erreicht. Der zweite kritische Wert ist der Zeitpunkt, wenn der flüssige Wassergehalt in der Mitte des Brotes seinen Höchstwert erreicht. Der dritte kritische Wert ist das Niveau des Spitzenwassergehaltes in der Mitte.

Die Ergebnisse zeigten, dass der simulierte Wassergehalt an der Oberfläche rapide sinkt, wenn die Temperatur zunimmt. Der simulierte Wassergehalt auf halbem Weg zum Zentrum nimmt zunächst etwas zu und beginnt dann zu sinken, die simulierte Temperatur bleibt auf einem Plateau, während der Wassergehalt anfängt zu sinken. In der Mitte nimmt der Wassergehalt am Anfang zu und beginnt dann langsam zu sinken. Das mathematische Modell reagierte auf den Zeitschritt sehr sensibel und befriedigende Ergebnisse wurden nur durch eine Reihe von Zeitschritten, zwischen 15 s und 100 s erzielt. Kleinere Zeitschritte führten zu einem fehlerhaften und abweichenden Ergebnis, während ein größerer Zeitschritt zu einem unbrauchbaren Ergebnis führte.

Die Effizienz eines Brotbackofens mit Direktheizung wurde mit Methoden der Energie und Exergie untersucht. Die Werte der Energie-und Exergieeffizienz für den mit Erdgas beheizten Ofen wurden ausgewertet und die Effizienzverbesserung vor und nach der Installation des neuen regenerativen Brenners auf dem Backofen wurde analysiert.

Nomenclature

AFR - air-fuel ratio on mass basis, kg (air) kg^{-1}(fuel)

A_S - area, m^2

b - breadth, m

c - specific heat capacity, J kg^{-1} K^{-1}

c - amount concentration, mol m^{-3}

c_p - specific heat capacity at constant pressure, J kg^{-1} K^{-1}

D - diffusion coefficient, m^2 s^{-1}

E - energy, J

E - exergy, J

E_D - exergy destruction, J

e - mass-specific exergy or energy, kJ kg^{-1}

$\bar{e}$ - mole -specific exergy or energy, kJ kmol^{-1}

F - fraction of radiation (view factor), 1

F - specific weight, N m^{-3}

g - acceleration due to gravity, m s^{-2}

G - mass velocity, kg h^{-1} m^{-2}

H_i - lower heating value, MJ kmol^{-1}

h - coefficient of heat transfer, W m^{-2} K^{-1}

h - mass-specific enthalpy, kJ kg^{-1}

$\bar{h}$ - mole -specific enthalpy, kJ kmol^{-1}

h' - enthalpy of liquid water, kJ kg^{-1}

h'' - enthalpy of saturated vapor, kJ kg^{-1}

IVF - Initial Velocity Field, m s^{-1}

IP - Initial Pressure, kPa

k - thermal conductivity, W m^{-1} K^{-1}

k_d - mass transfer coefficient, kg m^{-2} s^{-1}

k'_d - mass transfer coefficient with respect to mole fraction, kg m^{-2} s^{-1}

L - characteristic length, m

m - mass, kg

M - radiant excitance (emitted radiant flux), W m^{-2}

M - molar mass, kg mol^{-1}

N - mass flux of H_2O evaporating, kg m^{-2} s^{-1}

Nu - Nusselt number, –

n - amount (of substance), mol

P - perimeter, m

p - pressure, Pa

Pr - Prandtl number, –

Q - heat, J

Q_{CV} - total heat transfer of control volume accompanying combustion, J

$\dot{Q}$ - heat flow rate, W

$\dot{Q}_V$ - heat flow rate per unit of volume, W m^{-3}

$\dot{Q}_A$ - heat flow rate per unit of area, W m^{-2}

Ra - Rayleigh number, –

Re - Reynolds number, –

R_C - drying rate in the constant rate drying period, kg m^{-2} s^{-1}

$\bar{R}$ - universal gas constant, kJ kmol^{-1} K^{-1}

s - mass-specific entropy, kJ kg^{-1} K^{-1}

$\bar{s}$ - mole -specific entropy, kJ kmol^{-1} K^{-1}

T - temperature; thermodynamic temperature, K; Celsius temperature, °C

t - time, s

U - overall coefficient of heat transfer, W m^{-2} K^{-1}

u - speed, m s^{-1}

V - volume, m^3

V - water vapor content, kg (H_2 0,g) kg^{-1}(product)

v_H - humid volume, m^3 kg^{-1}

W - liquid water content, kg ($H_2$0) kg^{-1}(product)

x - mass ratio of water vapour to dry air, kg ($H_2$0, g) kg^{-1}(dry air)

x_M - log mean inert mole fraction, –

y - mole fraction for condensed phase, –

x, y, z - Cartesian space coordinates, m

α_V - coefficient of thermal expansion, K^{-1}

$\partial f/\partial x$ - partial derivate of function $f(x,y,z)$, with respect to variable x

$\partial f/\partial t$ - partial derivate of function f, with respect to time t

$\mathrm{d}f/\mathrm{d}t$ - 1st derivate of function f, with respect to time t

Abbreviations

CFD - Computational Fluid Dynamics

FDM - Finite difference method

FEM - Finite element method

FVM - Finite volume method

Greek symbols

δ - thickness, m

ϕ - volume fraction, –

ρ - mass density, kg m^{-3}

ν - kinematic viscosity, $m^2\ s^{-1}$

η - dynamic viscosity, Pa s

γ - ratio of specific heats, –

Φ - radiant power (radiant energy per time), W

ρ - reflectance, reflection factor, –

α - absorptance, absorption factor, –

ε - emissivity, –

σ - Stefan—Boltzmann constant, $W\ m^{-2}\ K^{-4}$, $5.67051(19) \times 10^8\ W\ m^{-2}\ K^{-4}$

I - irradiance (radiant flux received), $W\ m^{-2}$

λ - latent heat of vaporization, kJ kg^{-1}

Λ - Lagrange multiplier vector

σ - normal stress, Pa

ω - mass fraction,1

a - thermal diffusivity, $m^2\ s^{-1}$

ε - exergy efficiency, %

η - energy efficiency, %

Subscripts and superscripts

$(\cdot)_{amb}$ - ambient

$(\cdot)_{ash}$ - ash

$(\cdot)_{ap}$ - apparent

$(\cdot)_{bak}$ - baking

$(\cdot)_{bb}$ - black body

$(\cdot)_{b/d}$ - bread / dough

$(\cdot)_{cnd}$ - conduction

$(\cdot)_{cab}$ - carbohydrate

$(\cdot)_{cnv}$ - convection

$(\cdot)_{ca}$ - combustion air

$(\cdot)_{cg}$ - combustion gas

$(\cdot)_{dr}$ - dry

$(\cdot)_{e}$ - component exiting system

$(\cdot)_{env}$ - environment

$(\cdot)_{fat}$ - fat

$(\cdot)_{fib}$ - fiber

$(\cdot)_{f}$ - film

$(\cdot)_{ffs}$ - fluid flowing stream

$(\cdot)_{f}$ - formation

$(\cdot)_{fg}$ - flue gas

$(\cdot)_{g}$ - gas

$(\cdot)_{hel}$ - heating element

$(\cdot)_{i}$ - component incoming system

$(\cdot)_{int}$ - initial

$(\cdot)_{l}$ - liquid

$(\cdot)_{L}$ - loss

$(\cdot)_{M}$ - metal

$(\cdot)_{mix}$ - mixture

$(\cdot)_{m}$ - mutual

$(\cdot)_{mos}$ - moisture

$(\cdot)_{prt}$ - protein

$(\cdot)_{p}$ - product of combustion

$(\cdot)_{pa}$ - preheated combustion air

$(\cdot)_{R}$ - reactant of combustion

$(\cdot)_{reg}$ - regenerator

$(\cdot)_{rec}$ - recovery

$(\cdot)_{rad}$ - radiosity

$(\cdot)_{rad}$ - radiation

$(\cdot)_{rs}$ - radiating source

$(\cdot)_{sld}$ - solids

$(\cdot)_{srf}$ - surface

$(\cdot)_{S}$ - solid

$(\cdot)_{sat}$ - saturation

$(\cdot)_{t}$ - total

$(\cdot)_{tru}$ - true

$(\cdot)_{theo}$ - theoretical

$(\cdot)_{uhf}$ - unheated fluid

$(\cdot)_{w}$ - wet

$(\cdot)_{0}$ - conditions of the thermodynamic environment

$(\cdot)^{PH}$ - thermomechanical exergy

$(\cdot)^{CH}$ - chemical exergy

$(\cdot)^{o}$ - property at absolute values (reference temperature is 0 K)

List of content

List of figures

List of tables

1 Introduction

1.1 Background

Baking is a high energy demanding process, which requires special attention in order to know and improve its efficiency [1]. The bakery industry has witnessed a revolution over the past 150 years. The small artisan bakeries, which used to be present in every village, made way for a highly technological bakery industry. Industrial mono-production took over from the high variety bakeries as bread could be produced in a more efficient way. Productivity became the key of success. Different baking technologies were developed to respond better to the continuously growing market demand [2].

Computational simulation has proved its effectiveness in many areas it is still relatively new to the food industry. Food is a complex matrix and food processing has always been a fickle process. The pattern of fluid flow is thus complicated by many other factors. Some of these factors include simultaneous heat and mass transfer, multiple heat flow, phase change, change in physical structure, change in physical properties, etc.

Baking was chosen as the process of interest for bread baking. Baking is one of the oldest known methods for food processing. Over time, the products and design of ovens have changed, but the basic combinations of chemical and physical processes that are induced by heat transfer and transform dough into bakery products, are still of great importance to food manufactures and researchers. Although the individual transition processes that take place during baking are well understood, the design of industrial baking processes is still highly empirical today.

Computational fluid dynamic (CFD) modelling is an excellent tool for the baking industry, whereby the heat and mass transfer in the whole baking oven can be better understood. With such knowledge, the baking process can be further improved. It would greatly increase the production efficiency, product consistency, and product quality. Concurrently, it could also reduce energy consumption and food wastage.

The increasing cost of energy and the reduced availability of fuel in recent years provide considerable incentives to evaluate energy use in food processing operation. That leads to find reliable methods to reduce the energy consumption. Using energy methods to evaluate efficiency has been recognized for years, but the exergy method examines efficiency change in a more practical way. Exergy is defined as maximum theoretical work possibly obtained in a process or a system referring to environment. For example, if a flue gas exergy value is small, it shows that even if some energy is associated with flue gas, this part of energy becomes less available in reality. Exergy efficiency is a measure of how near a process approaches ideality and a measure of how near energy transfer approaches ideal transfer.

Exergy analysis which may be considered as accounting of the use of energy and material resources provide information on how effective a process takes place towards conserving natural resources. Industrial heating processes are very inefficient from the point of view of second law of thermodynamics. This is because of the fact that the exergy value of heat is much lower than its energy value [3].

1.2 Aim and Objectives

The aim of this study is to optimize baking conditions by using modelling and simulation techniques and discuss the efficiency improvement after the implementation of a new burner system on the baking oven. The techniques and methodologies developed in this study can also be applied to other food processes.

The objectives of this study are:

- To simulate the heat and mass transfer during baking using the CFD modelling technique.
- To develop model describes the mechanisms of simultaneous heat, water and vapour diffusion inside the bread during baking.
- Apply exergy analysis to industrial Baking oven.

1.3 Overview of the Thesis

In **Chapter 2**, state of the art is given on bread baking process, the classification of industrial bakeries, the energy related problems in modern bakery plants, the physical properties of bread and the mathematical models of the heat and mass transfer equation that are used in the study. This part is followed by literature review of different modeling techniques that have been recently implemented in the studies of bread baking process. The next part of Chapter 2 is devoted to the method of Computational fluid dynamics (CFD) and problems related to the modeling techniques, discretization and mesh generation. Description of software is followed by the overview of heat and mass transfer equations and codes in COMSOL. This part is followed by literature review of emitted gases during baking, regenerative technology, and exergy analysis.

Chapter 3 presents the heat and mass transfer analysis in bread during baking using COMSOL models. The existing bread baking conditions (e.g. temperature, air velocity, moisture) were simulated. These models can help engineers to determine the optimal heating conditions for whatever food may be baked in the oven. Also, simulations can be used to determine if the food will be cooked enough and not burned and to simulate an actual food item-before, during and after baking.

Chapter 4 shows the model for coupled heat and mass transfer in bread at different temperature. The model equations were solved using COMSOL Multiphysics. Special attention was focused on the thermal physical properties of food with functions of local values of temperature and moisture content. The model can be used for an evaluation of the time evolution of some characteristic parameters, namely the moisture content of food and its temperature, and to predict bread temperature and water content at different oven temperatures (180, 200, 220, 240 and 260 °C).

Chapter 5 presents the mathematical modeling for simultaneous heat, water, and vapor diffusion inside bread during baking. The model was developed to be used for prediction of the diffusion of water inside foods during heat processing. The model is based on Fourier's and Fick's Laws. The diffusion of liquid water is separated from the diffusion of water vapor. The doughs were dried in a conventional oven at 220 °C and the local water content and temperatures were measured during the drying in the center, halfway to the center and at the surface. Several critical values in the temperature and moisture profiles are also taken as the characteristic values of the process.

Chapter 6 provides the energy and exergy analysis of a continuous industrial baking process in direct heating oven with an analysis of the efficiency improvement before and after the implementation of a new burner system on a heating furnace. Exergy is a more practical tool compared to the conventional energy method when examining the thermal performance of the same baking oven and the same regenerator. Implementing regenerative technology results in enhanced system performance indicated by an exergy efficiency improvement. The regenerative burner system improves efficiency and achieves fuel saving.

2 State of the art

2.1 Energy Consumption in Bakeries

Energy efficiency is nowadays a subject deeply discussed in several fields, with a large potential in industry. Here proper process and energy management routines turns out to be essential to reduce the energy demand while keeping the control of the product quality. In this respect the bread baking, one of the pillars of food related industry, is an energy intensive process irrespective to the adopted oven technology or to the primary energy nature. Baking is the fundamental step of the bread production process and it entails a number of complex chemical and physical phenomena, critical to the final physical properties of bread, i.e. crust colour, crumb texture and taste. A careful balance throughout all the steps of the "manufacturing" cycle is vital to ensure the processes synchronization, in order to produce a consistent and satisfactory loaf of bread. A proper energy management of this process needs to consider such features to ensure a high-quality product. As such, process monitoring cannot be conveniently described using customary specific energy metric (correlating the energy demand to the amount of processed material) or full three-dimensional (3D) physic-based modeling as in computational fluid dynamics (CFD)[4].

Baking bread is considered to be an intensive energy process. There are little efforts into monitoring and reducing energy usage in bakeries. Energy consumption during baking is of the range of 450-650KJ per kg of food where most of the heat is used to heat the food, to evaporate water from the crust, to superheat water vapor (steam) that is transported through the crust and to superheat the dry crust [5].The average energy demanding in bread baking processes around 4 MJ kg^{-1}, compared with other thermal processes such as canning [6].

Paton et al. [7] identified that the heat loss of flue gases emitted during baking represents 82 % of total losses and the radiation loss depends upon the design and the insulation of bakeries. In general, it is between 0.5 % and 3 % from the heating value of the fuel. They also reported that the excess air value must be kept low as it needs to be heated resulting in a decrease of the flame temperature and an increase of the flue gas temperature, thereby deteriorating the efficiency.

Commercial bakery products in the United States such as breads, rolls, frozen cakes, pies, pastries, cookies, and crackers consume over $870 million of energy annually. Energy efficiency measures can reduce the energy costs of significant energy processes and increase earnings predictability [8].

Paton [9] developed a system-level thermodynamic analysis in order to measure and model heat streams in industrial bread ovens. The model was subjected to a sensitivity analysis to ensure the calculations could be trusted to give suitably accurate results. A number of measurement techniques were employed, and the methodology was designed to increase the potential for industry-wide use to assess the efficiency of ovens. The results showed that between 40 % and 49 % of heat is wasted in industrial ovens. The model has been successfully distributed to industry.

2.1.1 The Theory of Baking Bread

Bread is a basic dietary item dating back to the Neolithic era, which is prepared by baking that is carried out in oven. Control of the production and distribution of bread has been used as a means of exercising

political influence over the populace for at least the last two millennia. Several experimental and mathematical models are developed for clear understanding of baking [10].

During the baking process, radiation, conduction, and convection each play a part as a means by which heat is transferred to the batch to be baked. The hot oven gases have carried heat to the solid surfaces by convection. This heat is largely passing on through the walls, sole and crown of all ovens by conduction that carries heat always from hot parts to cooler parts making the heat flow more efficient. Convection currents are largely employed in hot air ovens and most traveling ovens by forced convection. Radiation also takes place from all bodies and the hotter the body the faster it radiates. It plays a very large part in equalizing the temperature differences inside the oven [11].

Kulp [12] reported that as the dough temperature increases in the oven, carbon dioxide in the gaseous phase expands. Other important changes occurring in the oven include physicochemical reactions of flour proteins and thermal changes of starch. Eliasson, Larsson [13] reported that when the dough is put into the oven after fermentation, a considerable increase in volume occurs - the oven spring. The increase in volume induces considerable stress on the air/water interface in the dough.

The increase of volume observed during oven spring is a consequence of the increase in temperature, which induces changes in both dispersed and continuous phases of the dough. These changes result in the volume expansion and the setting of the crumb. The rate of temperature increases and the final temperature reached differ in different parts of the dough, and this is especially true for the center of the dough compared to the surface. The increase in temperature directly influences the dough in several ways, including yeast activity, the solubility of gases, and volume expansion of evaporated gases.

The flour constituents, the starches gelatinize, and the protein undergoes certain changes. As a result of the physical changes related to the included gas, an enormous increase in volume occurs, and this increase in volume has some indirect effects on the dough.

Convection currents enhance uniform heat distribution throughout the oven and many commercial designs are fitted with fans to supplement natural convection currents and to reduce the thickness of boundary films. This approach increases heat transfer coefficients and improves the efficiency of energy utilization.

Conduction of heat through the baking hearth or conveyor belt increases the temperature difference at the base of the food and causes differences in the rate of baking.

The low thermal conductivity of foods causes low rates of conductive heat transfer and is an important influence on baking time.

The size of the pieces of bread determines the distance that heat must travel to bake the center of the bread adequately. When a food is placed in an oven, moisture at the surface is evaporated and removed by the hot air. The low humidity of air in the oven establishes moist vapor pressure gradients, which cause movement of moisture from the interior of the food to the surface; the extent of moisture loss is determined by the nature of food and the rate of heating. When the rate of moisture loss exceeds the rate of movement from the interior, the zone of evaporation moves inside the food, the surface dries out, its temperature rises to the temperature of the hot air and a crust is formed.

Because baking takes place at atmospheric pressure and moisture escapes freely from the food, the internal temperature of the food does not exceed 100 °C. The more rapid heating and higher

temperature cause complex changes to the components of the food at the surface. These changes both enhance eating qualities and retain moisture in the bulk of the food.

2.1.2 The Effect of Heat on Baking Bread

Eliasson, Larsson [13] reported that when the dough is put into the oven, heat is transferred by several mechanisms, including convection, radiation, conduction and the evaporation of water. Heat transfer inside the dough is thought to occur through the mechanisms of heat conduction and evaporation – condensation.

The dough surface is cold compared with the surroundings, and moisture condenses onto it from the air. The condensation makes the surface temperature rises to the dew point very quickly, as soon as the surface has reached the dew point temperature, evaporation begins, causing a loss in weight. The weight loss during baking depends on the maximum surface temperature; the higher the maximum surface temperature, the higher the weight loss.

The increase in surface temperature causes the evaporation of water from a zone just below the crust. Part of the water vapor passes through the crust into the surrounding air, but part of it moves toward the cooler regions inside the crumb. Here, the water vapor condenses and causes an increase in the crumb temperature. It has been suggested that evaporation-condensation is the major mechanism of heat transfer in the bread. Although conduction is thought to play a minor role, it is nevertheless essential. If conduction was the only or the main mechanism for heat transfer in the dough, heat transfer in a gas-free piece of dough would be as rapid as the heat transfer in a fermented piece of dough. This is not the case, however, the temperature increases much faster in a fermented dough than in a gas-free dough. Heat transport in the dough is thus the result of a combination in the gas phase.

Evaporation-condensation is assumed to be the only mechanism of mass – (water) transfer. The transfer of water during baking is illustrated by the gradients in the water content of the loaf Differences occur in water content between crumb and crust.

The gas volume of a dough increases as a function of temperature until a certain temperature just above the gelatinization onset temperature of the starch. Not only does the total gas volume change, but its composition also changes with temperature. In the early stages of baking, the gas volume is composed almost entirely of CO_2, whereas the fraction of water increases with temperature. The heat transfer is related to the gas volume of the initial dough. The more gas included in the dough, the shorter the baking time (particularly if temperature in the center approaches 100 °C).

Fellows [14] pointed that a boundary film of air acts as a resistance to heat transfer into the food and to movement of water vapor from the food. The thickness of the boundary layer is mostly determined by the velocity of the air and the surface properties of the food. He also stated that baking is a unit operation uses heated air to alter the eating quality and sensory properties of foods and is usually applied to flour-based foods. The second purpose of baking is preserving the bread by the destruction of micro – organisms and reducing the water activity at the baking to improve palatability and to extend the range of tastes, aroma, and textures in the diet. Baking also destroys enzymes and microorganisms and lowers the water activity of the food to some extent, thereby preserving the food, and revealed that in an oven, heat is supplied to the food by radiation from the oven walls, by convection from circulating air and by conduction through the tray or conveyor on which the food is placed. Heat passes through the food by

conduction in most cases although convection currents are established during the initial heating. Air, other gases and moisture vapor inside the oven transfer heat by convection. The heat is converted to conductive heat at the surface of the food and at the oven walls.

2.2 Classification of Industrial Bakeries

Baking ovens should be constructed so as to have as reserve supply of heat as possible and should give up this heat slowly [11].

The following basic essentials must be taken into consideration in designing and building efficient baking ovens as mentioned by RD [15]:

- Application of heat-in what manner is the heat to be applied.
- Method of control of the required heat.
- Best manner of insulating the heat for best efficiency.
- Flexibility of the oven to bake a variety of products and the ability to bake the most desired products in the most efficient manner.
- Cost of construction.
- Overall ease of operation and maintenance of the baking unit.

Cauvain [16] indicated that, the furnace or oven physically consists of an enclosure (with a source of heat) that holds the materials being heated. The enclosure incorporates insulating or refractory materials to withstand the high temperatures of the process and to reduce heat losses from the enclosure to its surroundings.

Furnaces and ovens also incorporate conveying systems to charge raw materials into the heated area, and to remove the heat –treated materials from the heated area. In general, it is known that bakeries were classified according to different parameters as shown in Fig. 2.1.

The following are some of these classifications as reported in different reviews:

Direct – Heating Ovens

Fellows [14] showed that, in the direct heating ovens, air and products of combustion are recalculated by natural convection or by fans. The temperature in the oven is controlled automatically, by adjustment of air and fuel flow rates to the burners. He stated also that gas (as a commonly used fuel) is burned in ribbon burners located above and below conveyor belts in continuous ovens. The advantages of the direct heating ovens include:

1) Short baking time,

2) High thermal efficiencies,

3) Good control, and

4) Rapid start-up, as it is only necessary to heat the air in the oven.

However, care is necessary to prevent contamination of the food by undesirable products of combustion.

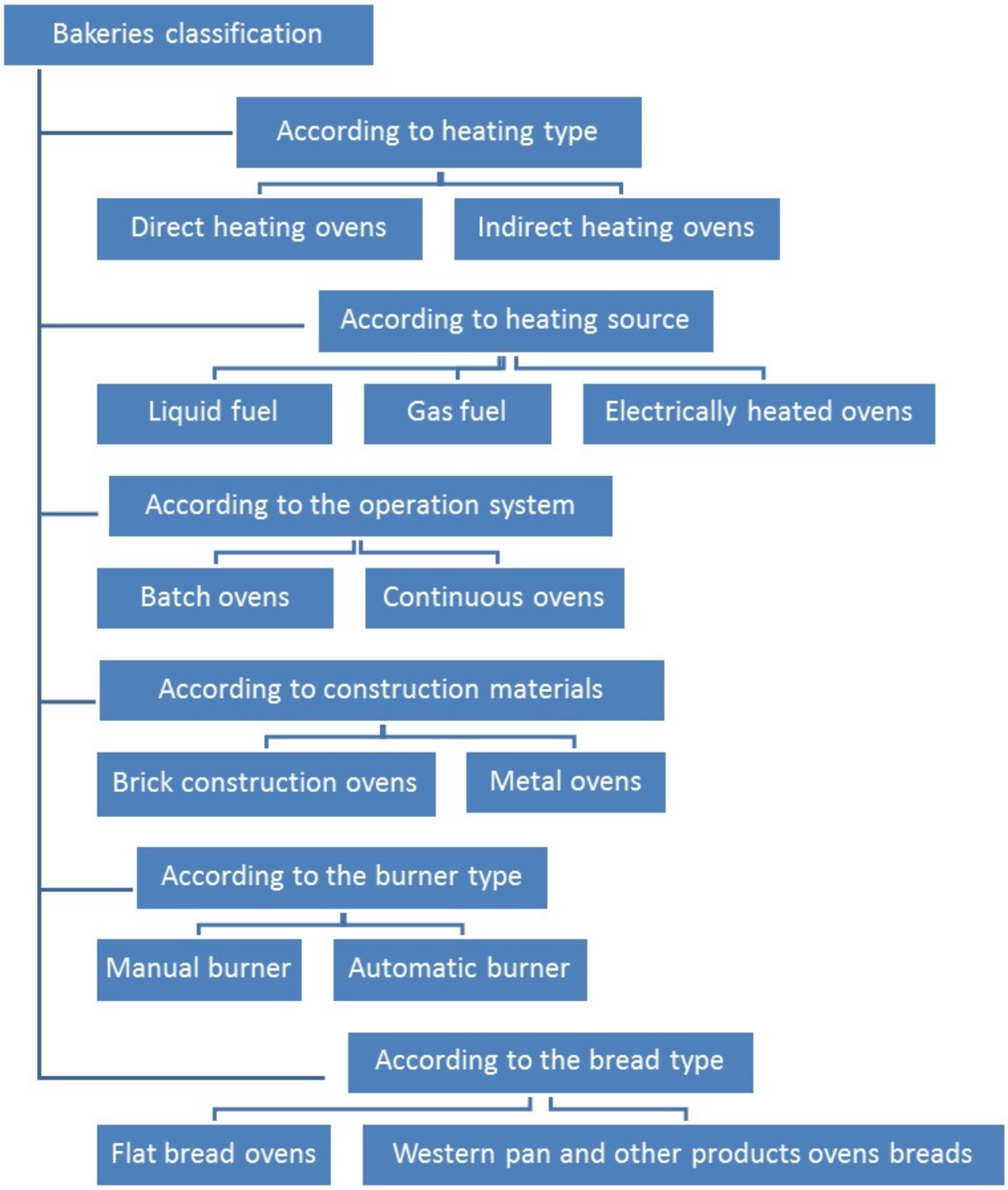

Fig. 2.1 Bakeries classification according to different parameters

Indirect Heating Ovens

In the indirect heating ovens, heat from the burning fuel is used to heat air, or steam pipes, which are then used to heat the baking chamber [14]. It is also stated that steam tubes are either heated by burning fuel or supplied with steam from a remote boiler.

Heated air is commonly recirculated through the baking chamber and a separate heat exchanger where the combustion gases are passed through banks of radiator tubes in the baking chamber, or fuel is burned between a double wall, and the combustion products are exhausted from the top of the oven.

Convective ovens require a pre-heating stage to achieve a homogenous temperature. Energy consumption is high during the pre-heating stage and proportional to pre-heating time. The pre-heating time depends on the set-point temperature [17].

Burning fuel Ovens

In the fuel-fired ovens, heat is supplied by combustion of fuel and is transmitted by different means of heat transfer [5]. This type of ovens depends on burning either the liquid or gas fuel to produce heat, as mentioned by Fellows [14].

Electrically Heated Ovens

Fellows [14] pointed that electric ovens are heated by induction heating elements or radiator plates.

Batch - Ovens

In batch ovens, the walls and base are heated whereas, in continuous ovens, radiators are located above, alongside and below a conveyor belt. Fellows [14] pointed that in the batch ovens, food is loaded into a baking chamber, either on trays or single and the more recent designs include the multi-deck oven. The main disadvantages of the batch ovens are higher labor costs and lack of uniformity in baking times, caused by the delay in loading and unloading.

In batch ovens operation, the furnace or oven is charged with a certain amount of raw material, and is heated for the proper duration to achieve temperature increase, chemical or physical change required. At this point, the heat source is removed, the treated material is discharged, a new batch is charged and the process is reported. In some batch furnaces, the temperatures maintained may vary during the process cycle [16].

Continuous and Semi-continuous Ovens

Continuous and semi-continuous ovens circulate the food through the oven, the movement of the food with or without fans to circulate the air ensures more uniform heating [14]. It is indicated that the operation is semi–continuous when the oven must be stopped to unload the food that takes place through the same door of loading (like in rotary – hearth rack ovens). These tunnel ovens (conveyor or traveling hearth ovens) are one type of continuous ovens.

Cauvain [16] reported that in the continuous operation, the furnace or oven is continuously operated at the operating temperature. The raw material is continuously charged at one end of the furnace and is conveyed to the other end. The material spends enough time in the furnace to achieve the temperature increase, the physical or chemical change required. This amount of time is sometimes known as the residence time. In some continuous furnaces, the conditions maintained vary with distance from the entrance.

In this operation, an eternal conveyor system is required to move the materials from the entrance to the exit of the oven.

2.3 Principles of Bread Baking Process

Bread production encompasses a number of fundamental biochemical, chemical and physical processes, such as evaporation of water, volume expansion, gelatinization of starch, protein denaturation, crust formation, carbon dioxide production, the formation of a porous structure and browning reactions.

Bread production on a commercial scale is frequently a continuous manufacturing process, with short shutdown periods occurring on a weekly basis to allow equipment to be cleaned and maintained. Several engineering / manufacturing issues in a commercial bakery need to be tightly controlled in order for it to be commercially successful. First and foremost, product quality is non-negotiable – this includes food safety, consistency of produce, taste, texture, appearance, and shelf-life. Furthermore, other factors such as minimizing interruptions to the manufacturing process to avoid wastage and keeping the production time at a minimum are important to keep financing costs low. Energy use is an increasingly important concern for commercial bakeries [18].

Flatbread is baked at temperatures of 300 °C – 350 °C in 4 min – 6 min [19]. It can also be baked at a substantially higher temperature, e.g. 400-600°C, during only 40 s – 60 s [20]. Other kinds of bread are normally baked at temperatures of 218 °C – 232 °C in 20 min – 25 min

The flatbread has a roundish flat shape of about Ø22 cm with two layers, and is produced as soft (130 g per loaf at 36 %humidity) or hard, the so-called well-baked, low moisture, high- quality bread (110 g per loaf at 26 %humidity) [21].The initial moisture content of dough is reported as 42.12 % for Magr flatbread, whereas after baking it ranged from 24.32 % to 29.25 %, dependent on the oven belt speed [22].

Bread can be produced by the following sequence of operations: weighing of ingredients, mixing, fermentation, scaling, rounding, bench proving, moulding, panning, pan proving, baking, and cooling.

Mixing (Formation of Dough)

After being weighed, ingredients are mixed in order to bring about a uniform mixture and form the smooth dough. In dough mass, gluten is developed to promote the elasticity that retains gases formed by yeast. In addition, mixing is to distribute yeast cells uniformly so that yeast can receive proper nutrition. Mixing has to be properly controlled to ensure optimum bread texture and volume. The most popular measurement to estimate dough development during mixing is that of mixing torque. AN alternative measurement is that of power consumption of mixer or work input into the dough [23]. Kilborn [24] described a device to produce mixing curves by monitoring mixing power, force (resistance of dough to a probe) and dough temperature. This device could detect dough consistency during mixing. Larsen, Greenwood [25] found that mixing curve showed lower dough consistency when dough water addition was increased. To expend the optimum work input of 43 kJ kg^{-1}, mixing time needed to be increased linearly when added water was increased from 54 % to 66 %. Wesley et al. [23] developed a non-invasive method of monitoring dough mixing using a diode array near infrared (NIR) spectrometer. NIR shows a reduction in the spectroscopically active component until mixture reaches the optimum dough development. This is because the amount of glutenin macro-polymer and extractable gliadin is reduced. However, the effect of the starch component on the NIR curves was still not clear. When the dough was over mixed, the NIR result showed an increase in the spectroscopically active component.

Moulding After Mixing

The dough is divided and rounded before being delivered to an intermediate prover. Then the dough is shaped into dough pieces by moulding prior to a final proving. Incorrect moulding practice can affect bread features including loaf shape and symmetry, volume, crumb structure, and crust color. During moulding, the dough is sheeted to expel most of the gas that was produced after mixing and during intermediate proving. Sheeting makes the dough more pliable and aligns the gluten stranding in a more

orderly fashion. Consequently, it lays the foundation for a fine even grain in the finished loaf. After sheeting, dough is rolled up. A curling chain is produced. More curls in the dough piece generally provide better crumb structure. The curled dough piece is sealed by applying pressure. Too high pressure can damage the fine cell structure. The fault is recognizable by the occurrence of some large, shallow and open cells [14].

Dough Proving

Fermentation starts after the dough is mixed. The made-up dough pieces are placed in a prover which is maintained at 38 °C and a high humidity by using hot water or steam. The period of proving depends on the amount of yeast and temperature. Higher yeast level tends to increase fermentation rate, then shorten proving time. However, some ingredients such as salt and sugar can affect yeast activity. Generally, yeast is active within the temperature range of 25 °C to 40 °C. The fermentation can be speeded up by increasing temperature within active range [14]. Young dough refers to the under proved dough. Old dough refers to the over proved dough. As proving proceeds, gluten absorbs water, as a result, dough becomes more pliable and smoother. By the action of the yeast during proving, ethyl alcohol is produced, and carbon dioxide is released [16].

Bread Baking

During baking, heat is applied, and the final leavening occurs before yeast is destroyed at 60 °C. As a result, a rapid expansion of water vapor and carbon dioxide produces oven spring. The top crust is pushed up. A baking temperature depends on size and richness of the product. For example, small products should be baked at 204 °C to 238 °C whereas richer products should be baked at lower temperatures. The baking process is the key step in bread making. It can be divided into 3 stages [26]. The first stage starts at around 204°C and is composed of one-fourth of a total baking time of 26 minutes. The temperature of the outer crumb increases at an average rate of 4.7 °C per minute to 60 °C. An increase in temperature enhances enzymatic activity and yeast growth resulting in an oven rise (a perceptible increase in loaf volume). When the temperature reaches 50 °C – 60 °C, most enzymes are inactivated, and yeast is killed. Consequently, carbon dioxide is released from the solution resulting in a rapid loaf expansion called oven spring. The volume increases by one-third of the original. Furthermore, surface skin loses elasticity, thickens and begins to appear browning color. In the second stage, the oven temperature is maintained at 238 °C for 13 minutes. Crumb temperature increases at a rate of 5.4 °C per minute to 98.4 °C – 98.9 °C before keeping constant. At this temperature, all reactions are maximized, including evaporation, starch gelatinization, and protein denaturation. The dough becomes crumb structure from outer to inner portions by penetrating heat. A typical browning crust can be observed when crust temperature reaches 150 °C – 205 °C. Finally, the volatilization of organic substances is designated as the bake-out-loss. This period also takes one-fourth of the total baking time.

Process mapping is defined as assessing the conditions that exist within an oven, and then using this data to interpret product transformations. Two very different baking processes were evaluated by Walker [27] using this approach, the slow (406 s) cookie baking process in which initial dough moisture content was 19 % d.b., and the faster (195 s) cracker baking process in which the initial dough moisture content was 35 % d.b.

Cooling

Baked products are cooled to allow steam and alcohol produced during baking to escape. At the beginning of a cooling process, in the crumb, heat, and mass are transferred by evaporation-condensation mechanism, because of a radiation heat transfer and a high vapor pressure gradient between the crumb center and crust surface. The mass transfer increases the apparent thermal conductivity of crumb. Therefore, cooling rate at this stage is the fastest. Then the cooling rate is slowed down because of the reduction of evaporation-condensation rate and radiation heat transfer rate. Cooling rate also depends on air temperature and relative air humidity. To increase the cooling rate by decreasing air temperature, the intense mass transfer may move towards the crust surface with a slow evaporation rate. Consequently, condensation might occur below the crust layer and cause a higher water activity which interacts with microbial growth during storage. Therefore, the condensation under crust has to be controlled by controlling the evaporation rate above the crust surface [28].

2.4 Physical Properties of Bread

Physical properties of bread are important for modeling, simulation, and optimization of the baking process. The Physical properties of bread such as thermal conductivity (k), specific heat (c_p), and density (ρ) are usually used in a mathematical model of heat transfer. An improved knowledge of these physical properties of bread is essential in accurately predicting temperature changes, process duration, and energy consumption during the baking process. Among these properties, specific heat and density are significant in analyzing mass energy balances; thermal conductivity is the key property in determining the rate of thermal energy transfer within a material by conduction; and the combination of these three properties, thermal diffusivity, is a key property in the analysis of transient heat transfer.

2.4.1 Specific Heat Capacity

The specific heat of food stuff is defined as the quantity of thermal energy associated with a unit mass of the food and a unit of change in temperature. This thermo-physical property is often referred to as heat capacity and is an essential component of a thermal energy analysis on a food product, a thermal process, or processing equipment used for heating or cooling of a food.

Specific heat capacity depends on the nature of the heat addition process in terms of either at constant pressure or at constant volume. However, since pressure change in heat transfer problems of food materials are usually very small, the specific heat at constant pressure is most often considered [29,30].

Specific heat is the ratio of heat losses or gained to temperature change for a unit mass [31to 34]:

$$c_p = \frac{Q}{m \cdot \Delta T} \tag{2.1}$$

where c_p [J kg^{-1} K^{-1}] is the specific heat capacity at constant pressure, Q [J] is the heat loss or gained, ΔT [K] is the temperature change, and m [kg] is the mass of the food.

Specific heat which takes into account the mass fraction of water proposed by Favre-Marinet, Tardu [32]:

$$c_p = 0.837 + 3.349 \cdot \omega_{\mathrm{H2O}} \tag{2.2}$$

where c_p [J kg^{-1} K^{-1}] is the specific heat capacity at constant pressure, and ω [–] is the mass fraction of different food elements that are indicated by the subscripts H_20 – for water.

Favre-Marinet, Tardu [32],[35] reported that the influence of product components was expressed in an empirical equation:

$$c_p = 4\,187 \cdot \omega_{\mathrm{H2O}} + 2\,093 \cdot \omega_{\mathrm{fat}} + 1\,256 \cdot \omega_{\mathrm{sld}} \tag{2.3}$$

where c_p [J kg^{-1} K^{-1}] is the specific heat capacity at constant pressure, and ω [–] is the mass fraction of different food elements that are indicated by the subscripts H_20 – for water, fat – for fat, and sld – for solids.

The relation between the composition of food and the specific heat proposed by Choi [36]:

$$c_p = 4\,180 \cdot \ \omega_{\mathrm{H2O}} + 1\,711 \ \cdot \omega_{\mathrm{prt}} + 1\,928 \cdot \omega_{\mathrm{fat}} + 1\,547 \cdot \omega_{\mathrm{cab}} + 0.908 \cdot \omega_{\mathrm{ash}} \tag{2.4}$$

where c_p [J kg^{-1} K^{-1}] is the specific heat capacity at constant pressure, and ω [–] is the mass fraction of different food elements that are indicated by the subscripts H_20 – for water, prt – for protein, fat – for fat, cab – for carbohydrate and ash – for ash.

Irudayaraj, Jun [35] gave equation for specific heat which takes into account the composition of food:

$$c_p = 4\,187 \cdot \ \omega_{\mathrm{H2O}} + 1549 \ \cdot \omega_{\mathrm{prt}} + 1675 \cdot \omega_{\mathrm{fat}} + 1424 \cdot \omega_{\mathrm{cab}} + 0.837 \cdot \omega_{\mathrm{ash}} \tag{2.5}$$

The specific heat of food products as a function of temperature and water content in a range of 303 K – 336 K and in a moisture content range of 0.1 % – 80 % was suggested by Gupta [37]:

$$c_p = 2\,477 + 2\,356 \cdot \omega_{\mathrm{H2O}} + 3.79 \cdot T \tag{2.6}$$

where c_p [J kg^{-1} K^{-1}] is the specific heat capacity at constant pressure, T [K] is the temperature, and ω [–] is the mass fraction of different food elements that are indicated by the subscript H_20 – for water.

More generalized equation for specific heat of food was published, for example, by Choi [36],[38,35,34] :

$$c_p = \sum_{j=I}^{n} \omega_j \ \cdot c_{p,j}$$

$$c_p = \omega_{\mathrm{H2O}} \cdot c_{p,\mathrm{H2O}} + \omega_{\mathrm{prt}} \cdot c_{p,\mathrm{prt}} + \omega_{\mathrm{fat}} \cdot c_{p,\mathrm{fat}} + \\ + \omega\_\mathrm{cab} \cdot c\_(p, \mathrm{cab}) + \omega\_\mathrm{ash} \cdot c\_(p, \mathrm{ash}) + \omega\_\mathrm{fib} \cdot c\_(p, \mathrm{fib}) \tag{2.7}$$

where c_p [J kg^{-1} K^{-1}] is the specific heat capacity at constant pressure by the subscripts H_20 – for water, prt – for protein, fat – for fat, cab – for carbohydrate and ash – for ash, and ω [–] is the mass fraction of different food elements that are indicated by the subscripts H_20 – for water, prt – for protein, fat – for fat, cab – for carbohydrate and ash – for ash.

To determine the specific heat of the major components of a food $c_{p,j}$ the empirical equations were used in Table 2.1, [29,35,39].

Table 2.1 Models of specific heat for major components of foods

Components	c_p / J kg^{-1} K^{-1}
Carbohydrate	$c_p = 1.5488 + 1.9625 \times (10)^{-3} \times T - 9399 \times (10)^{-6} \times T^2$
Ash	$c_p = 1.0926 + 1.8896 \times (10)^{-3} \times T - 3.6817 \times (10)^{-6} \times T^2$
Fiber	$c_p = 1.8459 + 1.8306 \times (10)^{-3} \times T - 4.650\,9 \times (10)^{-6} \times T^2$
Fat	$c_p = 1.9842 + 1.4733 \times (10)^{-3} \times T - 4.8008 \times (10)^{-6} \times T^2$
Protein	$c_p = 2.0082 + 1.2089 \times (10)^{-3} \times T - 1.3129 \times (10)^{-6} \times T^2$
Water (0 °C < T < 150 °C)	$c_p = 4.1762 - 9.0864 \times (10)^{-5} \times T + 5.4731 \times (10)^{-6} \times T^2$

2.4.2 Thermal Conductivity

Thermal conductivity measures the ability of a material to allow the flow of heat from its warmer surface through the material to its colder surface, determined as the heat energy transferred per unit of time and per unit of surface area divided by the temperature gradient, which is the temperature difference divided by the distance between the two surfaces (the thickness of the material). A simplified approximation for thermal conductivity is given as [29,31,40]:

$$k = \frac{\dot{Q} \cdot \delta}{A_S \cdot \Delta T} \tag{2.8}$$

where k [W m^{-1} K^{-1}] is the thermal conductivity, $\dot{Q}$ [W] is the rate of heat input, δ [m] is the material thickness parallel to heat flow, ΔT [K] is the temperature change, and A_S [m^2] is the contact area normal to direction of heat flow.

Most common models to predict thermal conductivity of foods are those assuming that different components are arranged in layers either parallel or normal to the heat flow, resulting in the following expressions based on the electric analogy of heat transmission [1].

Series model supposed that layers of components placed normal to the heat flow, in a series arrangement of resistances and the effective thermal conductivity can be calculated as follows:

$$k = \frac{1}{\sum_{i=1}^{n} (\phi_i / k_i)} \tag{2.9}$$

where k [W m^{-1} K^{-1}] is the thermal conductivity, k_i [W m^{-1} K^{-1}] is the thermal conductivity of each food composition, and ϕ_i [–] is the volume fraction of each food composition.

Parallel model supposed that layers of components are placed in the direction of the heat flow, in parallel arrangements of resistances. The effective thermal conductivity is given by:

$$k = \sum_{i=1}^{n} k_i \cdot \phi_i \tag{2.10}$$

The volume fractions can be calculated from the mass fractions ω_i and intrinsic densities ρ_i as:

$$\phi_i = \frac{\omega_i/\rho_i}{\sum_{i=1}^{n}(\omega_i/\rho_i)} \tag{2.11}$$

where ϕ_i [–] is the volume fraction of each food composition, ρ_i [kg m^{-3}] is the density of each food composition, and ω_i [–] mass or weight fraction of each food composition.

Random model, which is the weighted geometric mean of the component phases proposed by Valentas et al. [39]:

$$k = k_1^{\omega_1} \cdot k_2^{\omega_2} \cdot k_3^{\omega_3} \ldots \ldots k_n^{\omega_n} \tag{2.12}$$

where k [W m^{-1} K^{-1}] is the thermal conductivity, and ω [–] is the mass fraction.

Another empirical equation is developed for solid and liquid foods [41]:

$$k = 0.58 \cdot \omega_{\mathrm{H2O}} + 0.155 \cdot \omega_{\mathrm{prt}} + 0.16 \cdot \omega_{\mathrm{fat}} + 0.25 \cdot \omega_{\mathrm{cab}} + 0.135 \cdot \omega_{\mathrm{ash}} \tag{2.13}$$

where k [W m^{-1} K^{-1}] is the thermal conductivity, and ω [–] is the mass fraction of different food elements that are indicated by the subscripts H_20 – for water, prt – for protein, fat – for fat, cab – for carbohydrate and ash – for ash.

Farinu [29] considered thermal properties of 15 different food powders from literature and observed that all data points fall on the range defined by values predicted by series and parallel models. It was observed that the parallel model defined the upper limit while the series model defined the lower limit of the predictions.

An empirical relation for the determination of thermal conductivity of major components of foods is given in Table 2.2, [29,35,39].

Table 2.2 Models for thermal conductivity of major components of foods

Components	***K* / W m^{-1} K^{-1}**
Carbohydrate	k= 0.20141 + 1.3874 × (10)$^{-3}$ × T – 4.3312 × (10)$^{-6}$ × T^2
Ash	k= 0.32962 + 14011 × (10)$^{-3}$ × T – 2.9069 × (10)$^{-6}$ × T^2
Fiber	k= 0.18331 + 1.2497 × (10)$^{-3}$ × T – 3.1683 × (10)$^{-6}$ × T^2
Fat	k= 0.18071 + 2.7604 × (10)$^{-4}$ × T – 1.7749 × (10)$^{-7}$ × T^2
Protein	k= 0.17881 + 1.1958 × (10)$^{-3}$ × T – 2.7178 × (10)$^{-6}$ × T^2
Water	k= 0.57109 + 1.7625 × (10)$^{-3}$ × T – 6.7036 ×(10)$^{-6}$ × T^2

2.4.3 Density

Density is the ratio of mass to volume of a material. Density of food products is an important property in analyzing food processing operations. Density is closely related to porosity and moisture content of food. The structure of food materials can be characterized by density (apparent and true), porosity, specific volume, particle density shrinkage and so on. Among these, density and porosity are the most common structural properties.

Apparent density (ρ_{ap}): concerns powdered and porous materials, and it is determined by the mass of the sample and its apparent volume

$$\rho_{ap} = \frac{m_t}{V_t} \tag{2.14}$$

where ρ_{ap} [kg m^{-3}] is the apparent density, m_t [kg] is the total mass, and V_t [m^3] is the total volume of the sample including the pores.

True density (ρ_{tru}) is the density excluding all pores and it is determined by the mass of the sample and its true volume

$$\rho_{tru} = \frac{m_t}{V_t} \tag{2.15}$$

where ρ_{tru} [kg m^{-3}] is the true density, m_t [kg] is the total mass, and V_t [m^3] is the total volume of the sample (volume of dry solids and water).

Density is an intensive property it depends directly on the mass fractions of the major components of the food and can be found in Boukouvalas et al. [42],[35,39]:

$$\rho = \frac{1}{\sum_{i=1}^{n}(\omega_i/\rho_i)} \tag{2.16}$$

where ρ [kg m^{-3}] is the density of the product, ρ_i [kg m^{-3}] is the density of each food composition, and ω_i [–] mass or weight fraction of each food composition.

An empirical relation for the determination of density of major food components as a function of temperature is given in Table 2.3, [35,39,29].

Table 2.3 Models for density of major components of foods

Components	ρ / kg m^{-3}
Carbohydrate	$\rho = 1.5991 \times (10)^3 - 0.31046 \times T$
Ash	$\rho = 2.4238 \times (10)^3 - 28063 \times T$
Fiber	$\rho = 1.3115 \times (10)^3 - 0.36589 \times T$
Fat	$\rho = 9.2559 \times (10)^2 - 0.4175 \times T$
Protein	$\rho = 1.3299 \times (10)^3 - 0.5184 \times T$
Water (0 °C < T < 150 °C)	$\rho = 997.18 + 3.1439 \times (10)^{-3} \times T - 3.7574 \times T^2$

2.4.4 Thermal Diffusivity

Thermal diffusivity indicates how fast heat propagates through a sample while heating or cooling. Thermal diffusivity is a parameter used in the heat transfer calculation by conduction. The rate at which heat diffuses by conduction through a material depends on the thermal diffusivity and can be defined as

$$a = \frac{k}{\rho \cdot c_p} \tag{2.17}$$

where a [$m^2\ s^{-1}$] is the thermal diffusivity, ρ [$kg\ m^{-3}$] is the density of the product, k [$W\ m^{-1}\ K^{-1}$] is the thermal conductivity, and c_p [$J\ kg^{-1}\ K^{-1}$] is the specific heat capacity at constant pressure.

Thermal diffusivity can be determined either by direct experiment or estimated from the thermal conductivity, specific heat, and density.

2.4.5 Moisture Diffusivity

Moisture diffusivity (D) is the rate at which moisture diffuses through a material. Moisture diffusivity is an important transport property necessary for the design and optimization of all the processes that involve internal moisture movement. Fick's second law is used in liquid diffusion theory to establish moisture diffusion as a function of the concentration gradient [39]:

$$\frac{\partial c}{\partial t} = \frac{\partial}{\partial x}\left(D \frac{\partial c}{\partial x}\right) \tag{2.18}$$

where c [$mol\ m^{-3}$] is the amount of concentration, t [s] is the time, x [m] material thickness along direction of mass transfer, and D [$m^2\ s^{-1}$] is the diffusion coefficient.

2.5 Heat and mass Transfer in the Bread During Baking

2.5.1 Heat Transfer

Energy transfers from the surroundings to the product and from the surface to the inside of the product are the two main aspects of energy movement in the baking process. The heating of the product causes physio-chemical changes in the dough and dries the product by evaporation of water.

During baking, heat is transferred through the combination of all three well-known mechanisms: conduction, convection and radiation.

Conduction

Heat conduction is usually most effective in solids, in particular metals, due to the molecular structure that allows a large number of electrons to vibrate and therefore transfer heat. Thermal conductivity is a material specific property that is dependent on factors such as temperature, phase and material structure.

Midden [43] described the success of a baking operation as being dependent on "the ability of the product to transfer heat from its outer surface to its center" i.e. the rate at which conduction occurs from crust to crumb. As the temperature at the core of the dough/bread needs to be raised from ambient to approximately 100 °C, conduction within the bread has a great effect on the energy requirement of both the prover and oven.

Bread is a poor conductor of heat due to the cellular structure of gas cells trapped within the dough/bread. The thermal conductivity of dough/bread varies with temperature due physical changes in the material structure, i.e. volume expansion, increase in porosity, decrease in density and moisture

loss. Published temperature dependent values of thermal conductivity for white sandwich bread vary between 0.11 W m^{-1} K^{-1} and 0.85 W m^{-1} K^{-1} [44-46].

Conduction is the transfer of heat from higher temperature to lower temperature through the vibration of molecules. In order to find out how much the material (in this research, the container or dough/bread) rises in temperature, the heat diffusion equation [47] is employed:

$$\frac{\partial}{\partial x}\left(\frac{\partial T}{\partial x}\right)+\frac{\partial}{\partial y}\left(\frac{\partial T}{\partial y}\right)+\frac{\partial}{\partial z}\left(\frac{\partial T}{\partial z}\right)+\dot{Q}_{\mathrm{V}}=\rho\cdot c_p\cdot\frac{\partial T}{\partial t} \tag{2.19}$$

where x, y, and z = the horizontal, vertical, and depth space coordinates in the Cartesian system, respectively, T [K]is the variable temperature, $\dot{Q}_{\mathrm{V}}$ [W m^{-3}] is the volume heat source, ρ [kg m^{-3}] is the density of the material, c_{p} [J kg^{-1} K^{-1}] is the specific heat (at constant pressure) of the material, and t [s] is the variable time.

In order to solve this equation a number of assumptions are to be made. First, it is assumed that there is no variation in temperature in the x, y, and z directions; this causes the first three terms on the left side of (2.19) to be equal to zero. This results in the following equation:

$$\dot{Q}_{\mathrm{V}}=\rho\cdot c_p\cdot\frac{\partial T}{\partial t} \tag{2.20}$$

where $\dot{Q}_{\mathrm{V}}$ [W m^{-3}] is the volume heat source, ρ [kg m^{-3}] is the density of the material, c_p [J kg^{-1} K^{-1}] is the specific heat (at constant pressure) of the material, T [K] is the variable temperature, and t [s] is the variable time.

Since T is now only a function of t, the ∂ operator can be changed to d

$$\dot{Q}_{\mathrm{V}}=\rho\cdot c_p\cdot\frac{\mathrm{d}T}{\mathrm{d}t} \tag{2.21}$$

Multiplying both sides of (2.21) by dt:

$$\dot{Q}_{\mathrm{V}}\cdot\mathrm{d}t=\rho\cdot c_p\cdot\mathrm{d}T \tag{2.22}$$

Rearranging:

$$\rho\cdot c_p\cdot\mathrm{d}T=\dot{Q}_{\mathrm{V}}\cdot\mathrm{d}t \tag{2.23}$$

Multiplying both sides of (2.23) by c_{p}:

$$\mathrm{d}T=\frac{\dot{Q}_{\mathrm{V}}}{\rho\cdot c_p}\mathrm{d}t \tag{2.24}$$

Integrating, assuming ($\dot{Q}_{\mathrm{V}}/\rho\, c_{\mathrm{p}}$) is constant (to simplify the calculation):

$$\int\mathrm{d}T=\frac{\dot{Q}_{\mathrm{V}}}{\rho\cdot c_p}\int\mathrm{d}t \tag{2.25}$$

$$T = \frac{\dot{Q}_V}{\rho \cdot c_p} t + C \tag{2.26}$$

Where C is the constant of integration. Noting that at $t = t_0$, $T = T_0$

$$T_0 = \frac{\dot{Q}_V}{\rho \cdot c_p} t_0 + C \tag{2.27}$$

Rearranging:

$$T_0 - \frac{\dot{Q}_V}{\rho \cdot c_p} \cdot t_0 = C \tag{2.28}$$

$$T = \frac{\dot{Q}_V}{\rho \cdot c_p} \cdot t + T_0 - \frac{\dot{Q}_V}{\rho \cdot c_p} \cdot t_0 \tag{2.29}$$

$$T - T_0 = \frac{\dot{Q}_V}{\rho \cdot c_p} \cdot t - \frac{\dot{Q}_V}{\rho \cdot c_p} \cdot t_0 \tag{2.30}$$

$$T - T_0 = \frac{\dot{Q}_V}{\rho \cdot c_p} (t - t_0) \tag{2.31}$$

Since $\Delta T = T - T_0$ and $\Delta t = t - t_0$

$$\Delta T = \frac{\dot{Q}_V}{\rho \cdot c_p} \cdot \Delta t \tag{2.32}$$

Multiplying both sides of (2.32) by $\rho \cdot c_p$, and rearranging, results in the following equation:

$$\rho \cdot c_p \cdot \Delta T = \dot{Q}_V \cdot \Delta t \tag{2.33}$$

where ΔT is the temperature change of the container.

In order to apply (2.33) to the material being heated by the oven heating elements in this research, the heat flux of the heating elements upon the material is originally assumed to be equivalent to the heat source term $\dot{Q}_V$.

Convection

Convective heat transfer occurs when the movement of fluids causes momentum, energy and mass transfer [48].The rate of convective heat transfer is given by Newton's law of Cooling (2.34):

$$\dot{Q}_{cnv} = h_{cnv} \cdot A_S \cdot dT \tag{2.34}$$

where $\dot{Q}_{cnv}$ [W] is the heat flow rate, h_{cnv} [W m^{-2} K^{-1}] is the coefficient of heat transfer, A_S [m^2] is the area, and T [K]is the temperature.

where the convective heat transfer coefficient h_{cnv} is dependent on a number of physical characteristics of the fluid and flow parameters, thus, it is a difficult value to determine numerically or theoretically. Two methods are frequently used to calculate values – for simple flow problems it may be obtained by solving boundary layer equations, or for complex flow it can be correlated using experimental results [47].

The convective heat transfer coefficient h_{cnv} determines the rate of convective heat transfer from the air to the product surface inside a baking oven. Due to the scope for large variations in conditions in which bread is baked, values for h_{cnv} vary considerably for different studies. For the bread industry, the value of h_{cnv} = 10 W m^{-2} K^{-1} was first quoted by Rohsenow et al. [49] and subsequently used by Zhang, Datta [50]. A further value of convective heat transfer coefficient of 100 W m^{-2} K^{-1} was initially estimated by Therdthai et al. [51] and subsequently quoted by Wong et al. [46]. Another study used a value of 14 W m^{-2} K^{-1} for forced convection ovens with air velocities between 1.5 m s^{-1} and 2.5 m s^{-1} [45,52,53] quoted values of 17.53 W m^{-2} K^{-1} and 20 W m^{-2} K^{-1} respectively for bread baking applications but no details of how these values were obtained were given for either study. Šeruga et al. [54] determined heat transfer coefficients for baking Croatian flat bread by correlating dimensionless Nusselt number, Grashof number and Prandtl number. The value of heat transfer coefficient calculated for free convection was 9.756 W m^{-2} K^{-1}. Two types of convection are frequently discussed: free (or natural) convection and forced convection.

Natural Convection

In order to calculate whether the flow is laminar or turbulent, the Rayleigh number must be calculated. For a horizontal plate, the Rayleigh number is calculated as follows:

$$Ra = \frac{g \cdot \alpha_V \cdot (T_{srf} - T_{uhf}) \cdot L^3}{v \cdot a} \tag{2.35}$$

where T_{srf} [K] is the temperature of the heating element surface, T_{uhf} [K] is the temperature of the unheated fluid, L [m] is the characteristic length of the heating element surface, the variable g [m s^{-2}] is the acceleration due to gravity, the variables α^V [K^{-1}] is the volumetric thermal expansion coefficient, v [m^2 s^{-1}] is the kinematic viscosity, and a [m^2 s^{-1}] is the thermal diffusivity of the fluid.

Here, all of the fluid properties are evaluated at the film temperature T_f [K], given by:

$$T_f = \frac{T_{srf} + T_{uhf}}{2} \tag{2.36}$$

The variable α^V [K^{-1}] for ideal gases is defined as follows:

$$\alpha_V = \frac{1}{T_f} \tag{2.37}$$

For this geometry (horizontal flat plate), L is defined as:

$$L = \frac{A_S}{P} \tag{2.38}$$

where L [m] is the characteristic length of the heating element surface, A_S [m²] the surface area of the plate, and P [m] is the perimeter of the plate. At this point it must be stated that since this is a two-dimensional simulation, the depth of the plate must be specified: this (the third dimension) is 0.8 m.

Forced convection

In order to determine if the flow is laminar or turbulent, the Reynolds number is calculated:

$$Re = \frac{\rho \cdot u \cdot L}{\eta} \tag{2.39}$$

where Re [–] is the Reynolds number, ρ [kg m⁻³] is the density of the fluid, u [m s⁻¹] is the speed of the fluid, L [m] is the characteristic length, and η [Pa s] is the dynamic viscosity of the fluid. If Re is less than 2300, the flow is considered laminar; if Re is greater than 2300, flow is considered turbulent. However, the Reynolds number at which flow becomes turbulent can be delayed to much higher values for rounded entrances, smooth walls, and steady inlet streams.

Thermal Radiation

Thermal radiation is often considered the most complex mode of heat transfer [55] and occurs when high energy photons are emitted from a hot body in the form of electromagnetic waves. Unlike convection and conduction, no particles are involved in the transfer of heat. Every object that has a temperature greater than absolute zero will emit thermal radiation.

Chhanwal et al. [56] reported that thermal radiation is the dominant mode of the heat transfer in the tunnel oven, therefore radiation is the most extensively studied mode of heat transfer in the simulations.

The following methodology of radiation formulation (including equations and figures) is derived from Bergman et al. [47]. Figure 2.2 shows a schematic of an enclosure. Surfaces i and j are arbitrary surfaces. Here, surface i is receiving radiation in the form of irradiation I_i from surfaces 1, 2, and j; radiation is leaving surface i in the form of radiosity $M_{\mathrm{rad},i}$. The net radiation leaving surface i is Φ_i, T, A_S, and ε are the temperatures, areas, and emissivities of the surfaces, respectively; the terms in this figure will be subsequently described.

Diffuse means that the radiation emitted, reflected and/or absorbed by a surface is independent of direction. A gray surface is one for which the emissivity and absorptivity are independent of wavelength for the spectral region under consideration. In order to arrive at a relation describing radiation exchange between surfaces in an enclosure, the net radiation from a single surface will first be describe (Fig. 2.3).

The net rate Φ_i at which radiation leaves surface i involves the difference between surface i radiosity $M_{\mathrm{rad},i}$, and surface i irradiation I_i:

$$\Phi_i = A_{\mathrm{S},i} \cdot \left(M_{\mathrm{rad},i} - I_i\right) \tag{2.40}$$

where Φ_i [W] is the net radiation leaving surface i, $A_{S,i}$ [m²] is the surface area of surface i, $M_{\mathrm{rad},i}$ [W m⁻²] is the surface i radiosity, and I_i [W m⁻²] is the radiation arriving at surface i from the other surfaces in the enclosure.

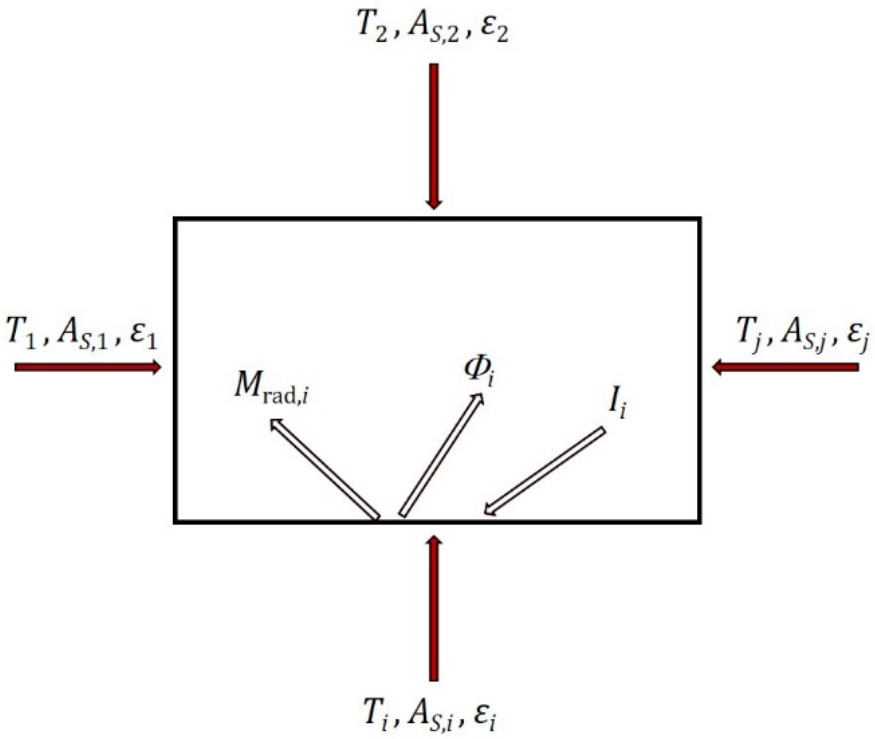

Fig. 2.2 Radiation exchange in an enclosure of diffuse, gray surfaces

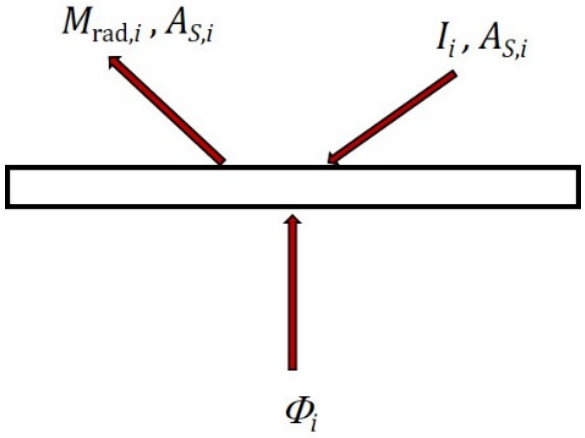

Fig. 2.3 Radiative balance according to (2.40)

The surface radiosity is defined as follows:

$$M_{\mathrm{rad},i} = M_i + \rho_i \cdot I_i \tag{2.41}$$

where M_i [W m^{-2}] is the emissive power of surface i, and ρ_i [–] is the reflectivity of surface i, $M_{\mathrm{rad},i}$ [W m^{-2}] is the surface i radiosity, and I_i [W m^{-2}] is the radiation arriving at surface i from the other surfaces in the enclosure.

For an opaque, diffuse, gray surface:

$$\alpha_i + \rho_i = 1 \tag{2.42}$$

where α_i [–] is the absorptivity of surface *i*. An opaque surface is one in which no radiation is transmitted through the surface.

Multiplying (2.42) by I_i:

$$\alpha_i \cdot I_i + \rho_i \cdot I_i = I_i \tag{2.43}$$

Substituting (2.41) into (2.22):

$$\Phi_i = A_{\mathrm{S},i} \cdot \left(M_i + \rho_i \cdot I_i - I_i\right) \tag{2.44}$$

Substituting (2.43) into (2.26); (see Fig. 2.4):

$$\Phi_i = A_{\mathrm{S},i} \cdot (M_i - \alpha_i \cdot I_i) \tag{2.45}$$

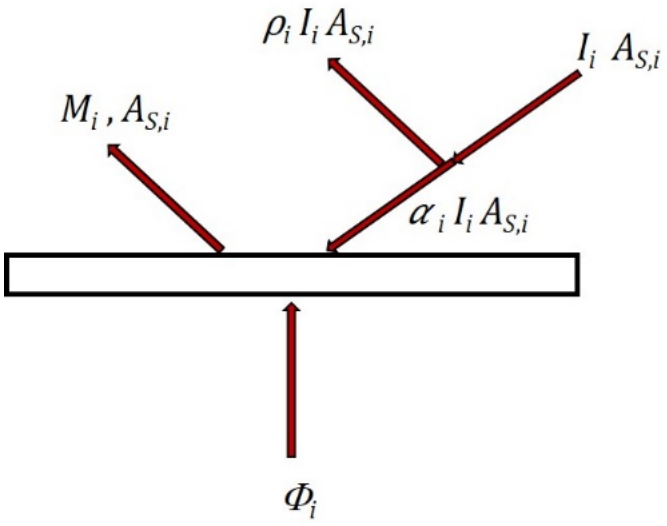

Fig. 2.4 Radiative balance according to (2.45)

For an opaque, diffuse, gray, surface:

$$\rho_i = 1 - \alpha_i = 1 - \varepsilon_i \tag{2.46}$$

where ε_i the total hemispherical emissivity of surface *i*. ε_i is defined as:

$$\varepsilon_i(T) = \frac{M_i(T)}{M_{\mathrm{bb},i}(T)} \tag{2.47}$$

where $M_{\mathrm{bb},i}$ [W m^{-2}] is the blackbody emissive power of surface *i*, and T [K] denotes the temperature of the surface.

A blackbody surface is a perfect emitter and absorber. The equation for $M_{\mathrm{bb},i}$ is:

$$M_{\mathrm{bb},i} = \sigma \cdot T_i^4 \tag{2.48}$$

where σ [W m^{-2} K^{-4}] is the Stefan-Boltzman constant.

Substituting (2.47) and (2.46) into (2.41):

$$M_{\mathrm{rad},i} = \varepsilon_i \cdot M_{\mathrm{bb},i} + (1 - \varepsilon_i) \cdot I_i \tag{2.49}$$

Solving (2.49) for I_i and substituting into (2.40):

$$\Phi_i = A_{\mathrm{S},i} \cdot \left(M_{\mathrm{rad},i} - \frac{M_{\mathrm{rad},i} - \varepsilon_i \cdot M_{\mathrm{bb},i}}{1 - \varepsilon_i} \right) \tag{2.50}$$

Rearranging terms on the right side of (2.49):

$$\Phi_i = \frac{M_{\mathrm{bb},i} - M_{\mathrm{rad},i}}{\frac{1 - \varepsilon_i}{\varepsilon_i \cdot A_{\mathrm{S},i}}} \tag{2.51}$$

In order to utilize (2.51), the surface radiosity $M_{\mathrm{rad},i}$ must be known. To determine this variable, it is necessary to consider the radiation exchange between the surfaces in the enclosure.

To compute the radiation exchange between any two surfaces (for example, surface *i* and surface *j*), the concept of a view factor must first be introduced. The view factor $F_{i,j}$ is the fraction of radiation leaving surface *i* that is intercepted by surface *j*. In this research a geometry the same and similar to that shown in Fig. 2.5 is employed:

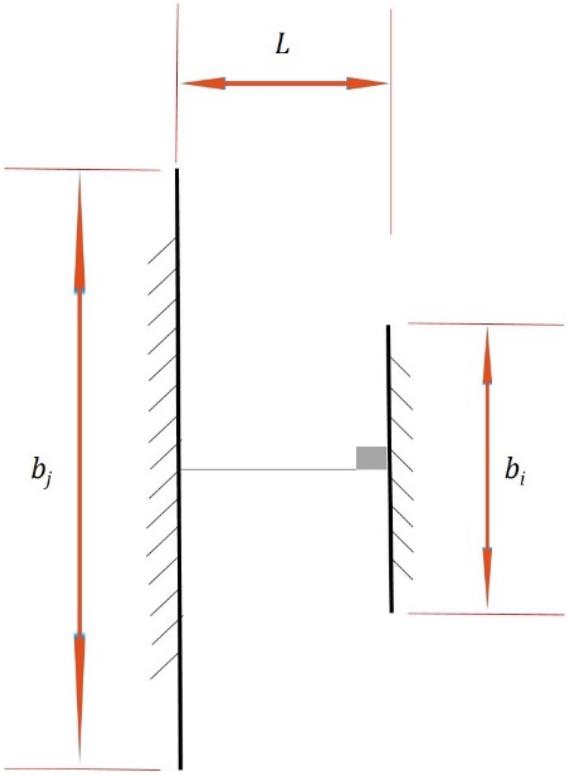

Fig. 2.5 Parallel plates with midline connected by perpendicular line

Figure 2.5 shows a schematic of parallel plates with their midline connected by a perpendicular line. For the geometry shown in Fig. 2.5 the view factor from Bergman et al. [47] is as follows:

$$F_{i,j} = \frac{\left[\left(B_i + B_j\right)^2 + 4\right]^{\frac{1}{2}} - \left[\left(B_i - B_j\right)^2 + 4\right]^{\frac{1}{2}}}{2B_i} \tag{2.52}$$

where $B_i = b_i / L$, $B_j = b_j / L$, b_i is the width of surface i, b_j is the width of surface j, and L is the perpendicular distance between the two surfaces.

Equation 2.52 is calculated from the view factor integral (a general expression for the view factor) in Bergman et al. [47]. Later in this radiation theoretical formulation there will be needed a view factor summation rule for surfaces exchanging radiation in an N-sided enclosure from Bergman et al. [47]:

$$\sum_{j=1}^{N} F_{i,j} = 1 \tag{2.53}$$

Referring back to Fig. 2.2, the irradiation of surface i can be evaluated from the radiosities of all the surfaces in an enclosure. From the definition of the view factor, it follows that the total rate at which radiation reaches surface i from all other surfaces, including i (Fig. 2.2), is:

$$A_{S,i} \cdot I_i = \sum_{j=1}^{N} F_{j,i} \cdot A_{S,j} \cdot M_{\mathrm{rad},j} \tag{2.54}$$

At this point another important view factor relation must be introduced. This relation is called the reciprocity relation, and is:

$$A_{S,j} \cdot F_{j,i} = A_{S,i} \cdot F_{i,j} \tag{2.55}$$

where $A_{S,i}$ [m²] is the area of surface i, and $A_{S,j}$ [m²] is the area of surface j, and $F_{j,i}$ is the fraction of radiation reaching surface i from surface j.

Substituting (2.55) into (2.54):

$$A_{S,i} \cdot I_i = \sum_{j=1}^{N} F_{i,j} \cdot A_{S,i} \cdot M_{\mathrm{rad},j} \tag{2.56}$$

Dividing both sides of (2.56) by $A_{S,i}$ and substituting into (2-40) for I_i:

$$\Phi_i = A_{S,i} \cdot \left(M_{\mathrm{rad},i} - \sum_{j=1}^{N} F_{i,j} \cdot M_{\mathrm{rad},j} \right) \tag{2.57}$$

Substituting the summation rule (2.53) into (2.57):

$$\Phi_{\mathrm{i}} = A_{\mathrm{S},i} \cdot \left(\sum_{j=1}^{N} F_{i,j} \cdot M_{\mathrm{rad},i} - \sum_{j=1}^{N} F_{i,j} \cdot M_{\mathrm{rad},j} \right) \tag{2.58}$$

Therefore:

$$\Phi_i = \sum_{J=1}^{N} A_{\mathrm{S},i} \cdot F_{i,j} \left(M_{\mathrm{rad},i} - M_{\mathrm{rad},j} \right) = \sum_{j=1}^{N} \Phi_{i,j} \tag{2.59}$$

Combining (2.51) and (2.59) results in:

$$\frac{M_{\mathrm{bb},i} - M_{\mathrm{rad},i}}{(1-\varepsilon_i)\left(\varepsilon_i \cdot A_{\mathrm{S},i}\right)^{-1}} = \sum_{J=1}^{N} \frac{\left(M_{\mathrm{rad},i} - M_{\mathrm{rad},j}\right)}{\left(A_{\mathrm{S},i} \cdot F_{i,j}\right)^{-1}} \tag{2.60}$$

Once the surface radiosity $M_{\mathrm{rad},i}$ is calculated from the (2.60), the heat transferred to the material (container or dough/bread) can be determined from (2.51), and the temperature rise of the material can then be determined from the heat diffusion equation.

2.5.2 Mass Transfer

Diffusion together with evaporation and condensation have been assumed to be the mass transfer mechanisms inside dough [57]. The transport of water is driven by the gradients in water content. Thorvaldsson, Skjöldebrand [58] found that at the center of a loaf, the measured water content decreased until the center temperature was at 70 °C ± 5 °C because of the volume expansion. However, the total water content of the loaf should be constant because dough does not have a continuous pore system. When the temperature reached 70 °C, some structural changes commenced, as a result, the discrete pore became continuous and then allowed water to move freely. To reduce the partial water vapor pressure due to the temperature gradient, water moves towards the loaf center and the surface by condensation and evaporation. As a result, crumb temperature increasing is accelerated. At the surface exposed to oven air where the partial water vapor pressure is far from saturation, the water vapor diffuses into the air, as a result, the surface starts to dry out [13]. At this stage, a differentiation in bread structure is observed. Crumb is a wet core that contains as much moisture as the dough. Crust is a dried portion, the longer the baking is, the higher the thickness [59]. In a study by Larsen, Greenwood [25],the moisture content in the center of crumb was measured at 45.7 %, whereas the edge was at 37.2 %.The moisture movement in crumb and crust can be described by Fick's law [60].

According to Baik et al. [61], for cookie baking in a continuous oven the constant rate drying period occupies about 40 % of the baking time.

When the bread at room temperature enters the hot oven there is an initial drying period when the drying rate is increasing; this period is often small and can be neglected in most circumstances, and then the constant rate drying period, after that the linear falling rate drying period. The falling rate drying period signifies the time when the drying rate is decreasing with time.

In this research, the moisture theoretical formulation (including all equations and figures) is derived from Geankoplis [62], and it is feasible to calculate the loss of moisture from the bread using a constant

drying rate analysis. This means that the rate at which the bread loses moisture to the oven air does not change with time.

In Fig. 2.6 the bread is being dried by a stream of air. The total rate of heat transfer to the drying surface is:

$$\dot{Q} = \dot{Q}_{\text{cnv}} + \dot{Q}_{rad} + \dot{Q}_{\text{cnd}} \tag{2.61}$$

where $\dot{Q}$ [W] is the heat flow rate, $\dot{Q}_{\text{cnv}}$ [W] is the convective heat transfer from the gas at temperature T_{ffs} to the solid surface at T_{srf}, $\dot{Q}_{\text{rad}}$ [W] is the radiant heat transfer from the radiating surface at T_{rs} to the solid surface, and $\dot{Q}_{\text{cnd}}$ [W] is the rate of heat conduction from the bottom.

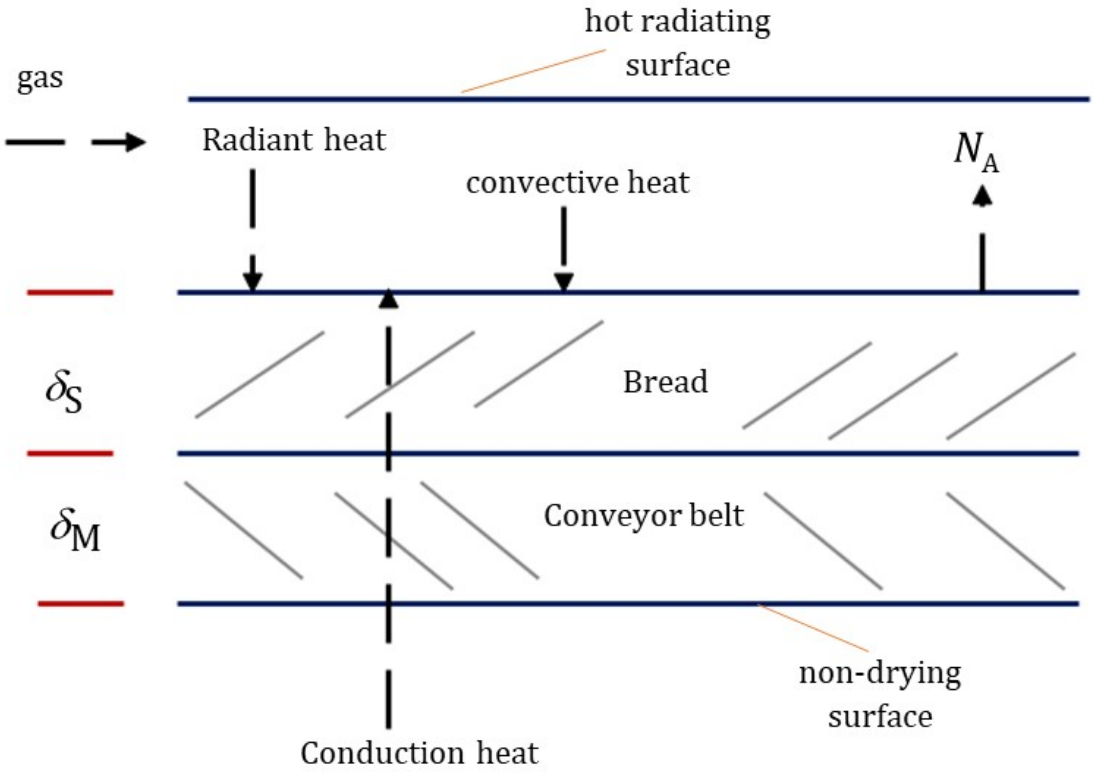

Fig. 2.6 Heat and mass transfer in drying a solid from the top surface.

The rate of convective heat transfer is as follows:

$$\dot{Q}_{\text{cnv}} = h_{\text{cnv}} \cdot (T_{\text{ffs}} - T_{\text{srf}}) \cdot A_{\text{S}} \tag{2.62}$$

where $\dot{Q}_{\text{cnv}}$ [W] is the convective heat transfer from the gas at temperature T_{ffs} to the solid surface at T_{srf}, A_{S} [m^2] is the exposed surface area, and h_{cnv} [W m^{-2} K^{-1}] is the convective heat transfer coefficient.

For air flowing parallel to the drying surface, the leading edge of the surface can cause turbulence. The following equation can be used to calculate h_{cnv} when the air temperature range is 45 °C to 150 °C and the air velocity range is 0.61 m s^{-1} to 7.6 m s^{-1}:

$$h_{\text{cnv}} = 0.0204 \times G^{0.8} \tag{2.63}$$

where G [kg h^{-1} m^{-2}] is the air mass velocity, and is calculated as:

$$G = u \cdot \rho \tag{2.64}$$

where u [m s^{-1}] is the speed, and ρ [kg m^{-3}] is the mass density.

$$\rho = \frac{1.0 + x}{v_H} \tag{2.65}$$

where ρ [kg m^{-3}] is the mass density, x [kg (H_20, g) kg^{-1}(dry air)] the specific humidity (also known as the humidity ratio) of the gas stream, and v_H [m^3 kg^{-1}] is the humid volume:

$$v_H = (2.83 \times 10^{-3} + 4.56 \times 10^{-3} x) T\ K \tag{2.66}$$

where T [K] is the temperature of the gas stream.

The coefficients in (2.66) are derived from the ideal gas equation at standard temperature and pressure, using the molecular weights of air and water.

The radiant heat transfer is calculated as:

$$\dot{Q}_{\text{rad}} = h_{rad} \cdot (T_{rs} - T_{\text{srf}}) \cdot A_{\text{S}} \tag{2.67}$$

where $\dot{Q}_{\text{rad}}$ [W] is the radiant heat transfer from the radiating surface at T_{rs} to the solid surface T_{srf}, A_{S} [m^2] is the exposed surface area and h_{rad} [W m^{-2} K^{-1}] is the radiation heat transfer coefficient.

$$h_{\text{rad}} = \varepsilon \cdot \sigma \frac{(T_{rs})^4 - (T_{\text{srf}})^4}{T_{rs} - T_{\text{srf}}} \tag{2.68}$$

where T_{rs} [K] is the radiating surface temperature , T_{srf} [K] is the solid surface temperature, ε [–] is the emissivity, σ [W m^{-2} K^{-4}] is the Stefan- Boltzman constant, and h_{rad} [W m^{-2} K^{-1}] is the radiation heat transfer coefficient.

The derivation of (2.68) will now be shown. For a small object (in this research, bread) in a large enclosure (in this research, the oven), the radiation to the small object is:

$$\dot{Q}_{\text{rad}} = A_{\text{S},1} \cdot \varepsilon \cdot \sigma \left(T_1^4 - T_2^4\right) \tag{2.69}$$

where $A_{S,1}$ is the area of the small object, ε is the emissivity of the object, σ is the Stefan- Boltzman constant, T_1 is the temperature of the object, and T_2 is the temperature of the enclosure. A radiation heat transfer coefficient h_{rad} can be defined as:

$$\dot{Q}_{\text{rad}} = h_{rad} \cdot A_{\text{S},1} \left(T_1^4 - T_2^4\right) \tag{2.70}$$

where $\dot{Q}_{\text{rad}}$ [W] is the heat transfer rate by radiation.

Equating (2.69) and (2.70), and solving for h_{rad} results in (2.71):

$$h_{\text{rad}} = \varepsilon \cdot \sigma \frac{(T_1)^4 - (T_2)^4}{T_1 - T_2} \tag{2.71}$$

Substituting the Stefan-Boltzman constant into (2.71) yields (2.72):

$$h_{\text{rad}} = \varepsilon \cdot (5.676)\ \frac{\left(\frac{T_1}{100}\right)^4 - \left(\frac{T_2}{100}\right)^4}{T_1 - T_2} \tag{2.72}$$

For the heat transfer by conduction from the bottom, the heat transfer is first by convection from the gas to the metal (in this research, the bread and/or conveyor belt), then by conduction through the metal, and finally conduction through the solid (bread). The heat transfer by conduction is:

$$\dot{Q}_{\text{cnd}} = U \cdot (T_{\text{ffs}} - T_{\text{srf}}) \cdot A_{\text{S}} \tag{2.73}$$

where $\dot{Q}_{\text{cnd}}$ [W] is the rate of heat conduction , A_{S} [m^2] is the exposed surface area, and U [W m^{-2} K^{-1}] is the overall heat transfer coefficient and is calculated as:

$$U = \frac{1}{\frac{1}{h_{\text{cnv}}} + \frac{\delta_M}{k_M} + \frac{\delta_S}{k_S}} \tag{2.74}$$

where U [W m^{-2} K^{-1}] is the overall heat transfer coefficient, h_{cnv} [W m^{-2} K^{-1}] is the convective heat transfer coefficient, δ_{M} [m] is the thickness of the metal, k_{M} [W m^{-1} K^{-1}] is the thermal conductivity of the metal, δ_{S} [m] is the thickness of the solid (bread), and k_{S} [W m^{-1} K^{-1}] is the thermal conductivity of the solid (bread).

The equation for the rate of mass transfer is:

$$N_{\text{A}} = k_{\text{d}} \cdot \frac{M_{\text{A}}}{M_{\text{B}}} \cdot (x_{\text{Sat}} - x) \tag{2.75}$$

where N_{A} [kg m^{-2} s^{-1}] is the flux of chemical A (water, in this research), k_{d} [kg m^{-2} s^{-1}] is the mass transfer coefficient, M_{A} [kg mol^{-1}] is the molecular weight of chemical A, M_{B} [kg mol^{-1}] is the molecular weight of chemical B (air, in this case), x_{Sat} [kg (H_20, g) kg^{-1}(dry air)] is the saturation humidity, and x [kg (H_20, g) kg^{-1}(dry air)] is the humidity. k_{d} is defined as :

$$k_{\text{d}} = \frac{k'_{\text{d}}}{x_{\text{M,B}}} \tag{2.76}$$

where k_{d} [kg m^{-2} s^{-1}] is the mass transfer coefficient, k'_{d} [kg m^{-2} s^{-1}] is the mass transfer coefficient with respect to mole fraction, and $x_{\text{M,B}}$ is the log mean inert mole fraction of chemical B. For a dilute mixture of chemical A in chemical B, $x_{\text{M,B}} \cong 1.0$, and then $k_{\text{d}} \cong k'_{\text{d}}$.

Equation (2.75) is derived by looking at the concept of wet bulb temperature. When a thermometer is covered by a wick. The wick is kept wet with water and immersed in a flowing stream of air-water vapor having a temperature T (dry bulb temperature) and humidity x. At steady-state, water is evaporating from the wick to the gas stream.

A heat balance on the wick can be made. The amount of heat lost by vaporization is:

$$\dot{Q} = M_{\mathrm{A}} \cdot N_{\mathrm{A}} \cdot \lambda \cdot A_{\mathrm{S}} \tag{2.77}$$

where $\dot{Q}$ [W] is the amount of heat lost by vaporization M_{A} [kg mol^{-1}] the molecular weight of the water is, N_{A} [kg m^{-2} s^{-1}] is the flux of water evaporating, A_S [m^2] is the surface area, and λ [kJ kg^{-1}] is the latent heat of vaporization. The flux N_{A} is:

$$N_{\mathrm{A}} = \frac{k'_{\mathrm{d}}}{x_{\mathrm{M,B}}} \cdot (y_{\mathrm{srf}} - y_{\mathrm{env}}) = k_{\mathrm{d}} \cdot (y_{\mathrm{srf}} - y_{\mathrm{env}}) \tag{2.78}$$

where k'_{d} and $x_{\mathrm{M,B}}$ are defined as before, y_{srf} is the mole fraction of water vapor in the gas at the surface, and y_{env} is the mole fraction in the gas. As stated before, for dilute mixtures, $x_{BM} \cong 1.0$, and then $k_y \cong k'_y$. The relation between H and y is:

$$y_{\mathrm{env}} = \frac{\frac{x}{M_A}}{\frac{1}{M_{\mathrm{B}}} + \frac{1}{M_{\mathrm{A}}}} \tag{2.79}$$

where M_{B} [kg mol^{-1}] is the molecular weight of air and M_{A} [kg mol^{-1}] is the molecular weight of water. Since x is small, as an approximation:

$$y_{\mathrm{env}} \cong \frac{xM_{\mathrm{B}}}{M_{\mathrm{A}}} \tag{2.80}$$

Substituting (2.80) into (2.78):

$$N_{\mathrm{A}} = \frac{k'_{\mathrm{d}}}{x_{\mathrm{M,B}}} \cdot (y_{\mathrm{srf}} - y_{\mathrm{env}}) = k_{\mathrm{d}} \cdot (y_{\mathrm{srf}} - y_{\mathrm{env}}) = k_{\mathrm{d}} \cdot \left(\frac{x_{\mathrm{srf}} \cdot M_{\mathrm{B}}}{M_{\mathrm{A}}} - \frac{x \cdot M_{\mathrm{B}}}{M_{\mathrm{A}}}\right) \tag{2.81}$$

$$N_{\mathrm{A}} = k_{\mathrm{d}} \cdot \frac{M_{\mathrm{B}}}{M_{\mathrm{A}}} \cdot (x_{\mathrm{srf}} - x) \tag{2.82}$$

Substituting (2.82) into (2.77):

$$\dot{Q} = M_{\mathrm{B}} \cdot k_{\mathrm{d}} \cdot \lambda \cdot (x_{\mathrm{srf}} - x) \tag{2.83}$$

The rate of convective heat transfer from the gas stream at T_{env} to the wick at T_{srf} is:

$$\dot{Q} = h_{\mathrm{cnv}} \cdot (T_{\mathrm{env}} - T_{\mathrm{srf}}) \cdot A_{\mathrm{S}} \tag{2.84}$$

where h_{cnv} [W m^{-2} K^{-1}] is the convective heat transfer coefficient, and A_{S} [m^2] is the surface area. Equating (2.83) to (2.84) and rearranging:

$$\frac{\mathrm{x} - x_{\mathrm{srf}}}{T_{\mathrm{env}} - T_{\mathrm{srf}}} = \frac{h_{\mathrm{cnv}} / M_{\mathrm{B}} \cdot k_{\mathrm{d}}}{\lambda} \tag{2.85}$$

The ratio $h_{cnv}/(M_B\ k_d)$ is known as the psychrometric ratio, and has been experimentally determined for water vapor-air mixtures to be approximately 0.960 to 1.005. The value of $h_{cnv}/(M_B\ k_d)$ can then be approximated to be equal to c_S , which is the humid heat of an air-water vapor mixture, and is the amount of heat required to raise the temperature of 1 kg dry air plus the water vapor present by 1 K or 1 °C. c_{mix} is assumed constant over the temperature ranges encountered at 1.005 J kg^{-1}(dry air) K^{-1} and 1.88 kg^{-1}(H_20, g). Therefore, c_{mix} is defined as follows:

$$c_{\text{mix}} = (1.005 + 1.88H)10^3 \tag{2.86}$$

Referring back to Fig. 2.6, and rewriting (2.77) in terms of the surface:

$$\dot{Q} = M_A \cdot N_A \cdot \lambda \cdot A_S \tag{2.87}$$

Combining (2.61), (2.62), (2.67), (2.73), (2.75), and (2.87):

$$R_C = \frac{\dot{Q}}{A_S \cdot \lambda} = \frac{(h_{\text{cnv}} + U)(T_{\text{ffs}} - T_{\text{srf}}) + h_{\text{rad}}(T_{rs} - T_{\text{srf}})}{\lambda} = k_d \cdot M_B\ (x_{\text{Sat}} - x) \tag{2.88}$$

where R_C [kg m^{-2} s^{-1}] is the rate of drying in the constant drying period. This period occurs when there is a sufficient amount of water on the surface of the solid. Eq. 2.88 gives the surface temperature T_{Srf} greater than the wet bulb temperature. The above equation can be rearranged to facilitate trial and error solution as follows:

$$\frac{(x_{\text{Sat}} - x) \cdot \lambda}{h_{\text{cnv}}/k_d M_B} = \left(1 + \frac{U}{h_{\text{cnv}}}\right)(T_{\text{ffs}} - T_{\text{srf}}) + \frac{h_{\text{rad}}}{h_{\text{cnv}}}(T_{rs} - T_{\text{srf}}) \tag{2.89}$$

2.6 Modelling of Bread Baking

Modeling is important to design, optimize and control a system. This is because a mathematical model describes how the process inputs affect various outputs [63]. Most modern control strategies rely to an extent on some form of process model. In food processes involving transformations and heat – mass momentum transfer coupled with intrinsic chemical reaction, the complex interrelationship is poorly understood. This is mainly because of a lack of information on kinetics, thermodynamic and transport properties of heterogeneous foodstuff [64].

2.6.1 Mathematical Modelling and Their Application in Bread Baking

Computer simulation is a powerful tool for prediction and optimal design of food engineering operations. Partial differential equations describing momentum, heat, and mass transfer coupled with equilibrium and kinetic equations, which usually form a model for a processing operation, can be solved easily with today's computing capabilities [65].

Zanoni et al. [66] proposed a mechanistic model to describe the heat and mass transfer phenomena causing a series of physical, chemical and structural transformations in bread. Temperature, moisture, crust thickness, and increased volume were determined. Initially, convective evaporation of water

occurs at the bread surface exposed to air and the crumb temperature increases linearly with time towards a constant value of 100 °C. Massive unbound water evaporates at this temperature with water boiling phenomenon. Therefore, this study assumed that the constant temperature of 100 °C was the evaporation-front temperature. In the crust, a bread portion above the evaporation front, bound water evaporates. As a result, the crust temperature increases and tends to the oven temperature. The crust becomes thicker when the evaporation-front progressively advances towards the inside. For microwave heating of dough, Tong, Lund [57] presented a1-dimensional mathematical model of heat diffusion in Cartesian co-ordinates with internal heat generation. The model was developed based on a principal model involving water transfer in vapor phase, water content in the hygroscopic range and equilibrium moisture content at the product surface during baking. The considered parameters included water diffusivity, bulk density, thermal conductivity, latent heat, dielectric constant, and constant surface heat transfer coefficient. With similar parameters, Zanoni et al. [59] developed a 2-dimensional axi-symmetric heat diffusion model. The phenomena were described separately for the upper and lower parts (crust and crumb). The upper part (crust) temperature was determined by equations including heat supply by convection, conductive heat transfer toward the inside, and convective mass transfer toward the outside. The lower part (crumb) temperature was determined by the Fourier's law. In addition to the Cartesian coordinate models, a 1-dimensional cylindrical co-ordinate model was also established by Vries et al. [67].

A mathematical model describing the heat and mass transfer in butter cookies during baking was formulated by Stenby Andresen [68]. The model was solved numerically by the use of a finite element method. Model optimization and validation was successfully carried out against experimental data obtained in the new pilot plant oven. The effect of the baking tray on mass transfer was examined through comparison of different modeling set-up and experimental data. It was found that while the baking tray is likely to reduce the evaporation from the bottom surface, it is not correct to assume that no evaporation takes place at the covered surface.

Feyissa [69] studied combined heat and mass transfer during processing of solid foods such as baking and frying processes. Modelling of heat and mass transfer during baking and frying is a significant scientific challenge. During baking and frying, the food undergoes several changes in microstructure and other physical properties of the food matrix. The heat and water transport inside the food is coupled in a complex way, which for some food systems it is not yet fully understood. A typical example of the latter is roasting of meat in convection oven, where the mechanism of water transport is unclear. Establishing the robust mathematical models describing the main mechanisms reliably is of great concern. A quantitative description of the heat and mass transfer during the solid food processing, in the form of mathematical equations, implementation of the solution techniques, and the value of the input parameters involves uncertainty.

Paton et al. [7] presented methodology quantifies the energy required to bake the dough, and to conduct a detailed analysis of the breakdown of losses from the oven. In addition, a computational fluid dynamics (CFD) optimisation study is undertaken, resulting in improved operating conditions for bread baking with reduced energy usage and baking time. Overall, by combining the two approaches, the analyses suggest that bake time can be reduced by up to 10% and the specific energy required to bake each loaf by approximately 2 %. For UK industry, these savings equate to more than £0.5 million cost and carbon reduction of more than 5000 tones CO_2 per year.

In study by Paton et al. [7], computational fluid dynamics (CFD) is combined with experimental analysis to develop a rigorous scientific framework for the rapid generation of forced convection oven designs. A design parameterization of a three-dimensional generic oven model is carried out for a wide range of oven sizes and flow conditions to optimise desirable features such as temperature uniformity throughout the oven, energy efficiency and manufacturability. Coupled with the computational model, a series of experiments measuring the local convective heat transfer coefficient (h_c) are undertaken. The facility used for the heat transfer experiments is representative of a scaled-down production oven where the air temperature and velocity as well as important physical constraints such as nozzle dimensions and nozzle-to-surface distance can be varied. An efficient energy model is developed using a CFD analysis calibrated using experimentally determined inputs. Results from a range of oven designs are presented together with ensuing energy usage and savings.

Powathil [70] developed two-dimensional model to examine the behavior of the problem in a two-dimensional environment. Two different numerical schemes, implicit finite difference scheme and finite element scheme are used to implement this mathematical model for baking and an efficient code is written in MATLAB to simulate the model and then to study its behavior. Then the profiles for temperature and moisture distribution during baking are plotted. Some critical values are also calculated to study the performance of the schemes used.

Sablani et al. [60] described a general equation for the temperature and moisture distribution within bakery products, which unfortunately contains a few errors. A corrected model for the combined heat and mass transfer in dough during baking can be presented as follows:

$$\rho_{\mathrm{ap}} \cdot c_p \frac{\partial T}{\partial t} = \nabla(k \cdot \nabla T) + \rho_{\mathrm{ap}} \cdot \lambda \cdot \frac{\partial c}{\partial t} \tag{2.90}$$

with the boundary conditions:

$$k \nabla T \boldsymbol{n} = h_{\mathrm{cnv}} \cdot (T_{\mathrm{ffs}} - T_{\mathrm{srf}}) + \varepsilon \cdot \sigma \cdot \left(T_{\mathrm{rs}}^4 - T_{\mathrm{srf}}^4\right) \tag{2.91}$$

$$D \nabla c \, n = k_{\mathrm{d}} \cdot (c - c_{\mathrm{env}}) \tag{2.92}$$

where ρ_{ap} [kg m^{-3}] is apparent density, c_p [J kg^{-1} K^{-1}] is specific heat, T [K] is temperature, t [s] is time, k [W m^{-1} K^{-1}] is thermal conductivity, λ [kJ kg^{-1}] is latent heat, C [kg m^{-2} s^{-1}] is absolute moisture content, h_{cnv} [W m^{-2} K^{-1}] is convective heat transfer coefficient, T_{rs} [K] is the radiating surface temperature , T_{srf} [K] is the solid surface temperature, T_{ffs} [K] is the fluid flowing stream temperature, σ [W m^{-2} K^{-4}] is Stefan-Boltzmann constant and ε [–] is emissivity, D [m^2 s^{-1}] is water diffusivity, k_{d} [m s^{-1}] is convective mass transfer coefficient.

Thorvaldsson, Janestad [31] further divided moisture into liquid water and water vapor, which diffused separately and simultaneously inside dough. A saturation equilibrium was assumed between the liquid water and water vapor.

Considering kinetic reactions, starch gelatinization was found to follow the first-order kinetics as follows [53]:

$$(1-\alpha) = \exp(-k \cdot t) \tag{2.93}$$

The gelatinization degree (α) was also defined as a function of time (t) as follows:

$$\alpha(t) = 1 - \frac{Q(t)}{Q_{\max}} \tag{2.94}$$

where α is the degree of gelatinization and t is time. $Q(t)$ and $Q_{\max}$ are heat uptakes evaluated for partially baked and raw dough, respectively.

Zanoni et al. [53] established the first model that combines the chemical-physical transformation model (i.e., starch gelatinization) with physical heat and mass transfer model. The model is useful to predict baking index with respect to different baking conditions.

In order to quantify the browning of bread crust during baking, Zanoni et al. [53] developed the following mathematical model for non-enzymatic browning reaction

$$\Delta E_{\infty} - \Delta E = \Delta E_{\infty} \exp(-k \cdot t) \tag{2.95}$$

where ΔE is color difference tending asymptotically to $\Delta E_{\infty} = 52$ which corresponded to the burnt sample and t is baking time (s).

In addition to kinetic reactions, volume expansion due to the thermally-induced release of carbon dioxide gas and water vapor from aqueous dough phase could be estimated by the following mathematical model:

$$V = \frac{4}{3}\pi R^3 \cdot N \cdot \rho + 1 \tag{2.96}$$

where V [–] is relative volume, R [m] is gas bubble radius, N [kg^{-1}] is number of gas cells in the dough, and ρ [$kg\ m^{-3}$] is density of gas-free dough.

The model showed a good agreement with the published data from literature, although the effect of elasticity was ignored.

2.6.2 Computational Fluid Dynamics (CFD) Modelling

Computational Fluid Dynamics (CFD) is a numerical technique for solving partial differential equations. The main characteristic of this technique is the immediate discretization of the equation of flow into the physically three-dimensional space. The solution domain is divided into a number of cells known as control volume. This process is called grid generation. For computation, the scalar values such as pressure, dissipation, and kinetic energy of turbulence are determined at the volume center whereas the three components of vector variables such as velocity are determined on the volume faces [71].

Computational fluid dynamics modeling of entire bread baking process is very complicated due to involvement of simultaneous physiochemical and biological transformations. Bread baking is a fickle process where composition, structure, and physical properties of bread change during the process. Computational fluid dynamics finds its application in modeling of such complex processes [72].

Nicolas et al. [73] used COMSOL Multiphysics® to model bread baking, considering heat and mass transfer coupled with the phenomenon of swelling. This model predicts the pressures, temperatures and water contents evolutions in the dough for different energy requests.

There are numerous advantages of using CFD techniques. It save time and cost in engineering design, but it is also used for addressing operational issues with equipment, conducting parametric studies, predicting flow in regions inaccessible to experimental measurements, and visualizing flow fields [74]. CFD is an analysis mechanism that should be used in conjunction with, rather than instead of experimental measurement.

In the bread industry, CFD has been used predominantly for analysis of airflow within baking ovens. For industrial ovens air distribution, air temperature and air velocity are all important factors to maximize heat transfer. Several CFD studies of baking ovens have been previously published, however there are significant issues affecting the accuracy of the results published. Some of the differences in the results can be attributed to varying oven designs, operating conditions and product types.

On the oven side, CFD modelling has been used to deal with the complexity of heat distribution, product geometry and oven configuration. To establish a model covering the temperature distribution of the whole oven chamber, CFD modeling may be the most effective method for it. To prevent leakage of gas inside a heating duct to an oven chamber, Fuhrmann et al. [75] used CFD to simulate the fluid mechanical and thermodynamic state in the oven to ensure that the system could maintain the pressure in the heating ducts lower than the ambient pressure. To investigate the proportion of heat transfer modes including radiation and convection inside natural convection and forced convection ovens. In addition, CFD approach was applied to study the effect of a perforated plate on improving the homogeneity of the velocity field and pressure drop over the baking chamber of a laboratory batch oven. Fluid flow was assumed to be laminar [67]. For a microwave baking oven, Verboven et al. [76] used CFD simulation to find a solution to increase the mass transfer coefficient and the uniformity of heat transfer coefficient at the product surface, so that the microwave baked product quality could be improved.

Chhanwal et al. [77] developed a computational fluid dynamic (CFD) model to study the temperature and browning profile of bread. Phase change during evaporation as well as evaporation–condensation mechanism during baking process was incorporated in this model. Simulation results were validated with experimental measurements of bread temperature at three different positions. Crumb temperature does not cross 100°C due to corporation of evaporation–condensation mechanism in this model [76]. Baking process completes within 25 min of processing time once the temperature of crumb becomes stable at 98 °C. Formation of crust and browning of bread surface were studied using earlier reported kinetic model and it predicted more browning at bread edges than the surfaces. However, predicted browning index was well within the range (<52).

In study by Khatir et al. [78], experimental and computational fluid dynamics (CFD) analyses of the thermal air flow distribution in a 3-zone small scale forced convection bread-baking oven are undertaken. Following industrial bread-making practice, the oven is controlled at different (constant) temperatures within each zone and a CFD model is developed and validated against experimental data collected within the oven. The CFD results demonstrate that careful selection of the flow model, together with implementation of realistic boundary conditions, give accurate temperature predictions throughout the oven. The CFD model is used to predict the flow and thermal fields within the oven and

to show how key features, such as regions of recirculating flow, depend on the speeds of the impinging jets.

Methodology of Computational Fluid Dynamics

Three common steps are used to formulate Computational Fluid Dynamics analysis:

1) pre–processing, 2) solving, and 3) post–processing.

Pre-processing (geometry creation and grid generation)

Geometry is created by fundamental geometric entities including points, lines, curves and surfaces. In grid generation, the whole geometry is then discretized by grids into small volumes composed of edges (1 – dimensional element), faces (2 – dimensional element) and blocks (3 – dimensional element). Each edge is composed of lines and curves that consist of grid points. It is used as a connecting element to create faces by surface discretization. Finally, each face is connected with other faces to create a block or volume. The set of volumes is the whole geometry. Grid generation can be done in 2 ways: structured grid generation and unstructured grid generation. The structured grid generation is based on the transfinite interpolation method. It can be used with uniform, exponential, geometric, and hyperbolic tangent grid point distribution along edges. The results are in tetrahedral faces and hexahedral volumes. For the unstructured grid generation, the different topological requirements are more than those for the structure grid generation. Unstructured grids including triangular face, prism, and pyramid are created within unstructured domains. In 2 – dimensional model, an unstructured domain consists of open surface sets. In contrast, an unstructured domain in 3 – dimensional model consists of closed surface sets. The results are in triangular faces, prisms, and pyramids. Due to the assumption of constant values over a whole control volume, the volume size may be reduced to increase the accuracy of the model. In other words, it needs to be ensured that the grid density is high enough to produce a reasonable solution. Then the number of volumes is increased. As a result, computational time is increased. In addition to the factor of number of grid, grid qualities such as skew quality, aspect ratio, face angle, and so on, have to be checked as well.

A CFD solver

Firstly, checks the pre-processing steps are compatible with the operations and equations that have been applied. The choice of turbulence model is made – turbulence models are sets of equations that have been devised to estimate flow characteristics of unpredictable three-dimensional fluid flow. The solution generated will never be exact – the residuals (degree of error) converge to approach the exact solution with an iterative approach. The computing part of the solving phase can use considerable time and resources, depending on: the parameters selected in the preprocessing stage, the quantity and quality of the processor(s) used and the degree of convergence or stability required for the problem to be considered solved.

Post-processing

Due to the magnitude of data that CFD solutions generate, post-processing requires careful thought and understanding to display results in the most informative format. Results can be displayed in visualized format, numerical results, or graphically. The most common options to display results include Geometry or mesh, Vector plots, contour plots, surface or planar plots and x-y plots or graphs, and particle tracking.

Depending upon the problem specified in the pre-processing phase, outputs would usually be flow characteristics such as: pressure, velocity, heat transfer, lift, drag, or many other forces and fluxes.

Discretisation and Mesh Generation

Discretisation of the flow domain is necessary to solve the governing equations. Discretisation is used to divide the flow domain into many smaller volumes, which generates a mesh (or grid). Flow domain discretisation and mesh generation is an important part of CFD problem formulation as it determines exactly how many calculation points there will be and therefore the computational demand of the solution process. Mesh refinement at the proximity of the nodes affects the accuracy of the interpolation equations used to approximate the governing differential equations. Generally speaking, regimes of complex flow require fine grids to adequately resolve the large flow gradients associated with rapidly varying flow fields.

Meshes can be one, two or three-dimensional, depending upon the nature of the flow problem. The quality and efficiency of a mesh is highly dependent on the meshing software used and the skill of the operator generating the mesh. Meshes can be broadly categorised as 'structured', 'unstructured' or 'hybrid'. The mesh is made up of cells containing nodes at which the flow variables of interest will be determined. Solving discretised forms of the governing flow equations at each of these nodes allows the flow variables (for example velocity, pressure etc.) to be approximated. Interpolation between each node then allows surface plots of the flow variables to be generated. Depending on the discretization method chosen, the governing equations must be expressed in either integral or differential form. The three main discretization methods are the Finite Difference Method (FDM), the Finite Volume Method (FVM) and the Finite Element Method (FEM).

The Finite Element Method

The FEM is often used in structural engineering or fluid dynamics problems where the fluid is interacting with a solid medium. The method uses shape functions to divide the geometry into a fixed number of elements [79].The discretised equations of fluid flow are interpolated across each element to approximate a solution for nodes – this approximated solution is in the form of a set of algebraic equations which then require solving to determine the solution across the fluid volume.

The starting point in the finite element method is the partition of the geometry into mesh elements, which are small units of a simple shape. Once the mesh has been created, approximations to the dependent variables can be introduced. For this discussion, one can start with the case of a single dependent variable u. The idea is to approximate u with a function that one can describe with a finite number of parameters called degrees of freedom. Inserting this approximation into the weak form of the equation generates a system of equations for the degrees of freedom.

One can start with a simple example: linear elements in one dimension (1 – D). Assume that the mesh consists of only two mesh intervals: $0 < x < 1$ and $1 < x < 2$. Linear elements means that on each mesh interval the continuous function is line ar (affine); therefore, the only fact one needs to know in order to characterize u uniquely is its values at the node points $x_1 = 0$, $x_2 = 1$, $x_3 = 2$. Identify these as $U_1 = u\,(0)$, $U_2 = u\,(1)$, $U_3 = u\,(2)$; these are the degrees of freedom. One can then write

$$U(X) = U_1\varphi_1(X) + U_2\varphi_2(X)\, U_3\varphi_3(X) \tag{2.97}$$

where φ_i (x) are certain piecewise linear functions. Specifically, φ_i (x) is the function that is linear on each mesh interval, and equals 1 at the i^{th} node point, and equals 0 at the other node points. For example:

$$\varphi_i\,(x) = \begin{cases} 1 - x & if\ 0 \le x\ \le 1 \\ 0 & if\ 1 \le x\ \le 2 \end{cases} \tag{2.98}$$

The φ_i (x) are called the basic functions. The set of functions u (x) is a linear function space called the finite element space.

The preceding examples are special cases of the Lagrange element. Consider a positive integer k, the order of the Lagrange element. The functions u in this finite element space are piecewise polynomials of degree k; in other words, on each mesh element u is a polynomial of degree k. To describe such a function it is sufficient to give its values in the Lagrange points of order k. These are the points whose local (element) coordinates are integer multiples of $1/k$. For a triangular mesh in 2 – D with k = 2, this means that there are node points at the corners and side midpoints of all mesh triangles. For each of these node points p_i, there exists a degree of freedom $U_i = u\ (p_i)$ and a basis function φ_i. The restriction of the basis function φ_i to a mesh element is a polynomial of degree (at most) k in the local coordinates such that φ_i = 1 at node i, and φ_i = 0 at all other nodes. Therefore, the basic functions are continuous and:

$$u = \sum_{\mathrm{i}} \mathrm{U}_i \cdot\ \varphi_i \tag{2.99}$$

The next step in the finite element method is the discretization of the partial differential equation that describes the physics of the COMSOL simulation; a 2 – D stationary problem will be considered for simplicity. The starting point is the weak formulation of the problem. First is the discretization of the constraints:

$$0 = R^{(2)}\ \mathrm{On}\ \Omega \tag{2.100}$$

$$0 = R^{(1)} \mathrm{on\ B} \tag{2.101}$$

$$0 = R^{(0)} on\ \mathrm{P} \tag{2.102}$$

where R(n) is the Euclidean n-space, and Ω, B, and P are the are domain, boundary, and point. The weak equation is then discretized. The weak equation is the differential equation (such as the Navier-Stokes equation) that is rewritten without derivatives of the unknown function, usually by multiplying by an arbitrary "test function" (here the basis function), and then integrating. A discretization of the stationary problem is then:

$$0 = \boldsymbol{L}(\boldsymbol{U}) - N_F(\boldsymbol{U})\boldsymbol{\Lambda} \tag{2.103}$$

$$0 = M(\boldsymbol{U}) \tag{2.104}$$

where L is the residual vector, U is the solution vector, Λ is the Lagrange multiplier vector, N_F is the constraint force Jacobian matrix, and M is the constraint residual; Λ and U are then solved for.

The Finite Difference Method

The FDM is the oldest discretization method and is typically best suited to structured meshes where the elements are less irregular. The method uses Taylor series expansion to approximate the finite differences using the governing equations. The FDM is generally only used for specialist CFD problems.

The Finite Volume Method

The Finite Volume Method (FVM) is the most popular method used in general purpose CFD packages. The geometry is divided into a series of cell volumes and the flow variables are applied to the centre of each element (nodal point) [80]. Integral forms of the governing flow equations are solved across each element. The FVM is used in software applications such as ANSYS Fluent and Open FOAM and is the most popular discretization method as it conserves mass, energy and momentum at a cell level, which ensures that these same three quantities are also consistently conserved for any given control volume.

2.7 Heat and mass Transfer Equations and Codes in COMSOL

2.7.1 Description of COMSOL Code

COMSOL Multiphysics is a powerful interactive environment for modeling and solving all kinds of scientific and engineering problems. The software provides a powerful integrated desktop environment with a Model Builder where you get full overview of the model and access to all functionality. With COMSOL Multiphysics you can easily extend conventional models for one type of physics into multiphysics models that solve coupled physics phenomena – and do so simultaneously. Accessing this power does not require an in-depth knowledge of mathematics or numerical analysis [81].

Using the built-in physics interfaces and the advanced support for material properties, it is possible to build models by defining the relevant physical quantities – such as material properties, loads, constraints, sources, and fluxes – rather than by defining the underlying equations. You can always apply these variables, expressions, or numbers directly to solid and fluid domains, boundaries, edges, and points independently of the computational mesh. COMSOL Multiphysics then internally compiles a set of equations representing the entire model. When solving the models, COMSOL Multiphysics uses the proven finite element method (FEM). The software runs the finite element analysis together with adaptive meshing (if selected) and error control using a variety of numerical solvers. The studies can make use of multiprocessor systems and cluster computing, and you can run batch jobs and parametric sweeps.

2.7.2 Conduction Heat Transfer in COMSOL

COMSOL uses equations similar to those described in conduction section. COMSOL uses (2.19) to calculate the temperature distribution in the material (container or dough/bread).

2.7.3 Convection Heat Transfer in COMSOL

Dimensional free (natural) Convection Theoretical Formulation in COMSOL

This formulation is outlined in Multiphysics, Module [82]. The steady state Navier-Stokes equations (including the continuity equation) shown below govern the fluid flow within the room and oven enclosure:

$$\rho \cdot (u.\nabla) \cdot u = -\nabla p + \nabla . \eta (\nabla u + (\nabla u)^T) + F \tag{2.105}$$

$$\nabla . u = 0 \tag{2.106}$$

where ρ [kg m^{-3}] is the density of the fluid, u [m s^{-1}] is the velocity vector, p [Pa] is the pressure, η [Pa s] is the dynamic viscosity of the fluid, and F [N m^{-3}] is the source term. The superscript T is the transpose of the vector.

The volume force F is set to:

$$F = (\rho_{\text{uhf}} - \rho) \cdot g \tag{2.107}$$

where ρ_{uhf} [kg m^{-3}] is the density of the unheated fluid and g [m s^{-2}] is the acceleration due to gravity; ρ is calculated according to the Boussinesq approximation:

$$\rho = \rho_{\text{uhf}} \cdot \left(1 - \frac{T - T_{\text{uhf}}}{T_{\text{uhf}}}\right) \tag{2.108}$$

where T [K] is the variable temperature of the fluid and T_{uhf} [K] is the temperature of the unheated fluid. The Boussinesq approximation is desirable because it allows one to solve for the compressibility of air as a function of temperature (as opposed to pressure) only.

The fluid flow boundary conditions are as follows: the walls of the heating elements and the oven are specified as no-slip meaning the fluid velocity vector is 0, or u = 0. The boundaries of the room are specified as open, and the equation for this condition is:

$$(-p \cdot \boldsymbol{I} + \eta \cdot (\nabla u + (\nabla u)^T) \cdot \boldsymbol{n} = -\sigma \cdot \boldsymbol{n} \tag{2.109}$$

where $\boldsymbol{I}$ is the identity matrix, $\boldsymbol{n}$ is the normal vector, and σ [Pa] is the normal stress. For this research, σ= 0, which means that there is nothing stopping the fluid from entering or exiting the boundary.

The heat balance within the room and oven enclosure is obtained via the conduction-convection equation:

$$\rho \cdot c_p \cdot u.\nabla T - \nabla . (k \nabla T) = 0 \tag{2.110}$$

where c_p [J kg^{-1} K^{-1}] is the specific heat of the fluid at constant pressure, k [W m^{-1} K^{-1}] is the thermal conductivity of the fluid, and T is the temperature of the fluid.

The boundary conditions for the heat transfer of natural convection formulation will now be presented. For the heating elements, the boundaries are specified as having a constant temperature of $T = T_0$. The

boundaries of the oven walls are specified as insulated, meaning that there is no heat flux across the boundaries as shown in (2.111):

$$\boldsymbol{n}.(k\nabla T) = 0 \tag{2.111}$$

Nondimensional free (natural) Convection Theoretical Formulation in COMSOL

This formulation is outlined in Tabatabaian [83]. The incompressible Navier-Stokes equations (including the continuity equation) shown below govern the fluid flow within the room and oven enclosure:

$$\rho \cdot (u.\nabla) \cdot u = -\nabla p + \nabla.\, \eta\,(\nabla u + (\nabla u)^T) + \rho_0 \cdot g \cdot \alpha_V\,(T - T_0) \tag{2.112}$$

$$\nabla.u = 0 \tag{2.113}$$

where ρ [kg m^{-3}] the density of the fluid, u [m s^{-1}] is is the velocity vector, p [Pa] is the pressure, η [Pa s] is the dynamic viscosity of the fluid, ρ_0 [kg m^{-3}] is the reference density, g [m s^{-2}] is gravity acceleration, α_V [K^{-1}] is the coefficient of volumetric thermal expansion, T [K] is temperature, and T_0 [K] is the reference temperature. In this model the Rayleigh number (Ra) is employed, and is defined as:

$$Ra = \frac{c_p \cdot \rho^2 \cdot g \cdot \alpha_V \cdot T \cdot L^3}{\eta \cdot k} \tag{2.114}$$

where c_p [J kg^{-1} K^{-1}] the specific heat of the fluid, L [m] is the length of a heating element, and k [W m^{-1} K^{-1}] is the thermal conductivity. The Prandtl number (Pr) is also used in this model, and is defined as:

$$Pr = \frac{\eta \cdot c_p}{k} \tag{2.115}$$

Specifying the body force in the y-direction for the momentum equation to F_y:

$$F_y = \left(\frac{Ra}{Pr}\right)(T - T_0) \tag{2.116}$$

and the fluid properties to $c_P = Pr$, and $\rho = \eta = k = 1$ produces a set of equations with nondimensional variables p, u and T. Temperature T_0 is the low (cold) temperature.

The fluid flow boundary conditions are as follows: the walls of the heating elements and the oven are specified as no-slip meaning the fluid velocity vector is 0, or u =0.

The boundaries of the room are specified as no-slip. The heat balance with in the room and oven enclosure is shown by the following equation:

$$\rho_0 \cdot c_p \cdot u.\nabla T - \nabla.(k\nabla T) = 0 \tag{2.117}$$

The boundary conditions for the heat transfer of nondimensional natural convection formulation will now be presented. For the heating elements and oven walls, the boundaries are specified as having a

constant temperature of $T = T_0$. The boundaries of the room are specified as insulated, meaning that there is no heat flux across the boundaries as shown in (2.118):

$$\boldsymbol{n}.(k\nabla T) = 0 \tag{2.118}$$

2.7.4 Radiation Heat Transfer in COMSOL

COMSOL uses equations very similar to those described in thermal radiation section. In order to model radiation exchange between surfaces it is necessary to use COMSOl's Heat Transfer Module, which is an add-on to the COMSOL Multiphysics software. This theoretical formulation is outlined in Multiphysics, Module [82].

COMSOL's Surface-to-Surface boundary condition feature handles surface to surface radiation with view factor calculation. The heat flux Φ on the surface-to-surface boundary is:

$$\Phi = A_S \cdot (M_{\text{rad}} - I) \tag{2.119}$$

where Φ [W] is the heat flux, A_S [m^2] is the surface area, M_{rad} [W m^{-2}] is the surface radiosity, and I [W m^{-2}] is the radiation arriving to the surface from the other surfaces in the enclosure. I [W m^{-2}] is calculated according to the following equation:

$$I = I_{\text{m}} + F_{\text{amb}} \cdot \sigma \cdot T_{\text{amb}}^4 \tag{2.120}$$

$$M_{rad} = (1 - \varepsilon) \cdot [I + \varepsilon \cdot \sigma \cdot T^4] \tag{2.121}$$

where I_{m} [W m^{-2}] is the mutual irradiation arriving from other boundaries in the model, F_{amb} [–] is the ambient view factor whose value is equal to fraction of the field of view that is not covered by other boundaries, σ [W m^{-2} K^{-4}] is the Stefan- Boltzman constant, M_{rad} [W m^{-2}] is the surface radiosity, and I [W m^{-2}] is the radiation arriving at the surface from the other surfaces in the enclosure, and T_{amb} [K] (ambient temperature) is the assumed far-away temperature in the directions included in T_{amb}.

The view factor calculation in COMSOL for this research uses the Hemicube method, which can be thought of as rendering digital images of the model geometry in five different directions (in 3 – D; in 2 – D, only three directions are needed) and counting the pixels in each mesh element to determine its view factor.

The boundaries in the COMSOL model are assigned as follows: the faces of the heating elements facing the dough/bread are specified as having a constant temperature.

$$T = T_0 \tag{2.122}$$

and the surfaces of the material and heating elements are each specified as having an appropriate emissivity ε.

The faces of the heating elements not facing the dough/bread may be specified as having a constant temperature, or as being insulated according to (2.123):

$$\boldsymbol{n}.(k\nabla T) = 0 \tag{2.123}$$

2.8 Emitted Gases During Baking

Baking bread use large quantities of energy and emit hazardous air pollutants. These industries strive to recover waste heat and reduce pollution. In baking industries, by-products of high temperature combustion are essential elements to be controlled for air pollution. The two oxides of nitrogen related to combustion are nitric oxide (NO) and nitrogen dioxide (NO_2). NOx refers to either one of these gases, which are considered toxic and play a major role in the formation of acid rain, smog and ozone.

The common source of air emissions from baking is high temperature combustion generates NO_x. Through combustion, hydrocarbon fuel transforms to CO_2, and sometimes it also transforms to CO due to uncompleted combustion.

In high temperature combustion, the amount of NO_x generation is related to flame ambient temperature and oxygen concentration of combustion air. It means that the higher flame ambient temperature, the more NO_x generated; the higher oxygen concentration, the more NO_x generated. In baking furnace, combustion temperature is directly related to the flame temperature.

Regenerative burner technology has been introduced to reduce the emerging influence of global warming and acid rain by reducing CO_2 emission and NO_x emission. This study aims in part to examine the flue gas emission improvement that the regenerative burners can make on a baking oven.

2.9 Regenerator

Thermal energy savings can be made in many ways. For example, unit fuel consumption could be decreased through operational improvements, such as optimizing furnace pressure controls and air to-fuel ratios which will prevent overheating. These energy saving techniques improve combustion performance and baking efficiency thereby increasing energy savings.

Besides operational improvements, hardware improvements such as strengthening furnace insulation and furnace seals, and utilizing ceramic fibers in furnace walls, will also reduce waste heat transferred through furnace enclosure which will, in turn, save on fuel consumption.

It is just as important to recover waste heat as it is to reduce waste heat. This is another solution to saving thermal energy. Waste heat in industries has a wide range of temperatures and exists in different forms, such as exhaust gas, exhaust steam, exhaust water, hot waste solids, hot waste liquid, heat convection, radiation from hot surfaces, and heat leaks.

A regenerative burner system is designed for recovering heat from the flue gas, preheating air for combustion, mixing air and fuel and igniting combustion. The system consists of burner monitoring and control instruments which are also essential to the system. The regenerator is one part of a regenerative burner system.

The regenerator is a heat exchanger that is usually used for recovering waste heat in flue gases from equipment, such as the boiler or furnace. When combustion takes place in a furnace, fossil fuel (for example, coal, natural gas) and air forms high temperature products of combustion (POC) and exhausts

high temperature flue gas. Before the flue gas exits to the atmosphere, making flue gas flow through a regenerator can reduce flue gas temperature and reclaim heat. The reclaimed heat is often recycled for heating purposes, for example, to heat up water before it is supplied to the boiler, to warm up the air before proceeding with combustion, or for domestic heating of the water supply.

There are various types of regenerators, such as ball regenerators, tube regenerators and honeycomb regenerators, which are defined by various media material and different forms of heat transfer. In the ball regenerator, the ceramic ball media has strong endurance for high temperatures and brings the temperature of preheated air to a level close to the temperature of flue gas, thus the ball generator offers an efficient heat recovery when compared to using conventional methods such as a tube heat exchanger.

The regenerative burner is usually equipped on a natural gas-fired furnace or oil fuel furnace. The burner is designed for reduction of NO_x emissions generated by oxidation of nitrogen in the air. During high temperature combustion, the concentration of NO_x increases when the flame temperature is rising. The regenerative burner ignites fuel at a lower temperature so as to reduce the flame temperature and to lower NOx concentration. The flame's chemical environment, primarily the oxygen concentration within the flame, is another important variable. For achieving low NOx generation, combustion should be controlled to take place at the suppression of maximum flame temperature, and at the prevention of excess amounts of oxygen.

Not only the NO_x, but also the CO emission level is lower than the level of the conventional counterpart because better control of the air-fuel ratio makes completed combustion. Reduced CO_2 emission is also achieved because less fuel is required to be consumed in the process.

2.10 Exergy Analysis

As the first law of thermodynamics deals with the quantity of energy and asserts that energy cannot be created or destroyed, the second law of thermodynamics deals with the quality of energy which is subject to degradation during a process as a result of the entropy production [84].

We make our whole technological world run by grabbing as much as we can of the energy flow available from concentrated energy sources like fuels to run an infinite variety of machines, electrical generators and vehicles. However, when we change energy from one form to another, from energy in a fuel to pushing a piston or even water running down from a dam to the dynamos below, it is impossible for us to get to use all of the energy in the concentrated energy source for the jobs we want it to do. Some always must be wasted, mainly as unusable heat to the environment [85].

The performance of engineering systems is degraded by the presence of irreversibilities, and the entropy production is a measure of the magnitudes of the irreversibilities present during that process. The greater the extent of irreversibilities, the greater the entropy production. Therefore, entropy production can be used as a quantitative measure of irreversibilities associated with a process. It is also used to establish criteria for the performance of engineering devices. It is now becoming a technological challenge to build high performance engineering devises that are not only efficient from the quantity of energy viewpoint (the first law) but also efficient in conserving the quality of energy (second law) by minimizing the entropy production [84].

Exergy conscious utilization of energy sources would help advance technological development towards resource-saving and efficient technology can be achieved by improving design of processes with high exergetic efficiency. Application of the exergy analysis in design and development of sustainable processes also provides information for long-term planning of resource management [86].

Exergy is defined as the maximum amount of work that can be produced by a stream or system as it is brought into equilibrium with a reference environment, and it can be thought of as a measure of the usefulness or quality of energy. Exergy is consumed during real processes due to irreversibilities and conserved during ideal processes. Exergy quantities are evaluated with respect to a reference environment. The intensive properties of the reference environment in part determine the exergy of a stream or system. The exergy of the reference environment is zero. The reference environment is in stable equilibrium, with all parts at rest relative to one another No chemical reactions can occur between the environmental components. The reference environment acts as an infinite system and is a sink and source for heat and materials. It experiences only internally reversible processes in which its intensive state remains unaltered.

Exergy analysis involves the application of exergy concepts, balances, and efficiencies to evaluate and improve energy and other systems. Many engineers and scientists suggest that devices can be well evaluated and improved using exergy analysis in addition to or in place of energy analysis. Exergy analysis has been applied to a wide range of processes and systems. Increases in efficiency are subject to two constraints, which are often poorly understood: (i) theoretical limitations, which establish the maximum efficiency theoretically attainable for a process by virtue of the laws of thermodynamics, and (ii) practical limitations, which further limit increases in efficiency. First, consider practical limitations on efficiency. In practice, when selecting energy sources and utilization processes the goal is not to achieve maximum efficiency but rather to achieve an optimal trade-off between efficiency and such factors as economics, sustainability, environmental impact, safety, and societal and political acceptability. This optimum is dependent on many factors controllable by society; furthermore, these factors can be altered to favor increased efficiency.

Now, consider theoretical limitations on efficiency. To assess the potential for increased efficiency, the theoretical limits must be clearly understood. In the past, lack of clarity on this issue has often led to confusion, in part because energy efficiencies generally are not measures of how close the performance of a process or device approaches the theoretical ideal. The consequences of such confusion can be very significant. For example, extensive resources have occasionally been directed toward increasing the energy efficiencies of devices that in reality were efficient and had little potential for improvement. Conversely, at other times devices have not been targeted for improved efficiency, even though the difference between the actual and maximum theoretical efficiencies, which represents the potential for improvement, has been large. The difficulties inherent in energy analysis are also attributable to the fact that it considers only quantities of energy and ignores energy quality, which is continually degraded during real processes. Exergy analysis, as discussed earlier, overcomes many of the problems associated with energy analysis.

In the absence of nuclear, magnetic, electrical, and surface tension effects, the total exergy of a system consists of four components: physical exergy, chemical exergy, kinetic exergy, and potential exergy. For many engineering applications, the kinetic and potential exergy changes are negligible, leaving just the change in physical and chemical exergy.

Physical exergy is the maximum theoretical useful work obtainable as the system passes from its initial state (T, P, x) to the restricted dead state (T_0, P_0, x) while heat transfer takes place only between the system and the environment. Chemical exergy is the maximum theoretical useful work obtainable as the system having the temperature and pressure of the reference environment is brought in to chemical equilibrium with this environment while interacting only with this environment.

The exergy method is a tool for measuring the efficiency of processes or systems, especially energy intensive systems. Some researchers have used exergy methods in many science studies and engineering applications, for example, thermodynamics [87] and thermal engineering [88-90]. Some discussions specifically focus on topics in air conditioning systems such as refrigerating compressor cycling [91,92], dehumidification [93], absorption [94] and other psychrometric processes [95]. Many exergy researches are also conducted in fields of thermal storage [96], fuel cell [97]. Some applications using exergy method have been studied and successfully practiced in industries like combined heat and power, building design in heat pump system and refrigeration system [98], food process and sugar production [99], etc.

A novel concept is developed by Jentsch [100] that allows to interpret exergy associated with mass or energy transfers as a product of thermodynamic quality (transformability) and quantity (transformation energy). Systems based on the Integrated gasification combined cycle (IGCC) technology with carbon capture are analyzed by Sorgenfrei [101] regarding an efficient and flexible electric power generation Using advanced exergy analysis.

Meanwhile the exergy theory is used to study topics of environment impact. Any technologies that increase efficiency will use lesser resources (or exergy) to drive the processes for the same products or services. This leads to less extraction from the environment of energy resources. When a more efficient process uses lesser resources, a direct result is normally to emit lesser wastes to the environment. Due to the character of irreversibility, exergy destruction often disorders the whole system, or destroys the order in an organized system, such as an environmental system, so irreversibility of exergy destroys or impacts on environment [102]. By preserving exergy through increased efficiency (i.e. degrading as little exergy as possible for a process), environmental damage is reduced. The exergy associated with processed wastes emitted to the environment can be viewed as a potential for environmental damage [103].

Besides the exergy expression shown in this study, there are other different second-law-based methods of analysis [91]. These discrepancies of the methods are various from definitions, wordings and expressions of exergy, etc.

3 Heat and Mass Transfer Analysis in Bread Baking Using COMSOL Models

The baking of bread can be defined as the process which transforms a raw dough into a light, porous, readily digestible and flavorful product. During this process, a number of phenomenal changes happen inside the product, including volume expansion, crust formation, inactivation of yeast and enzymatic activities, protein coagulation and gelatinization of starch [104]. The dominating factors behind these changes are temperature and moisture content. Therefore, the modelling of heat – and mass transfer processes during baking is a topic of considerable interest.

Computational simulation is proved to be a valuable tool for the prediction of the nutritional, sensory and safety of food, as well as for the optimization of food processes and storage conditions, minimization of the trial and error experimental procedures. Computational design has already been recognized as a standard prototyping tool outside the food industry (e.g. automotive and aviation industry), where it has proved to have an advantage in terms of costs and development time. Most of the costs in food industry development concentrate on the design, prototyping, and testing phases. Numerical modeling technology offers an efficient and powerful tool for simulating the heating / cooling and other processes of the food industry. The use of numerical methods such as finite difference, finite element, and finite volume analysis to describe processes in the food industry has produced a large number of models. However, the accuracy of numerical models can further be improved by using more detailed information about the surface heat- and mass transfer coefficients, thermal physical food properties, volume change during processes and sensitivity analysis for justifying the acceptability of assumptions in modeling.

During baking, heat is transferred through the combination of all three well-known mechanisms: conduction, convection, and radiation. However, the actual forms of combination and proportions are very different for the heat transfer within the dough pieces than for the one within an oven chamber. Heat transfer in a piece of dough is the combination of a conduction from oven bands or baking tins to the dough, a conduction in the continuous liquid / solid phase of the dough and an evaporation–condensation in the gas phase of the dough.

Bread is baked at temperatures of 300 °C – 350 °C in 4 min –6 min [19]. It can also be baked at a substantially higher temperature, e.g. 400 °C – 600 °C, during only 40 s – 60 s [20]. Other kinds of bread are normally baked at temperatures of 218 °C – 232 °C in 20 min – 25 min.

The aim of this chapter is to simulate existing bread baking conditions, and employed this models to improve existing processes, and be used to create new processes and products.

3.1 Methodology

3.1.1 Analytical Calculation

First, the radiation calculations are performed, followed by the convection calculations. Analytical calculations of moisture loss from the dough/bread relevant to this research are calculated.

Radiation Analytical Calculation

The geometry shown in Fig. 2.5 is used in the analytical solution. For this analysis it is assumed that the dough/bread (which will be called surface 2) is opaque, diffuse, and gray, and that the heater surface (which will be called Surface 1) and surroundings (which will be called Surface 3) are blackbody surfaces. First, the values to calculate the view factor between the two surfaces can be substituted into (2.52). The surfaces can be related to the geometry of COMSOL model as follows (Fig. 3.1) Surface *i* corresponds to Surface 2, which is the dough/bread; Surface *j* corresponds to Surface 1, which is the heating element surface.

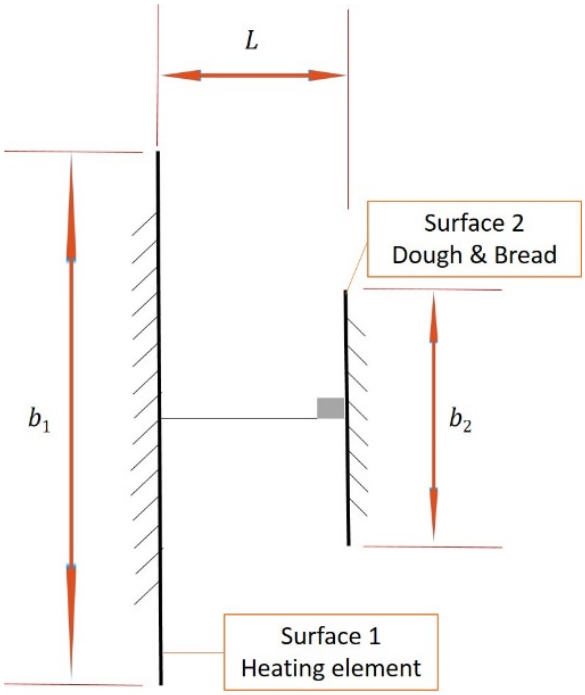

Fig. 3.1 Surfaces 1(heating element),2 (dough/bread)

$$B_i = B_2 = \frac{0.22}{0.5 - 0.01 - 0.15} = 0.647 \text{ m} \tag{3.1}$$

The values in (3.1) can be explained as follows (Fig. 3.2) Radiation effect on surface of container: COMSOL geometry): the numerator is b_2 = 0.22 m, which is the breadth of the dough; the denominator is L, which is the perpendicular distance between the surface of the dough and the surface of the heating element. L is equal to the vertical distance between the centers of the heating element and the dough, minus the vertical distance between the center and surface of the dough, minus the vertical distance between the center and surface of the heating element.

$$B_j = B_1 = \frac{4}{0.5 - 0.01 - 0.15} = 11.76 \text{ m} \tag{3.2}$$

The values in (3.2) are determined similarly to (3.1); only the numerator is different: the numerator is b_1= 4 m, which is the breadth of the heating element.

Substituting the values B_1 and B_2 into (2.52):

$$F_{2,1} = \frac{[(0.647 + 11.76)^2 + 4]^{1/2} - [(11.76 + 0.647)^2 + 4]^{1/2}}{2 \times (0.647)} = 0.7461 \tag{3.3}$$

The above view factor $F_{2,1}$ is necessary to calculate the radiation reaching Surface 2 (the dough/bread surface) from Surface 1 (the heating element surface). Later we will need the view factor $F_{2,3}$, which is the fraction of radiation leaving surface 2 (the dough/bread surface) that is intercepted by surface 3 (the surroundings). In order to calculate $F_{2,3}$, we use the view factor summation rule for surfaces exchanging radiation in an N-sided enclosure (2.53):

$$\sum_{j=1}^{N} F_{i,j} = 1 \tag{2.53}$$

For the current enclosure problem:

$$F_{2,1} + F_{2,2} + F_{2,3} = 1 \tag{3.4}$$

In (3.4), $F_{2,1}$ and $F_{2,3}$ have been previously explained; $F_{2,2}$ is the fraction of radiation leaving surface 2 (the dough/bread surface) that is intercepted by surface 2 (the dough/bread surface). Since surface 2 is not convex, $F_{2,2}$ =0. Substituting the known view factors into (3.4):

$$0.746\,1 + 0 + F_{2,3} = 1 \tag{3.5}$$

$$F_{2,3} = 0.014\,196 \tag{3.6}$$

Now we are ready to apply the foregoing analysis to find the amount of radiation that surface 2 (the dough/bread surface) intercepts. This will allow us to calculate the amount of energy the dough/bread absorbs, which will then enable us to determine the temperature rise in the dough/bread. The amount of energy the dough/bread absorbs is given by applying (2.51) to Surface 2 (the dough/bread surface):

$$\Phi_2 = \frac{M_{\mathrm{bb},2} - M_{\mathrm{rad},2}}{\frac{1 - \varepsilon_2}{\varepsilon_2 \cdot A_{\mathrm{S},2}}} \tag{3.7}$$

In order to find $M_{\mathrm{rad},2}$, we must apply (2.60) to Surface 2:

$$\frac{M_{\mathrm{bb},2} - M_{\mathrm{rad},2}}{(1 - \varepsilon_2) \cdot (\varepsilon_2 \cdot A_{\mathrm{S},2})^{-1}} = \frac{M_{\mathrm{rad},2} - M_{\mathrm{rad},1}}{(A_{\mathrm{S},2} \cdot F_{2,1})^{-1}} + \frac{M_{\mathrm{rad},2} - M_{\mathrm{rad},3}}{(A_{\mathrm{S},2} \cdot F_{2,3})^{-1}} \tag{3.8}$$

The temperatures of Surface 1 (the heating element surface), Surface 2 (the dough/bread surface) and Surface 3 (the surroundings) are specified as 493.15 K, 293.15 K (an initial value of room temperature, 20 °C), and 293.15 K (room temperature, 20 °C), respectively.

Applying (2.48) to Surfaces 3 (the surroundings) and 1 (the heating element), assuming that each surface is a blackbody:

$$M_{\text{rad},3} = M_{\text{bb},3} = \sigma \cdot T_3^4 = (5.670 \times 10^{-8}) \times (293.15\ )^4 = 418.7\ \text{W m}^{-2} \tag{3.9}$$

$$M_{\text{rad},1} = M_{\text{bb},1} = \sigma T_1^4 = (5.670 \times 10^{-8}) \times (493.15\ )^4 = 3353.5\ \text{W m}^{-2} \tag{3.10}$$

Applying (2.48) to Surface 2 (the dough/bread):

$$M_{\text{bb},2} = \sigma T_2^4 = (5.67 \times 10^{-8}) \times (293.15)^4 = 418.7\ \text{W m}^{-2} \tag{3.11}$$

Substituting values (here the emissivity is 0.9), and the dimensions are from Fig. 3.2 into (3.8):

$$\begin{aligned} &\frac{418.7 - M_{\text{rad},2}}{(1-0.9) \times \left[0.9 \times \left(\frac{\pi}{4} \times 0.22^2\right)\right]^{-1}} = \\ &= \frac{M_{\text{rad},2} - 3\ 353.506}{\left[\left(\frac{\pi}{4} \times 0.22^2\right) \times 0.985\ 8\right]^{-1}} + \frac{M_{\text{rad},2} - 418.7}{\left[\left(\frac{\pi}{4} \times 0.22^2\right) \times (0.0141)\right]^{-1}} \end{aligned} \tag{3.12}$$

$$M_{\text{rad},2} = 707.918\ \text{W m}^{-2} \tag{3.13}$$

Substituting values into (3.7):

$$\Phi_2 = \frac{418.7 - 707.918}{(1-0.9) \times \left[0.9 \times \left(\frac{\pi}{4} \times 0.22^2\right)\right]^{-1}} = -98.912\ 5\ W \tag{3.14}$$

In (3.14), since the equation originally assumed the energy to be leaving as positive, the negative sign indicates that the energy (98.9 W) is being absorbed by the container surface.

Convection Analytical Calculation

The temperature of the heating element is 493.15 K. Substituting the appropriate values from Fig. 3.7 into (2.36), (2.37), and (2.38):

$$T_{\text{f}} = \frac{493.15\ + 293.15}{2} = 393.15\ \text{K} \tag{3.15}$$

$$\alpha_V = \frac{1}{393.15} = 0.00254\ \text{K}^{-1} \tag{3.16}$$

$$L = \frac{4 \times 0.8}{4 + 0.8 + 4 + 0.8} = 0.33\ \text{m} \tag{3.17}$$

Properties at the average film temperature:

Thermal diffusivity (a) = 0.000 036 5 $\text{m}^2\ \text{s}^{-1}$, kinematic viscosity ($\nu$) =0.000 025 35 $\text{m}^2\ \text{s}^{-1}$, thermal conductivity ($k$) =0.032 73 $\text{W m}^{-1}\ \text{K}^{-1}$

Substituting the above values into (2.35):

$$Ra = \frac{(9.81) \times (0.002\,54) \times (493.15 - 293.15) \times (0.33)^3}{\left(25.35 \times 10^{-6}\right) \times \left(36.51 \times 10^{-6}\right)} \tag{3.18}$$

$$Ra = 1.991 \times 10^8 \tag{3.19}$$

This flow is considered laminar [47]. It is then appropriate to use the laminar flow application in the corresponding natural convection COMSOL simulations.

The general correlation between the Nusselt number and Rayleigh number is:

$$Nu = C \cdot Ra^m \tag{3.20}$$

where, m and C are constants. The value of the constants depends on geometry.

Sahin, Sumnu [105] proposed the following correlation for heat transfer:

$$\begin{cases} Nu = 0.54 \times (Ra)^{1/4} \text{ , for } 10^4 < Ra < 10^7 \\ Nu = 0.15 \times (Ra)^{1/3} \text{ , for } 10^7 < Ra < 10^{11} \end{cases} \tag{3.21}$$

From (3.19) and (3.21):

$$Nu = 0.15 \times (1.991 \times 10^8)^{\frac{1}{3}} = 87.58 \tag{3.22}$$

The convection heat transfer coefficient can be calculated from equation:

$$h_{\text{cnv}} = \frac{Nu \cdot k}{L} = \frac{87.58 \times 32.73 \times 10^{-3}}{0.33} = 8.687 \text{ W m}^{-2} \text{ K}^{-1} \tag{3.23}$$

Moisture Analytical Calculation

The goal here is to find the drying rate R_C, which is the amount of water in kg that has evaporated from the dough/bread per m² per unit time (chosen to be one hour). The starting point is (2.88), and this equation can be solved by using (2.71). At this point the values for (2.89) will be found.

$$\frac{(x_{\text{sat}} - x) \cdot \lambda}{h_{\text{cnv}}/k_y \cdot M_b} = \left(1 + \frac{U}{h_{\text{cnv}}}\right)(T_{\text{ffs}} - T_{\text{srf}}) + \frac{h_{\text{rad}}}{h_{\text{cnv}}}(T_{\text{rs}} - T_{\text{srf}}) \tag{3.24}$$

Where x [kg (H_20, g) kg^{-1}(dry air)] is the humidity, and x = 0.050 kg (H_20, g) kg^{-1}(dry air)[61]. T_{ffs} = 220 °C. x_{sat} is the saturation humidity and involves knowing or guessing T_{srf}, which is the surface temperature. Since T_{srf} is not known at this time, it must be guessed. T_{srf} will be above the wet bulb temperature T_W. T_W is determined from psychrometric chart program, which is about 56.5 degrees Celsius. Since T_{srf} will be above wet bulb temperature, estimate T_{srf} be 70 °C. x_{sat} is determined from psychrometric chart program, which is about 0.278 kg (H_20, g) kg^{-1}(dry air).

λ is the latent heat corresponding to the surface temperature T_{srf}. From the guessed T_{srf} 70 °C, find λ from the steam tables of Geankoplis [62]. The λ is calculated as 2626.8 kJ kg^{-1} – 292.98 kJ kg^{-1} = 2 333.82 kJ kg^{-1}.

Table 3.1 Excerpt of steam table. Geankoplis [62]

T / °C	p / kPa	h' / kJ kg^{-1}	h'' / kJ kg^{-1}
70	31.19	292.98	2626.8

The ratio $h_{cnv} / k_y M_b$ is approximately:

$$c_{\text{mix}} = (1.005 + 1.88\,H)10^3 \tag{3.25}$$

$$\text{c}_{\text{mix}} = \left(1.005 + (1.88 \times 0.05)\right) \times 10^3 \;=\; 1\,099\ \text{J kg}^{-1}\ \text{K}^{-1} \tag{3.26}$$

The value of U is found:

$$U = \frac{1}{\frac{1}{h_{\text{cnv}}} + \frac{\delta_{\text{M}}}{k_{\text{M}}} + \frac{\delta_{\text{S}}}{k_{\text{S}}}} \tag{3.27}$$

The remaining values for (3.27) are found (if possible) from corresponding models or simulations. Use k_{M} = 52 (W m^{-1} K^{-1}) for steel; use δ_{M} as 5 mm, which corresponds to an appropriate thickness of a conveyer belt, use δ_{S} = 0.02 m, from Fig. 3.2; and use k_{S} =0.1133 (W m^{-1} K^{-1}) from Table 3.4.

$$U = \frac{1}{\frac{1}{h_{\text{cnv}}} + \frac{\delta_{\text{M}}}{k_{\text{M}}} + \frac{\delta_{\text{S}}}{k_{\text{S}}}} = \frac{1}{\frac{1}{8.687} + \frac{0.005}{52} + \frac{0.02}{0.113\,3}} \tag{3.28}$$

$$U = 3.427\,7\ \text{W m}^{-2}\ \text{K}^{-1} \tag{3.29}$$

In order to find h_{rad}, a value for T_{rad} is specified as 220 °C (493.15 K), the emissivity of the dough bread is 0.9, and the guessed temperature of the surface is translated into Kelvin; substituting in (2.72):

$$h_{\text{rad}} = (0.9) \times (5.676)\frac{\left(\frac{493.15}{100}\right)^4 - \left(\frac{343.15}{100}\right)^4}{493.15 - 343.15} \tag{3.30}$$

$$h_{\text{rad}} = 15.42\ \text{W m}^{-2}\ \text{K}^{-1} \tag{3.31}$$

Substituting the acquired values into (2.89):

$$\frac{(0.278 - 0.05) \times (2\,333.82 \times 10^3)}{1\,099} = \\ = \left[\left(1 + \frac{3.427\,7}{8.687}\right) \times (220 - T_{\text{srf}})\right] + \left[\left(\frac{15.42}{8.687}\right) \times (220 - T_{\text{srf}})\right] \tag{3.32}$$

This gives a T_{Srf}=67.238 6 °C; substituting into (2.88) to obtain the drying rate R_C:

$$R_C = \frac{[(8.6 + 3.4) \times (220 - 67.2)] + [15.42 \times (220 - 67.2)]}{2\,333.8 \times 10^3} \tag{3.33}$$

$$R_C = 0.001\,8\ kg\ \mathrm{m}^{-2}\ \mathrm{s}^{-1} \tag{3.34}$$

$$R_C = 0.001\,8 \times 360\,0 = 6.48\ \mathrm{kg\ m}^{-2}\ \mathrm{hr}^{-1} \tag{3.35}$$

3.1.2 COMSOL Models

Radiation COMSOL Model

Figure 3.2 shows the COMSOL geometry of the model. The distance between the center of heating element to the center of dough/bread is 0.5 m, the heating element height (thickness) is 0.3 m, and width is 4 m, and the bread diameter is 0.22, and height (thickness) is 0.02 m.

The mesh used is COMSOL's initial mish (not refined). The base COMSOL Multiphysics license and Heat Transfer Module are used in this model.

The thermal properties of dough and bread [106] are presented in Table 3.2. It must be noted that the porosity of bread affects its density: the higher the porosity, the lower the density.

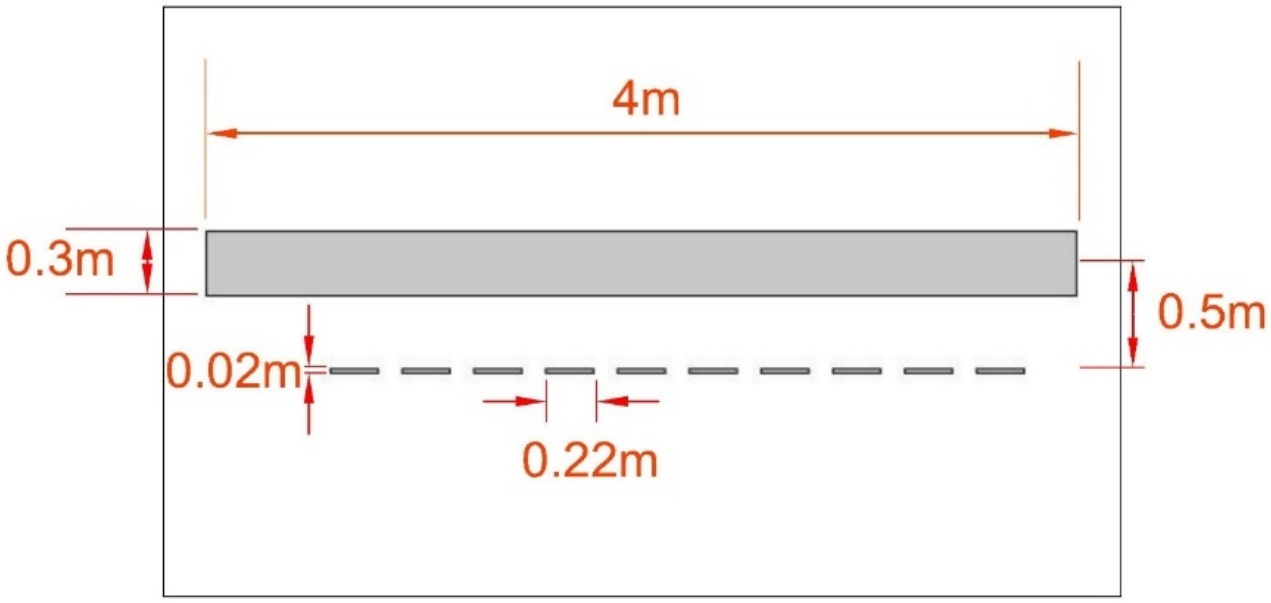

Fig. 3.2 Radiation COMSOL model geometry

Table 3.2 Thermal properties of dough and bread

T / °C	ρ / kg m^{-3}	c_p / J kg^{-1} K^{-1}	k / W m^{-1} K^{-1}
28	420	2883	0.20
120	380	1470	0.07
227	340	1470	0.07

Radiation COMSOL Model with Constant Properties:

The first attempt at modeling food within an oven considered taking an average each of the following thermal properties: conductivity, specific heat, and density. Using the data in Table 3.2, these averages are as follows: average thermal conductivity is 0.1133 W m^{-1} K^{-1}, average specific heat is 1941 J kg^{-1} K^{-1}, average density is 380 kg m^{-3}.

The material properties and initial conditions for the heating element are shown in Table 3.3, and default mesh is used for heating element. The domain of the heating element has the same geometry and location as shown in Fig. 3.2.

The material properties and initial conditions for the dough/bread are shown in Table 3.4. These properties are average thermal properties and the domain mesh for the dough/bread is refined twice (using COMSOL's default mesh refinement parameters). The domain of the dough/bread has the same geometry and location as shown in Fig. 3.2.

The boundary conditions for the radiation effect on dough/bread, COMSOL model are shown in Table 3.5.

Table 3.3 Heating element material properties and initial conditions, radiation effect on dough/bread, COMSOL model

T / °C	ρ / kg m^{-3}	c_p / J kg^{-1} K^{-1}	T_{int} / K	M_{rad}/ W m^{-2}
52	7800	465	293.15	0

Table 3.4 Dough/bread material properties and initial conditions, radiation effect on dough/bread, COMSOL model

k / W m^{-1} K^{-1}	ρ / kg m^{-3}	c_p / J kg^{-1} K^{-1}	T_{int} / K	M_{rad}/ W m^{-2}
0.1133	380	1941	293.15	0

Table 3.5 Boundary conditions, radiation effect on dough/bread, COMSOL model

ε_{hel} / –	$\varepsilon_{b/d}$ / –	T_{hel} / K
1	0.9	493.15

Radiation COMSOL Model with Varying Properties.

The next step is to model the food with properties that vary with temperature (but not moisture). This model is similar to Zhou, Therdthai [106], who modeled the dough/bread with only temperature-dependent properties; their justification is that the moisture content difference in dough versus crumb is not significant, and that bread is significantly more crumb than crust. They therefore did not model the dough/bread as having moisture – dependent properties. First, a curve is fitted to the density data in Table 3.2 via quadratic regression to yield the (3.36):

$$\rho = 0.000\,3\,T^2 - 0.647\,4\,T + 587.2 \tag{3.36}$$

Figure 3.3 shows a graph of the dough/bread density versus temperature, along with polynomial fitted to the data.

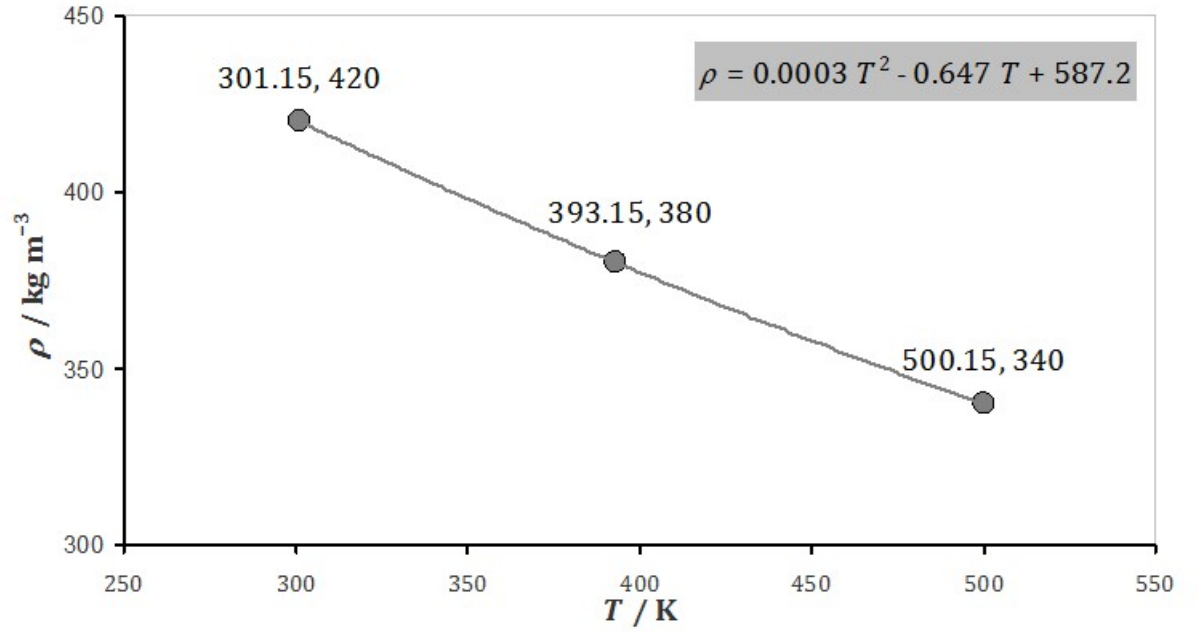

Fig. 3.3 Dough/bread density versus temperature

This model (and the other models involving temperature – varying properties) uses the COMSOL Multiphysics License in conjunction with the Heat Transfer Module. All of the models involving temperature-varying properties use the default mesh. The geometry for the models are the same as in Fig. 3.2, and the boundary specifications are the same as in Table 3.5.

The material properties and initial conditions for the heating element for all of the models having dough/bread temperature-varying properties are shown in Table 3.6. The initial surface radiosity is from (3.10).

The material properties and initial conditions for the dough/bread for temperature-varying density model are shown in Table 3.7. The initial temperature is room temperature, and the initial surface radiosity is from (3.13).

Table 3.6 Heating element material properties and initial conditions, radiation effect on dough/bread with temperature-varying density, COMSOL model

k / W m^{-1} K^{-1}	ρ / kg m^{-3}	c_p / J kg^{-1} K^{-1}	T_{int} / K	M_{rad}/ W m^{-2}
52	7800	465	493.15	3353.5

Table 3.7 Dough/bread material properties and initial conditions, radiation effect on dough/bread with temperature-varying density, COMSOL model

k / W m^{-1} K^{-1}	ρ / kg m^{-3}	c_p / J kg^{-1} K^{-1}	T_{int} / K	M_{rad}/ W m^{-2}
0.1133	(3.15)	1941	293.15	707.918

Next, a curve is fitted to the specific heat data in Table 3.2 via quadratic regression to yield (3.37):

$$C_p = 0.077\,2\,T^2 - 68.944\,T + 16\,646 \qquad (3.37)$$

Figure 3.4 shows a graph of the dough/bread specific heat versus temperature, along with polynomial fitted to the data. The material properties and initial conditions for the dough/bread for the temperature – varying specific heat model are shown in Table 3.8.

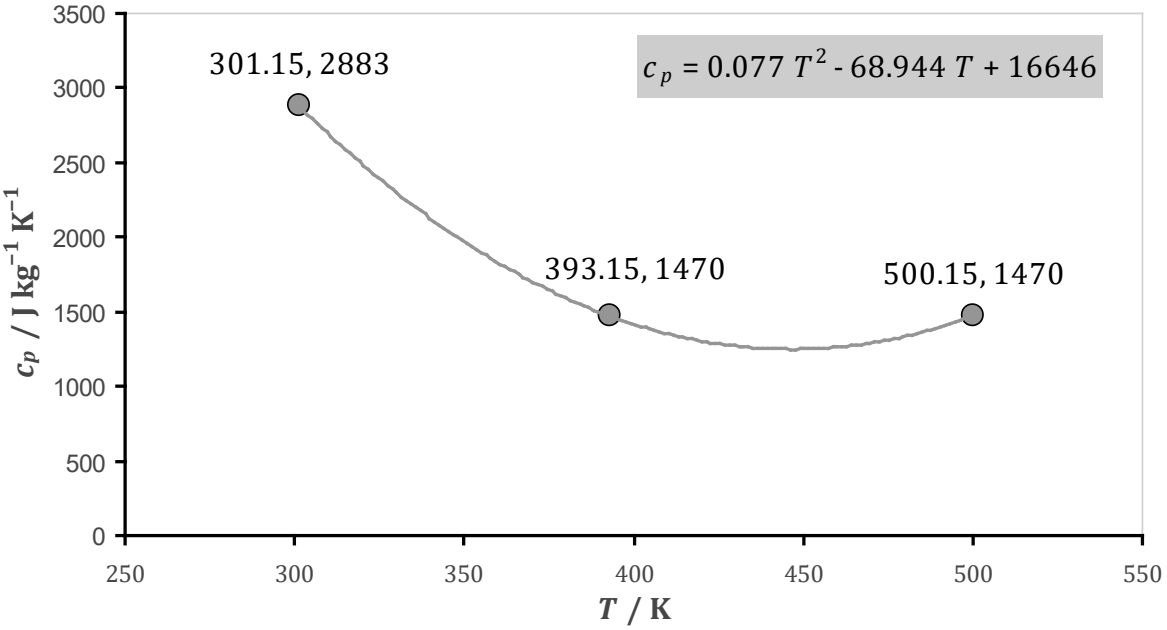

Fig. 3.4 Dough/bread specific heat versus temperature

Table 3.8 Dough/bread material properties and initial conditions, radiation effect on dough/bread with temperature – varying specific heat, COMSOL model

k / W m^{-1} K^{-1}	ρ / kg m^{-3}	c_p / J kg^{-1} K^{-1}	T_{int} / K	M_{rad}/ W m^{-2}
0.1133	380	(3.16)	293.15	707.918

The thermal conductivity would decrease during the baking process, due to the fact that there is loss of water from the dough. A graph was made of the dough/bread thermal conductivity using Table 3.2; a curve was fitted to the graph, thereby giving an equation for thermal conductivity as a function of temperature. This equation was incorporated into the material properties of the dough/bread COMSOL model.

Fitting a curve to the data for conductivity yields (3.38):

$$k = 7 \times 10^{-6}\ T^2 - 0.006\,3\,T + 1.466\,2 \tag{3.38}$$

Figure 3.5 shows a graph of the dough/bread conductivity versus temperature, along with polynomial fitted to the data. The dough/bread has the properties and initial conditions listed in Table 3.9.

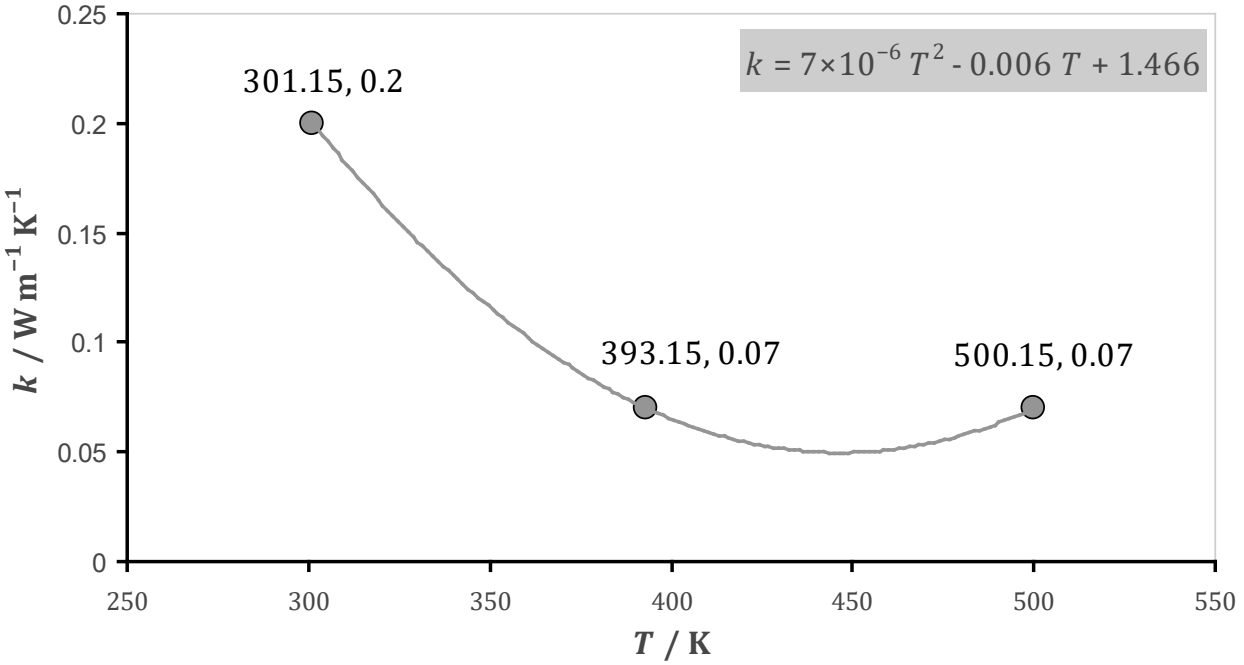

Fig. 3.5 Dough/bread conductivity versus temperature

Table 3.9 Dough/bread material properties and initial conditions, radiation effect on dough/bread with temperature-varying conductivity, COMSOL model

k / W m^{-1} K^{-1}	ρ / kg m^{-3}	c_p / J kg^{-1} K^{-1}	T_{int} / K	M_{rad}/ W m^{-2}
3.17	380	1941	293.15	707.918

Convection COMSOL Model:

According to Mirade et al. [107], for biscuit baking in band ovens, the total heat transfer is 37 % by convection.

Dimensional Convection COMSOL Model.

Figure 3.7 shows the COMSOL geometry of a room, and an oven with heating element. This model used the COMSOL Multiphysics license, and the Heat Transfer Module; the initial COMSOL mesh (unrefined) was employed. The temperature of heating element is 493.15 K, and the temperature of oven (top and bottom) is 293.15 K.

Table 3.10 shows the properties and initial condition (room temperature) of the fluid used in the COMSOL simulation of room and oven with heating element. The thermal and physical properties are from Bergman et al. [47], and the fluid property is from Simpson [108].The non-isothermal flow application is employed.

Nondimensional Convection COMSOL Model:

This model's oven and room definitions are as shown in Fig. 3.6. The geometry of the non-dimensional model are also the same as the dimensional model, and are shown in Fig. 3.7. This model uses COMSOL's Multiphysics license, with a default mesh.

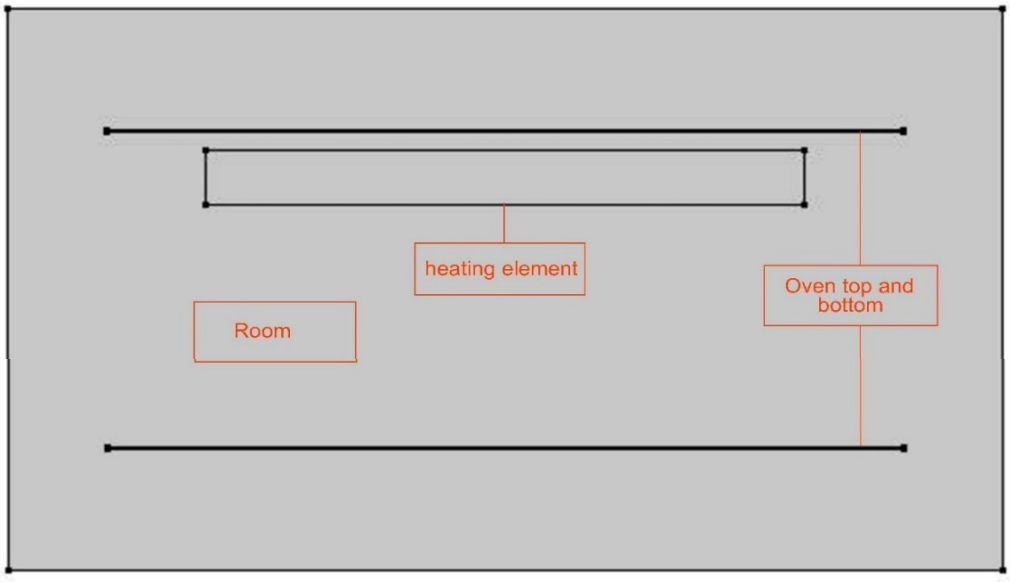

Fig. 3.6 Oven with heating element inside room, COMSOL model

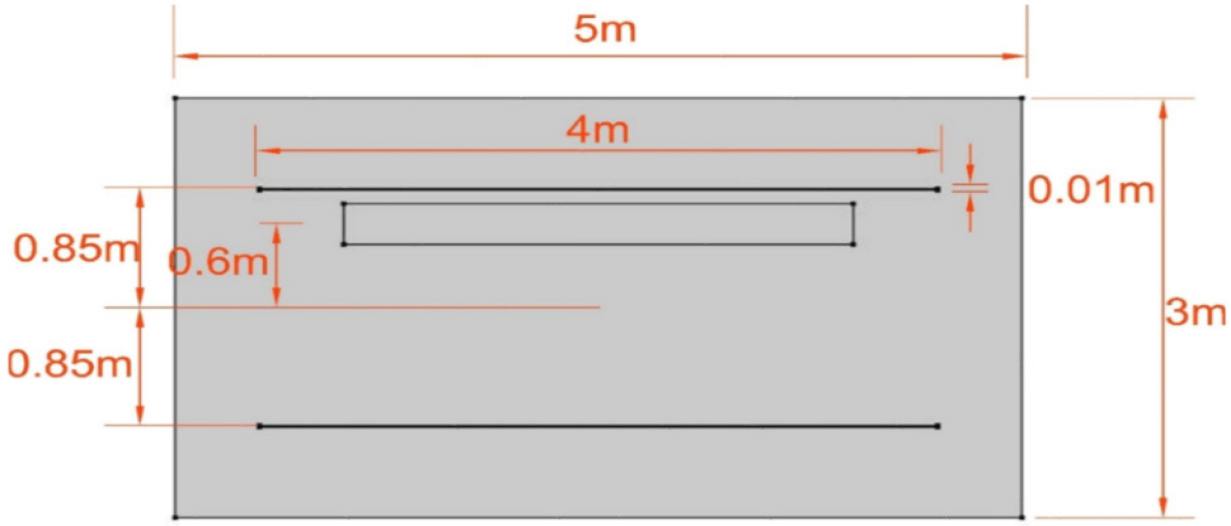

Fig. 3.7 Oven with heating element inside room, COMSOL geometry

Table 3.10 Fluid properties and initial condition, room and oven with heating element, COMSOL model

k / W m^{-1} K^{-1}	ρ / kg m^{-3}	c_p / J kg^{-1} K^{-1}	T_{int} / K	γ / –	η / Pa s
27E–03	Initially 1.21, then rho	1006	293.15	1.4	1.81E–05

Table 3.11 Fluid laminar flow material properties and initial condition, room and oven with heating element, nondimensional COMSOL model

ρ / kg m^{-3}	η / Pa s	IVF / m s^{-1}	IP / kPa	Ra / –
1	1	0	0	1,1E1,1E2,1E3,1E4,1E5

Fluid laminar flow material properties and initial condition for the room and oven with heating element for the non-dimensional COMSOL model are shown in Table 3.11. Fluid heat transfer material properties and initial condition for the room and oven with heating element for the non-dimensional COMSOL model are shown in Table 3.12. The values for both of these tables are obtained from Multiphysics, Module [82].

Table 3.12 Fluid heat transfer material properties and initial condition, room and oven with heating element, non-dimensional COMSOL model

p / kPa	k / W m^{-1} K^{-1}	c_p / J kg^{-1} K^{-1}	γ / –	T_{int} / K
0	1	Pr= 0.71	1	0

Moisture COMSOL Model

Moisture loss Without heat Transfer and Convection COMSOL Model

Figure 3.8 shows a COMSOL model. The geometry of the oven, heating element, and room are the same as in Fig. 3.7. The geometry of the dough is the same as the dough/bread geometry in Fig. 3.2. The base COMSOL Multiphysics license is employed; the Transport of Dilute Species application is used. The mesh is default (not refined).

The water content in dough/bread is approximately 42% by weight [22]. This means that for 100 kg of dough/bread 42 kg of it will be water. COMSOL's default units for c (concentration) are mol m^{-3}, so the conversion is calculated as follows:

$$\frac{42\ \text{kg water}}{100\ \text{kg bread}} \times \frac{\frac{1\,000\ \text{g water}}{1\ \text{kg water}}}{\frac{1\text{m}^3\ \text{bread}}{380\ \text{kg bread}}} \times \frac{\frac{1\ \text{mol water}}{18.015\ \text{g water}}}{1} = \frac{8\,859.28\ \text{mol water}}{\text{m}^3\text{bread}} \tag{3.39}$$

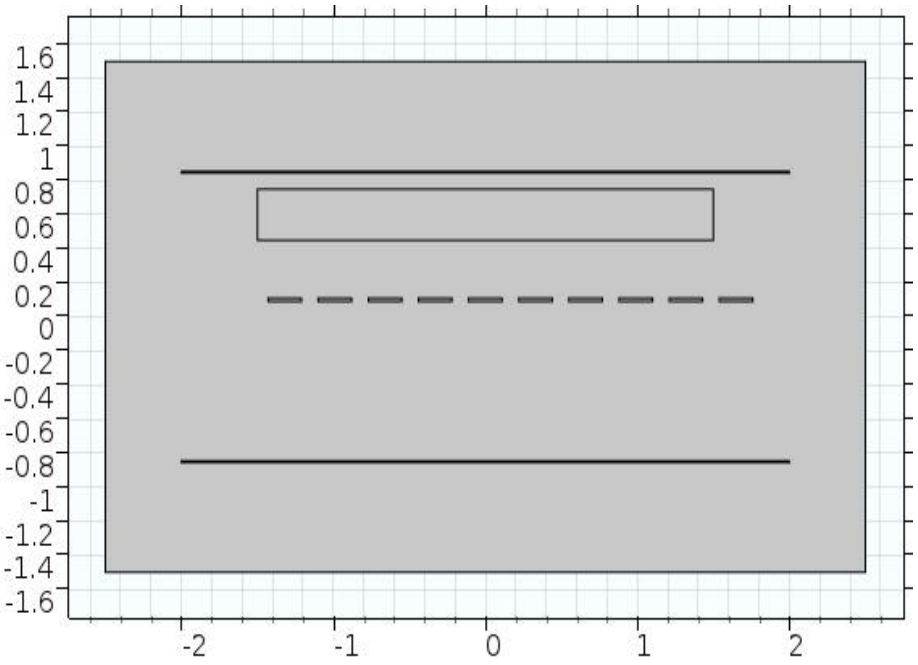

Fig. 3.8 Oven with dough/bread within heating element inside room, COMSOL model

Table 3.13 Room and dough/bread initial concentration and diffusion coefficients

	c_{int} / mol m^{-3}	D / m^2 s^{-1}
Room	0 (default)	5×10^{-9}, then 5×10^{-10}
dough/bread	8859.28 (from (3.39))	5×10^{-9}, then 5×10^{-10}

Table 3.13 shows the room and dough/bread initial concentration and diffusion coefficients for the COMSOL model without heat transfer and convection. The diffusion coefficient is obtained from a similar diffusion coefficient in Table 3.14.

Moisture loss with heat Transfer and Convection COMSOL Model

The base COMSOL Multiphysics license is used; The Transport of Dilute Species and Heat Transfer Applications are employed. The mesh used is default (not refined).

The properties, expression, values, and descriptions of the dough/bread for the moisture loss initial COMSOL model are shown in Table 3.14. The initial dough temperature is at room temperature, the density of the dough is from Table 3.4, the heat transfer coefficient is from the addition of (3.23) and (3.31); the initial dough moisture concentration is from Eladly et al. [22], air moisture concentration is from properties of the air at 220 °C, and humidity x = 0.050 kg (H_20, g) kg^{-1}(dry air),the specific moisture capacity from Eladly et al. [22], moisture conductivity, and surface moisture diffusivity are from Mondal, Datta [10], mass transfer coefficient in mass units is from (3.34). Latent heat of vaporization is from Table 3.1.

Table 3.14 Properties, values, and descriptions of the dough/bread for the moisture loss in COMSOL model

Symbol	Description	Value
T_{air}	oven air temperature	220 [°C]
T_0	initial dough/bread temperature	20 [°C]
ρ	dough/bread density	380 [kg m^{-3}]
h	heat transfer coefficient	24.1 [W m^{-2} K^{-1}]
M_{H2O}	the molar mass	18 [g mole^{-1}]
c_0	initial dough moisture concentration	$0.42 \times \rho/M_{H2O}$ [kg m^{-3}]
c_b	air moisture concentration	0.0354
C_m	specific moisture capacity (kg $_{mos}$/kg $_{b/d}$)	0.42 [kg m^{-3}]
k_m	moisture conductivity	1.53×10^{-6} [kg m^{-1} s^{-1}]
h_m	mass transfer coefficient in mass units	1.8×10^{-3} [kg m^{-2} s^{-1}]
D	diffusion coefficient	$k_m/(\rho \cdot C_m)$
k_c	mass transfer coefficient	$h_m/(\rho \cdot C_m)$
D_m	surface moisture diffusivity	5×10^{-10} [m^2 s^1]
λ	latent heat of vaporization	$2.33\times10^6 \cdot M_{H2O}$ [J kg^{-1}]

3.2 Results and Discussions

3.2.1 Radiation COMSOL Model

Radiation COMSOL Model with Constant Properties

Figure 3.9 shows the radiation effect on the dough/bread for a COMSOL solution after 1800 seconds. A surface integration on the dough/bread domain yielded a value of 1.7865 m^2K, which when divided by the area of the surface (0.0044 m^2) yields an average surface temperature of 406 K. This shows an increase in temperature from the initial temperature calculated as: 406 K (112.85 °C).

For the constant property simulation, the temperature of the center of the dough/bread first decreases, then increases as shown in Fig. 3.10; this is thought to be due to the fact that the initial radiosities of all the surfaces (dough/bread and heating element) are specified as zero, and the initial temperatures are specified as 293.15 K. In other words, it takes some time for the dough/bread to start having realistic values for its increase in temperature as the simulation converges.

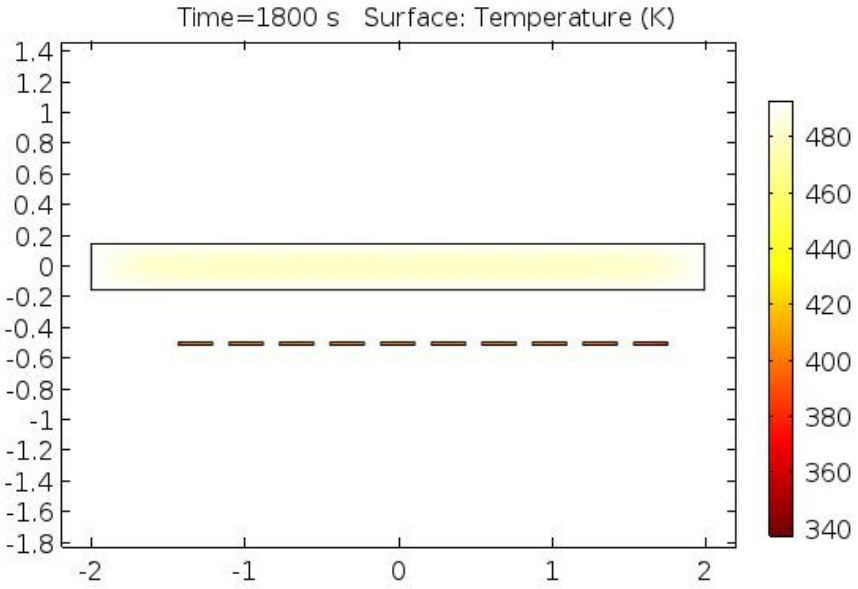

Fig. 3.9 Radiation effect on dough/bread at 1800 seconds

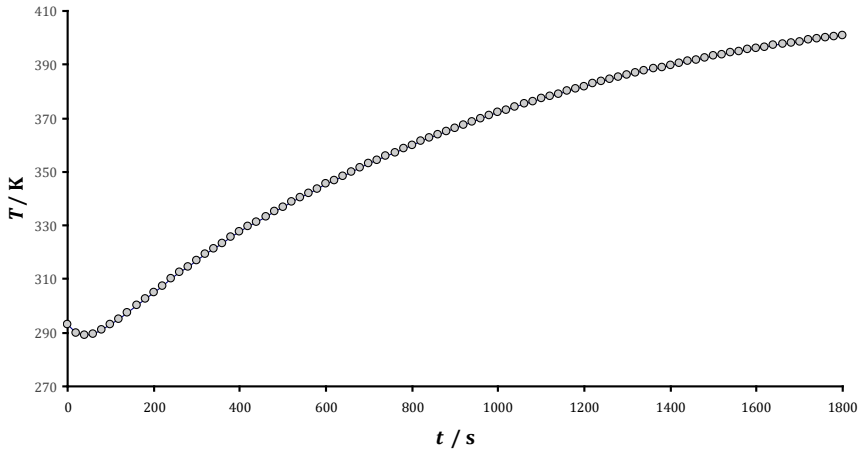

Fig. 3.10 Temperature versus time at center of dough/bread, radiation effect on dough/bread with constant properties

Radiation COMSOL Model with Varying Properties

Figure 3.11 shows the radiation effect on the dough/bread for a COMSOL solution after 1800 seconds. A surface integration on the dough/ bread domain yielded a value of 1.7186 m^2 K, which when divided by the area of the surface (0.0044 m^2) yields an average surface temperature of 390.59 K. This shows an increase in temperature from the initial temperature calculated as: 390.59 K (97.4 °C).

For the temperature –varying density simulation, the temperature at the center of the dough/bread first decreases in temperature, then increases. The reason for this is thought to be because as can be seen from Fig. 3.12, the density first rises with respect to time, then decreases with respect to time; therefore, the initial temperature drop of the dough/bread is due to higher density, and the temperature rise is due to the decreasing density.

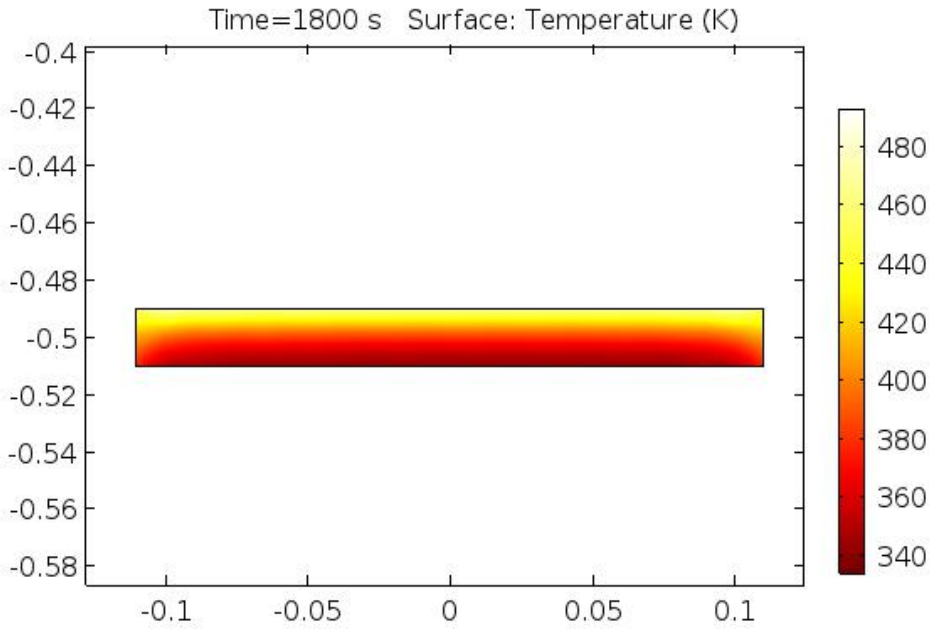

Fig. 3.11 Temperature versus time at center of dough/bread, radiation effect on dough/bread with temperature–varying properties

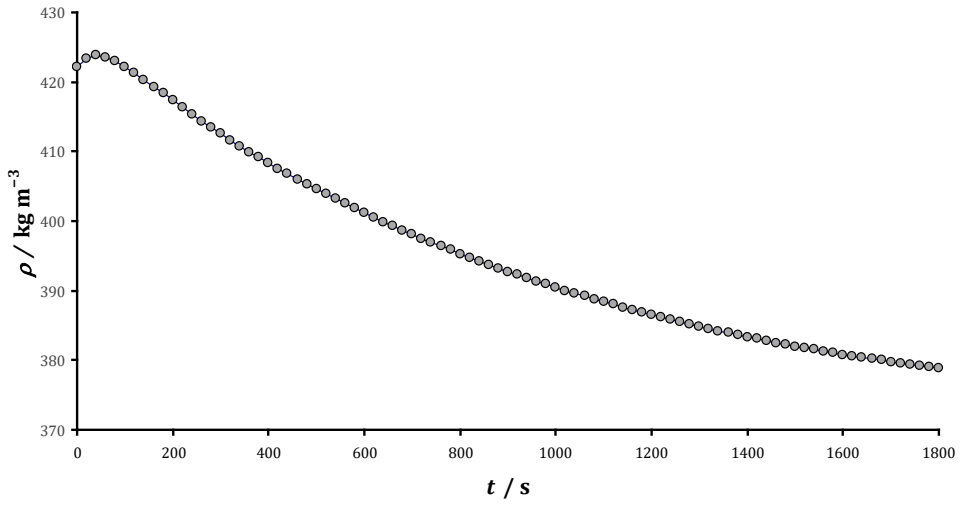

Fig. 3.12 Density of dough/bread at center versus time

From Fig. 3.13, the temperature of the dough/bread for the density–varying simulation is in general less than the constant property simulation, which is expected due to the fact that the density of the bread in the density-varying simulation is always higher (roughly 396.13 kg m^{-3} on the average) than the constant property simulation density (380 kg m^{-3}). A higher density means more energy is required to heat the dough/bread shown in Wong et al. [46], which is the same as stating that a higher density dough/bread has a lower temperature for a given amount of energy.

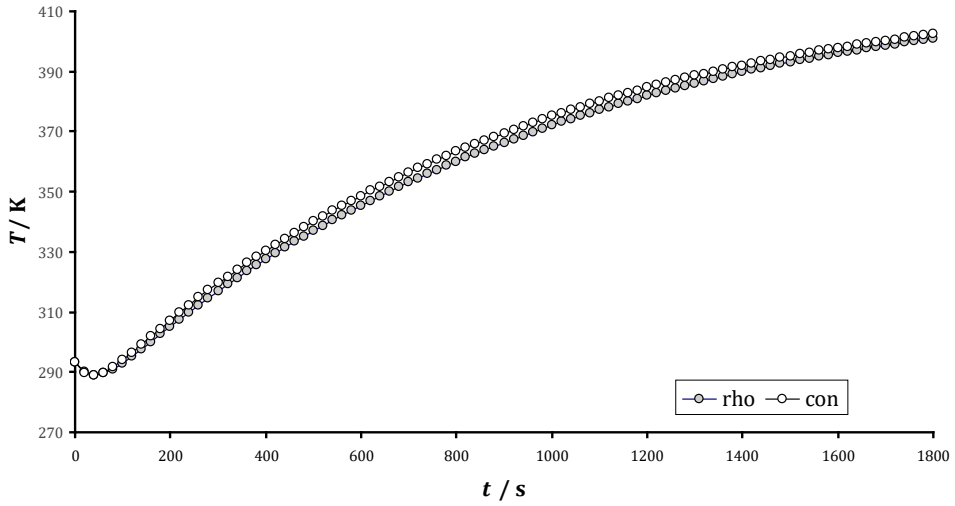

Fig. 3.13 Temperature versus time at center of dough/bread, radiation effect on dough/bread with temperature – varying density versus constant properties, COMSOL

For the simulation where the specific heat varies with temperature, the curve is qualitatively similar to the constant propertiy simulation curve. The temperature at the center of the dough/bread for the temperature-varying specific heat simulation is mostly below the curve for the constant property simulation as shown in Fig. 3.15. This is expected as the specific heat (an average of roughly 1995.8 J kg^{-1} K^{-1}, as seen in Fig. 3.14 in the temperature-varying simulation is always more than the constant property simulation specific heat (1941 J kg^{-1} K^{-1}); more energy is required to heat the dough/bread with a higher specific heat, as shown in Wong et al. [46].

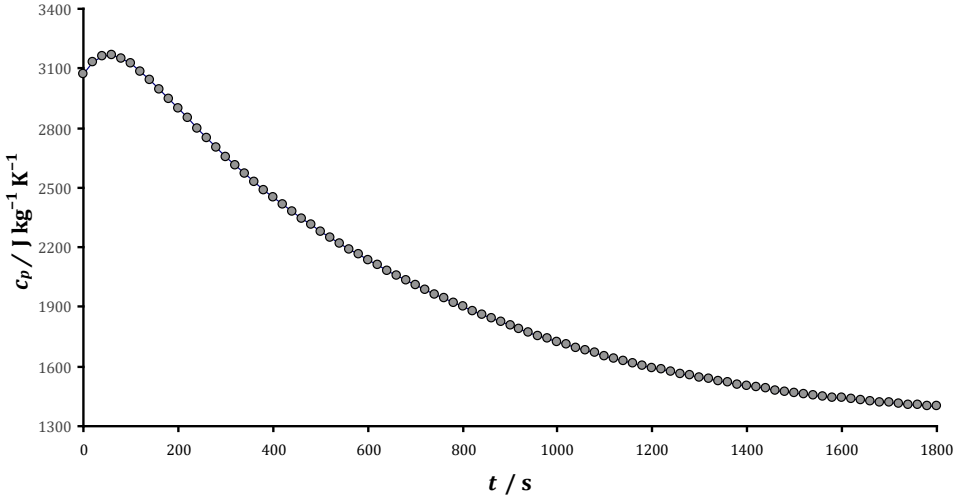

Fig. 3.14 Specific heat of dough/bread at center versus time.

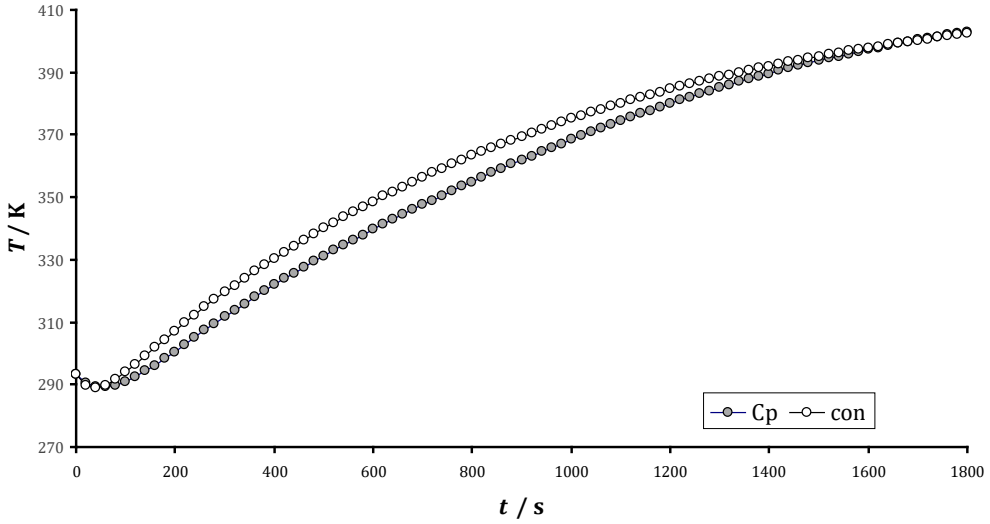

Fig. 3.15 Temperature versus time at center of dough /bread, radiation effect on dough/bread with temperature – varying specific heat versus constant properties, COMSOL

For the temperature-varying thermal conductivity simulation, the temperature at the center of the dough/bread was at first higher than the constant property simulation, then fell below the constant property simulation as shown in Fig. 3.17. The fact that the temperature is initially higher for the conductivity-varying simulation is expected due to the fact that the thermal conductivity (roughly an average of 0.124 W m^{-1} C^{-1}, as seen in Fig. 3.16) for this simulation is always higher than the thermal conductivity (0.1133 W m^{-1} C^{-1}) of the constant-property simulation; the heat will travel faster to the interior of the dough/bread for a higher thermal conductivity as shown in Wong et al. [46].

In summary, the physical properties can significantly affect the simulated temperature profiles, as stated in Wong et al. [46].

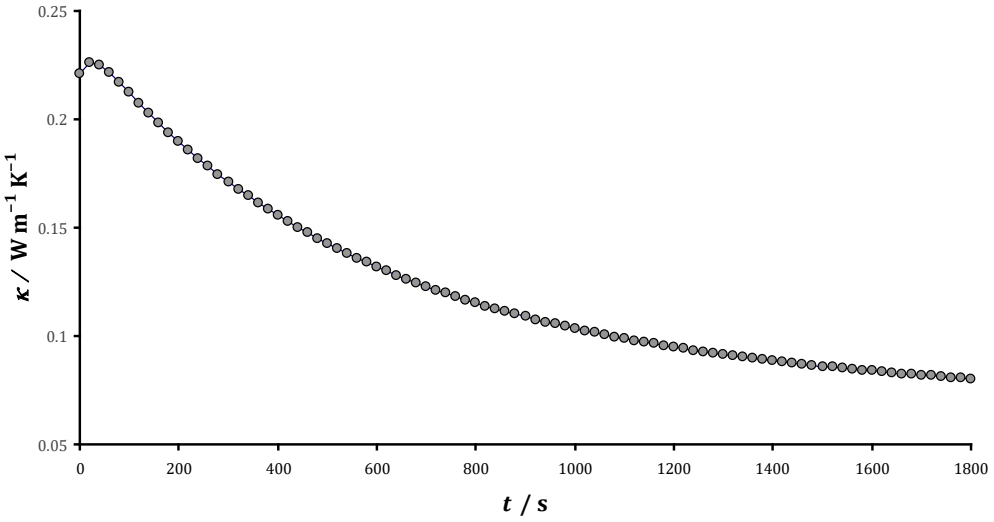

Fig. 3.16 Thermal conductivity of dough/bread at center versus time

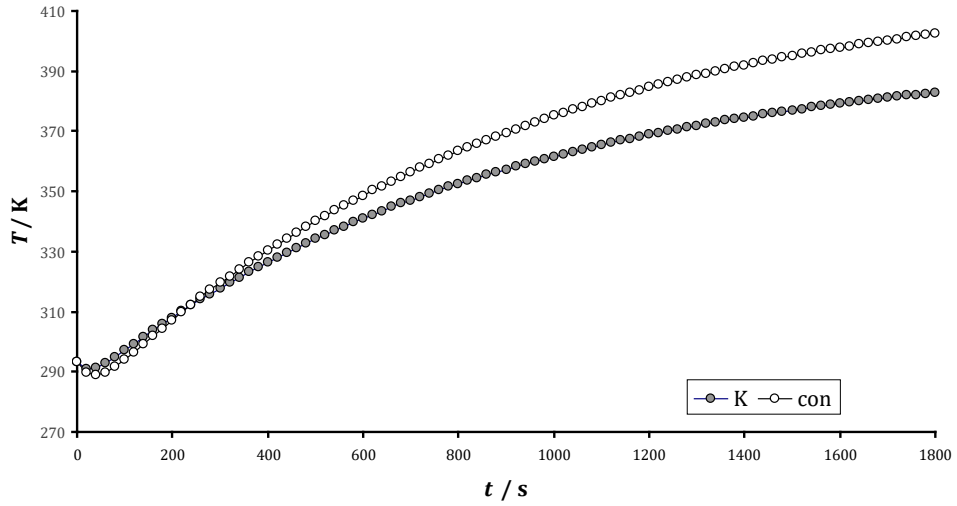

Fig 3.17 Temperature versus time at center of dough/bread, radiation effect on dough/bread with temperature – varying thermal conductivity versus constant properties, COMSOL

3.2.2 Convection COMSOL Model

The solution of dimension convection COMSOL model did not converge because the air heated by the element rises to the top of the oven, then out of the oven to the room.

Figure 3.18 shows the temperature and velocity fields for the non-dimensional free convection COMSOL simulation when the Raleigh number is equal to one. It can be seen from this figure that there are two distinct regions of cellular fluid flow: at the right side of the oven, there is a region of clockwise cellular flow, and at the left side of the oven, a region of counterclockwise cellular flow. These cellular flows are expected, given the location of the hot and cold areas of the temperature distribution. Compared to the dimensional free convection simulation the nondimensional simulation converged, and given the inputs of each model, the temperature and velocity distributions are qualitatively as expected.

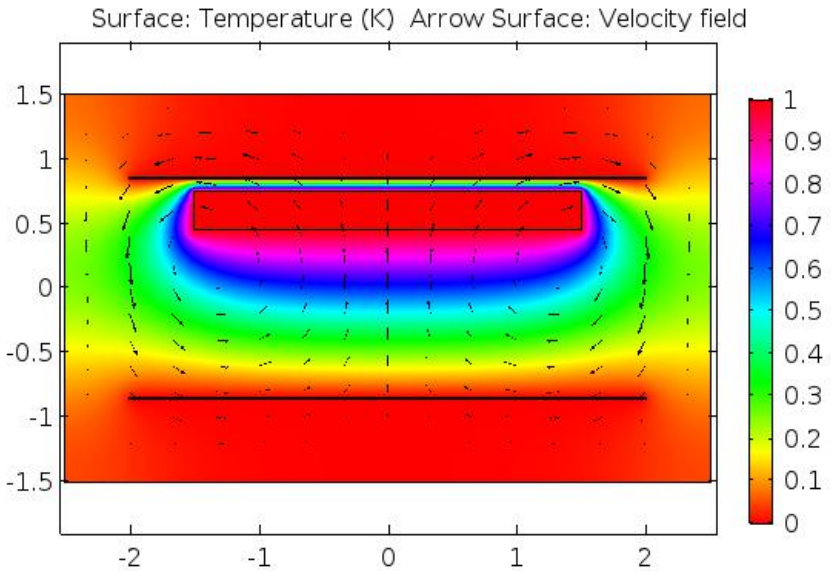

Fig. 3.18 Temperature and velocity fields, free convection COMSOL simulation, *Ra* = 1

Figure 3.19 shows the temperature and velocity fields of the non-dimensional free convection COMSOL simulation when Rayleigh number is equal to 1e05. Here the shape of the temperature distribution in

the vicinity of the heating element is more of a "butterfly" shape, compared to the when the Rayleigh number is equal to one, where the temperature distribution is more of an "oval" shape. This is expected since the higher the Rayleigh number the more disordered will be the temperature distribution and fluid flow.

Figure 3.21 shows the dimensionless velocity magnitudes versus Rayleigh numbers for the non–dimensional free convection simulations. As expected [82] with increasing the Rayleigh number, velocity increases.

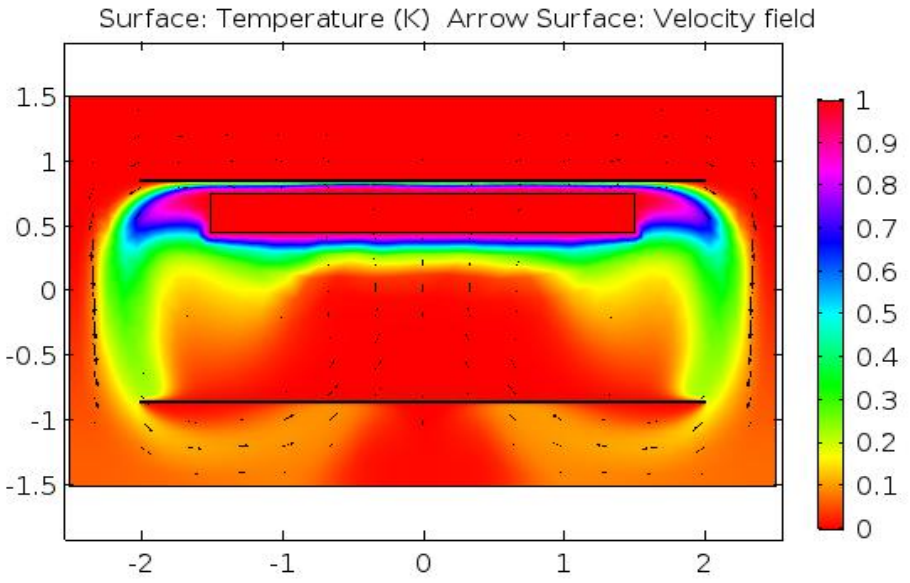

Fig. 3.19 Temperature and velocity fields, free convection COMSOL simulation, *Ra* = 1e5

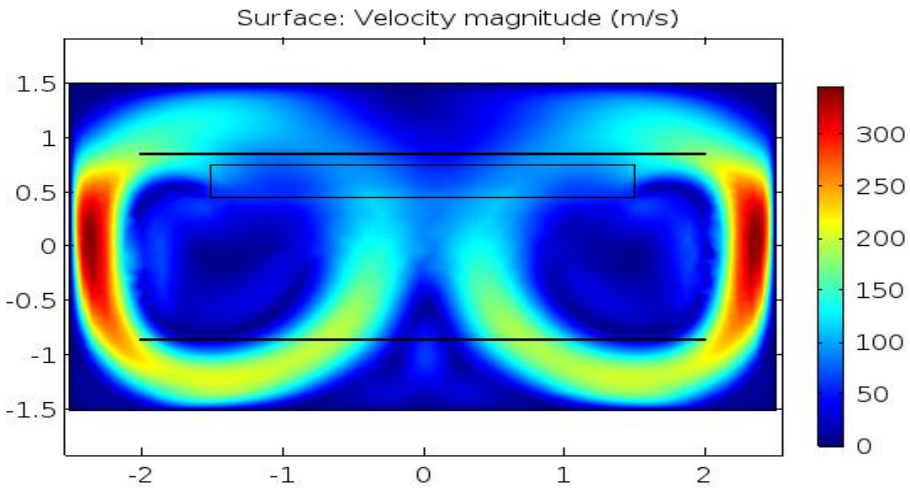

Fig. 3.20 Velocity magnitude, convection COMSOL simulation, *Ra* = 1e5

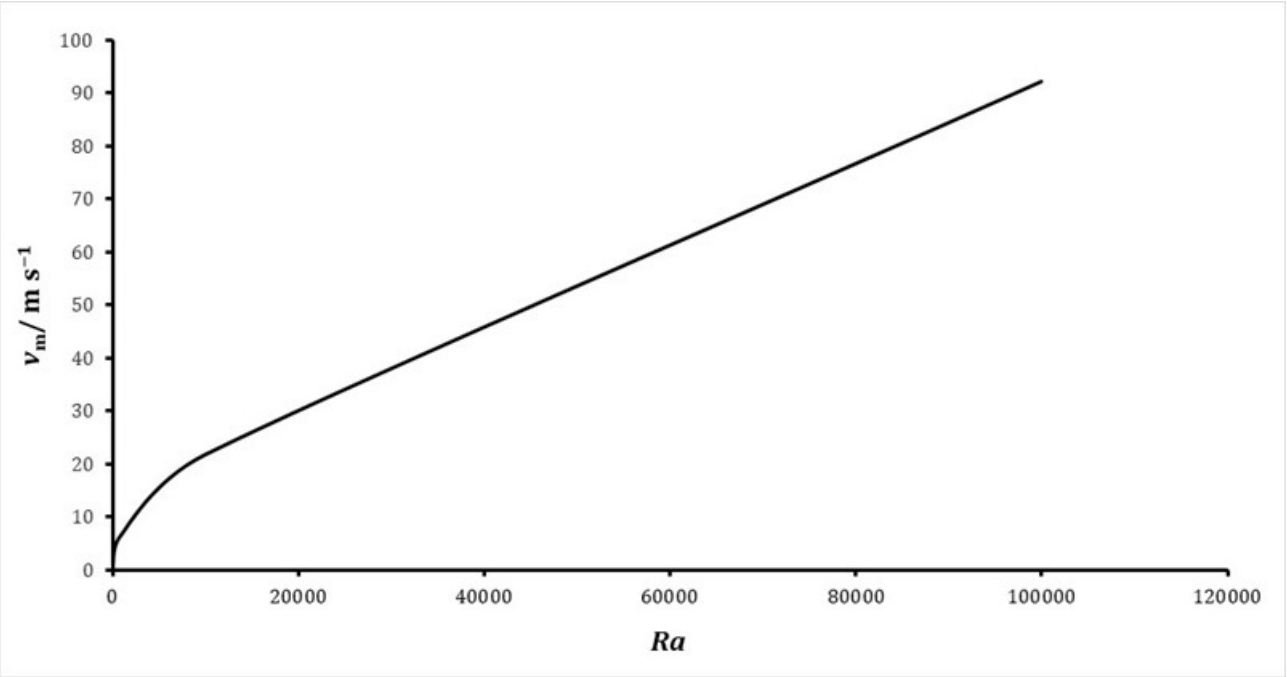

Fig. 3.21 The dimensionless velocity magnitudes versus Rayleigh numbers for the non-dimensional free convection simulations

3.2.3 Moisture COMSOL Model

Moisture Loss Without Heat Transfer and Convection COMSOL Model

Figure 3.22 shows the COMSOL result of the oven with dough/bread within heating element inside the room. It appears as though the moisture is leaving the dough/bread and diffusing to the room; this can be seen by observing that the moisture concentration is decreasing within the bread, and increasing in the room as shown in Fig. 3.23. A surface integration on the dough bread at 3600 seconds resulted in a value of 18.79 mol m^{-1}; this value divided by the area of the domain (0.02 × 0.22) = 4 270.454 5 mol m^{-3}.The loss of moisture from the dough bread is calculated as follows:

$$\frac{8\,859.28 \text{ mol water}}{\text{m}^3 \text{ bread}} - \frac{4\,270.4545 \text{ mol water}}{\text{m}^3 \text{ bread}} = \frac{4\,588.825 \text{ mol water}}{\text{m}^3 \text{bread}} \tag{3.40}$$

Now find kg water lost per m^3

$$4\,588.825 \times \frac{1}{1\,000} \times 18.015 = 82.667\,6 \text{ kg m}^3 \text{ hr}^{-1} \tag{3.41}$$

$$82.667\,6 \times \left[\left(\frac{\pi}{4} \times 0.22^2\right) \times 0.02\right] = 0.062\,849 \text{ kg hr}^{-1} \tag{3.42}$$

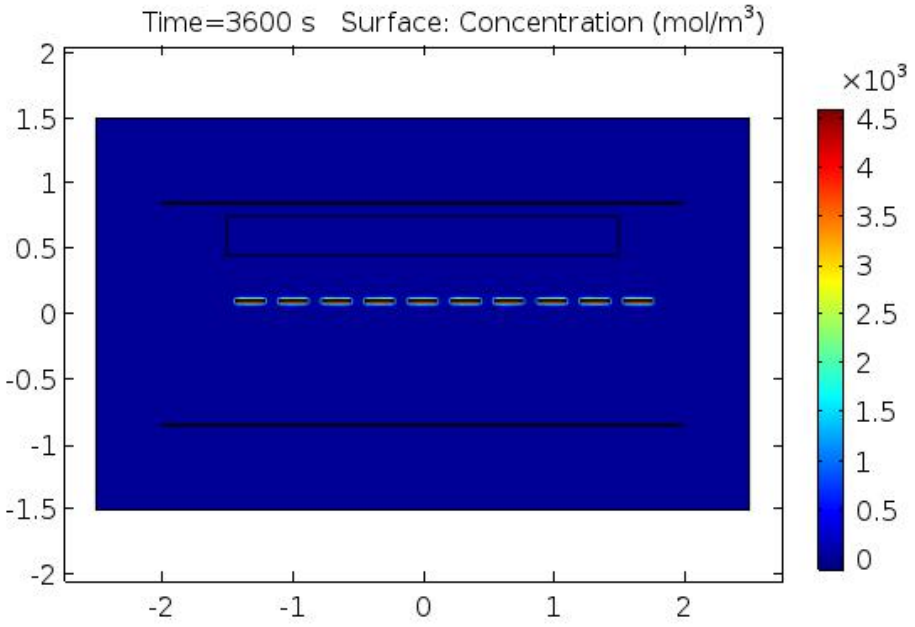

Fig. 3.22 Oven with dough/bread within heating elements inside room, COMSOL solution

For a diffusion coefficient of 5×10^{-10} m^2 s^{-1}. a surface integration on the dough/bread yielded a value of 4614.3 (mol m^{-3}). This result is used to calculate the moisture loss of the dough/bread as above. Table 3.15 shows the results of the two simulations; as expected, a lower diffusion coefficient resulted in a lower moisture loss from the dough/bread.

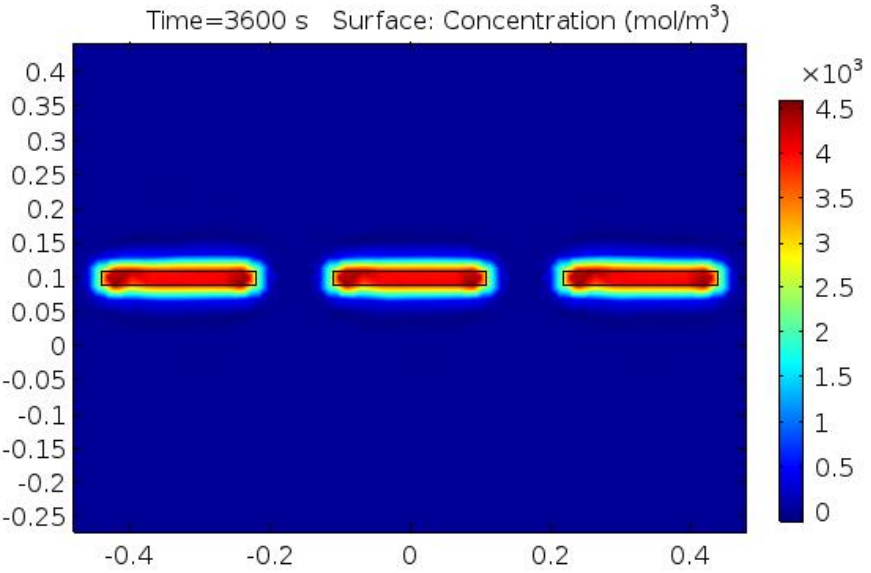

Fig. 3.23 Dough/bread, COMSOL solution

Table 3.15 COMSOL moisture simulations without convection and without heat transfer

D **/ m^2 s^{-1}**	**Moisture loss / kg hr^{-1}**
5×10^{-9}	0.062849
5×10^{-10}	0.05813

Moisture loss with heat transfer and convection COMSOL model:

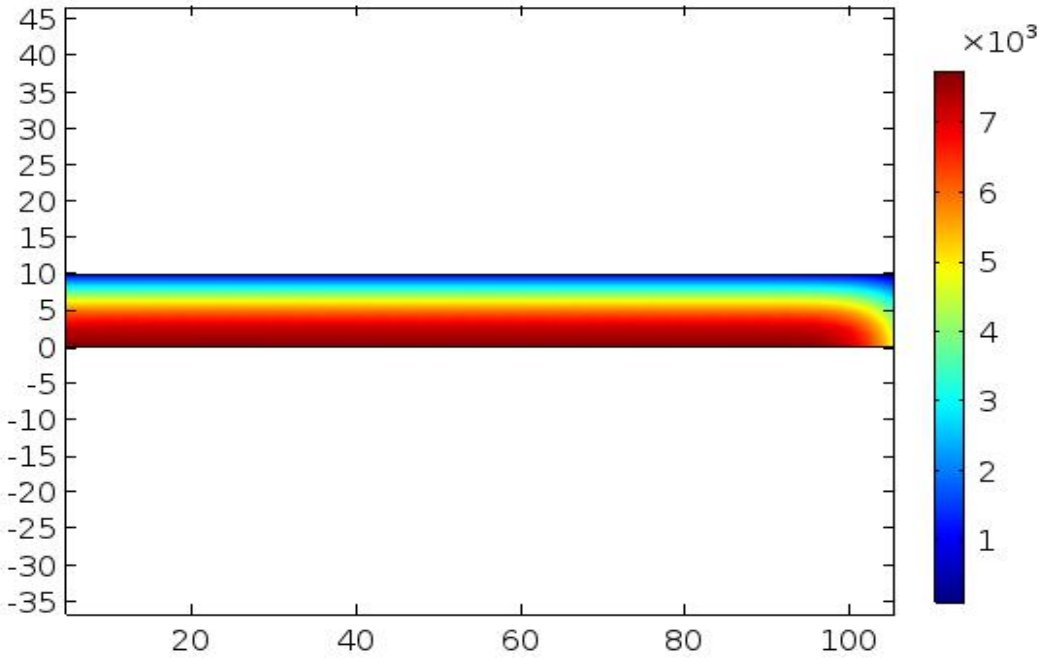

Fig. 3.24 Moisture concentration at 1800 seconds, COMSOL, using values from Table 3.14

Figure 3.24 shows a 2-D axisymmetric for moisture concentration at 1800 seconds in bread. The external surface is drier than the core. The water loss per hour is calculated as follows: at time 0, the moisture concentration in the dough is (8859.28 mol m^{-3}). At time 30 min, the moisture concentration in the dough is (4991.3 mol m^{-3}).

The amount of water lost from the dough/bread is:

$$8\,859.28 - 4\,991.3 = 3\,867.98 \text{ mol m}^{-3} \tag{3.43}$$

As shown in Table 3.16 When the initial moisture content of the dough/bread (c_0) was changed from $0.42\rho/M_{H2O}$ to $0.40\ \rho/M_{H2O}$, the moisture loss decreased; this is expected because the difference between the initial moisture content of the dough/bread and the moisture content of the air decreased. When the moisture concentration of the air (c_b) was decreased, the moisture loss of the dough/bread increased; this is expected because the difference between the moisture content of the air and the initial moisture content of the dough/bread increased. When the specific moisture capacity of the dough/bread (C_m) was increased, the moisture loss decreased; this is expected because it is believed that specific moisture capacity in similar to the specific heat capacity of a substance. The amount of energy required to increase the temperature of a substance is directly related to the magnitude of its specific heat, and this is analogous to the amount of energy required to reduce the moisture content of a substance being directly related to its specific moisture capacity. Finally, when the mass transfer coefficient in mass units (h_m) was increased, the moisture loss of the dough/bread increased; this is expected since the mass transfer coefficient is directly related to the moisture loss from the dough bread.

Table 3.16 Change in properties and values of the dough/bread for the moisture loss in COMSOL model

Symbol	Value	Moisture loss / mol m^{-3}
c_0	0.42 × ρ/M_{H2O}	3867.98
	0.40 × ρ/M_{H2O}	3690.8
c_b	0.0354	3867.98
	0.024	3876.2
C_m	0.42	3867.98
	0.73	2840.7
h_m	1.8e−3	3867.98
	2.5e−3	4052.5

4 Modeling Coupled heat and mass Transfer in Bread at Different Temperature

There are several studies in which the baking process has been reported, for example [57], where a computer model using the Crank–Nicholson finite-difference method has been developed in order to predict temperature and moisture content during microwave heating of the baked dough. The authors only considered the transport phenomena and neglected the deformation that takes place during baking. This work can very surely be extended by including the effect of volume expansion. De Cindio, Correra [109] studied the process of gas bubble expansion in leavened general goods and were able to accurately predict the softness, firmness (water content), and acidity of the leavened product. Lostie et al. [110] reported on the sponge cake batter baking process. Broyart, Trystram [111] developed a model for heat- and mass transfer phenomena and quality changes during continuous biscuit baking using both deductive and inductive (neural network) modelling principles. Bikard et al. [112] reported the simulation of bread making process using a direct 3D numerical method at microscale. Also, Baldino et al. [113] mathematically studied the behavior of the baking of semi-sweet short dough biscuits. Purlis [114] reported the heat- and mass balances for baking process.

Limited reports have been found to describe simultaneous heat and mass transfer during baking at different oven temperatures. Most of the previous research in this area assumed constant processing conditions and thermophysical properties. Consequently, while there does exist a body of relevant literature, there still remains a need for models that can be utilized for real world processing applications.

In this chapter, a theoretical model describing the transport phenomena involved in the bread baking process is discussed. Special attention was focused on the thermal physical properties of food with functions of local values of temperature and moisture content. The model can be used for an evaluation of the time evolution of some characteristic parameters, namely the moisture content of food and its temperature, and to predict bread temperature and water content at different oven temperatures (180 °C, 200 °C, 220 °C, 240 °C and 260 °C).

4.1 Methodology

During the convection baking process, heat was mainly transferred by convection from air to the product surface, and by conduction from surface towards the product center. Meanwhile, moisture diffuses outward towards the product surface, and is vaporized. Bread is modeled as a system containing three different regions:

- crumb - wet inner zone;
- crust - dry outer zone, and
- evaporation front - between the crumb and crust where temperature is 100°C and water evaporates, i.e. liquid-vapor transition [18,114].

To simulate simultaneous heat- and mass (moisture) transfer during the bread baking process of convection cooking, the following assumptions were made:

- no crust formation or shrinkage;

- mass transfer only as single species (i.e., only water), and
- moisture diffuses to the product surface, and is evaporated only at the surface.

The object of this study was cylindrical bread, the bread was 2 cm thick and 22cm in diameter. Due to the axisymmetric structure of the bread (Fig. 4.1), only one quarter of a planar intersection was simulated. The coordinate origin represented the center of the bread.

The properties, expression, values, and descriptions of the dough/bread for the COMSOL model are the same in Table 3.14.

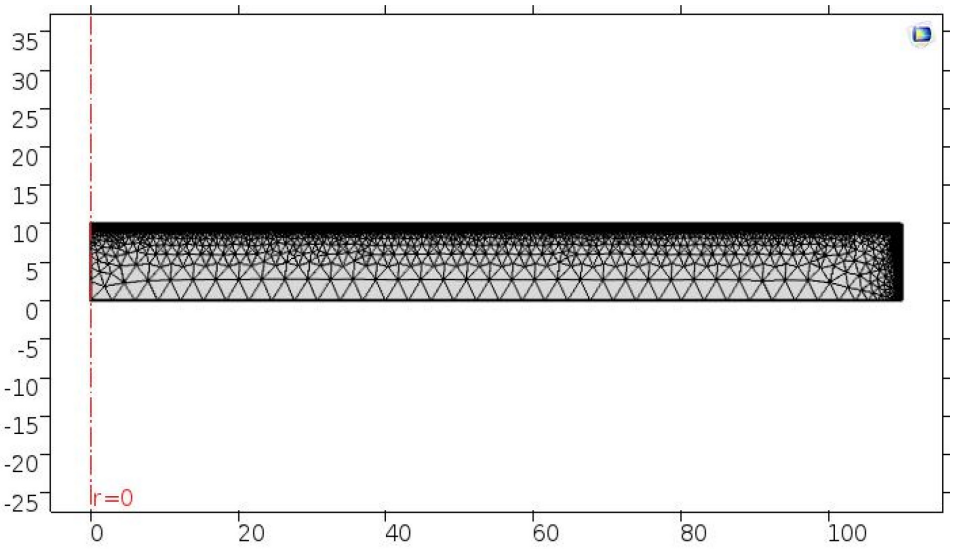

Fig. 4.1 Finite element mesh of the cross section of bread (in mm)

4.1.1 Governing Equations

The energy balance in the solid, based on Fourier's law, leads to

$$\rho \cdot c_p \cdot \frac{\partial T}{\partial t} + \nabla.(-K\nabla T) = 0 \tag{4.1}$$

Mass balance, based on Fick's law, leads to

$$\frac{\partial c}{\partial t} + \nabla.(-D\nabla c) = 0 \tag{4.2}$$

Supposing that the material parameters above (ρ, c_p, k and D), in the most general case, depend on local water concentration and food temperature, (4.1) and (4.2) form a system of non-linear partial differential equations. The thermal physical properties of bread used in the model baking process are based on Chen et al. [115].

$$\frac{1+c}{\rho} = \frac{1}{\rho_{dr}} + \frac{c}{\rho_w} \tag{4.3}$$

$$D = \frac{K}{\rho.c} \tag{4.4}$$

$$C_p = 3\,017.2 + 2.05\,T + 0.24\,T^2 + 0.002\,T^3 \tag{4.5}$$

$$K = 0.194 + 0.436\,c \tag{4.6}$$

4.1.2 Initial and Boundary Conditions

The initial conditions are given by the uniform distribution of temperature and moisture content:

$$(c)_{t_0} = c_0 \qquad (T)_{t_0} = T_0$$

The boundary conditions relative to (4.1) applied to the external surfaces of food where no accumulation occurs actually state that heat transported by convection from air to food is partially used to raise sample temperature by conduction, and partially to allow free water evaporation:

$$-\boldsymbol{n}(-K\nabla T) = \dot{Q}_{\mathrm{A}} + h_{\mathrm{cnv}} \cdot (T_{\mathrm{ffs}} - T_{\mathrm{srf}}) \tag{4.7}$$

The boundary conditions relative to (4.2) applied to external surfaces of food describe the balance between the diffusive flux of liquid water coming from the core of the product and the flux of vapor leaving the food surface which was transferred to the drying air:

$$-\boldsymbol{n} \cdot (-D\nabla c) = k_{\mathrm{d}} \cdot (c - c_{\mathrm{env}}) \tag{4.8}$$

The system of non-linear partial differential equations ((4.7) and (4.8)) were solved by the finite elements method developed by the COMSOL Multiphysics, using the time-dependent iterative non-linear solver already implemented in the Chemical Engineering Module.

4.2 Results and Discussions

In the bread baking process, temperature and water content distributions are important factors which determine the quality of the product. The water content distribution is influenced by the temperature distribution.

4.2.1 Temperature Evaluation

Figure 4.2 illustrates the temperature distribution in bread during the baking process at oven temperature 220 °C as the average temperature. The surface of the bread is at a much higher temperature than the inside part of the bread sample, and a large temperature gradient is developed in the region close to the surface. When the baking process starts, this large temperature gradient gradually shifts from near the surface to inside of the product.

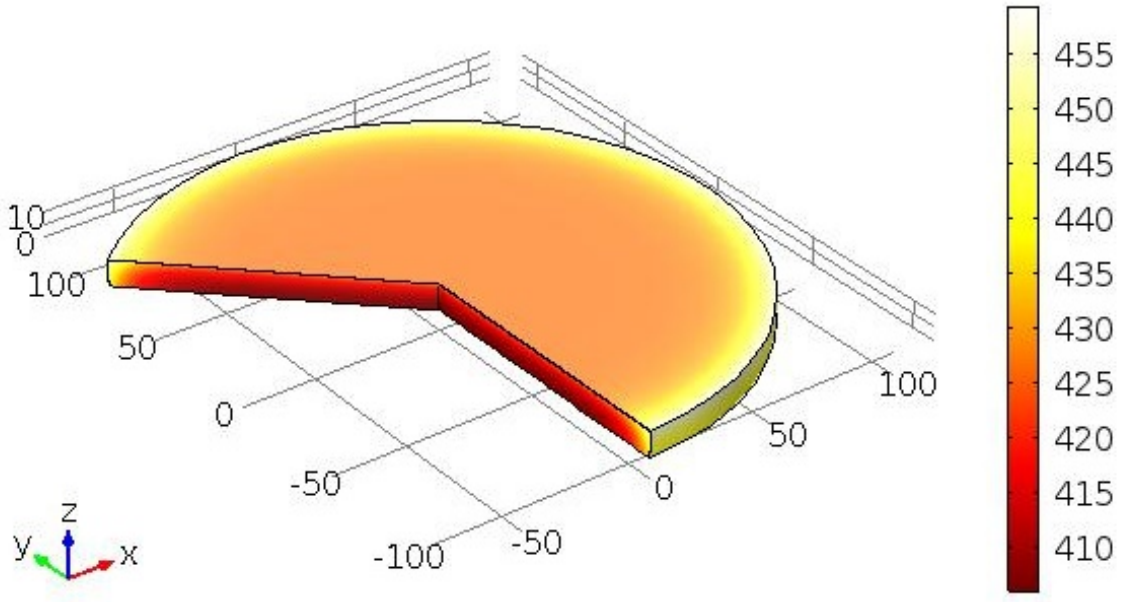

Fig. 4.2 A 3D temperature distribution (K) in bread during the baking process at an oven temperature of 220 °C as the average temperature

Figure 4.3 shows the predicted temperature of the crust of bread during the baking at different oven temperatures (180, 200, 220, 240 and 260 °C). The results indicate that the bread temperature increases with increasing oven temperature. It also indicates that when the oven temperature increases from 180°C to 260°C, the temperature at the crust of bread increases from 132.4 °C to 179.5 °C. The results show that the temperature increases with the increasing time, it increases from 20 °C to 132.4 °C when the time increases from 0 to 30 min at an oven temperature of 180°C. The temperature increases from 20 to 145.17 °C, 20 to 157.21 °C, 20 to 168.65 °C and 20 to 179.5°C at oven temperature of 200, 220, 240 and 260 °C, respectively.

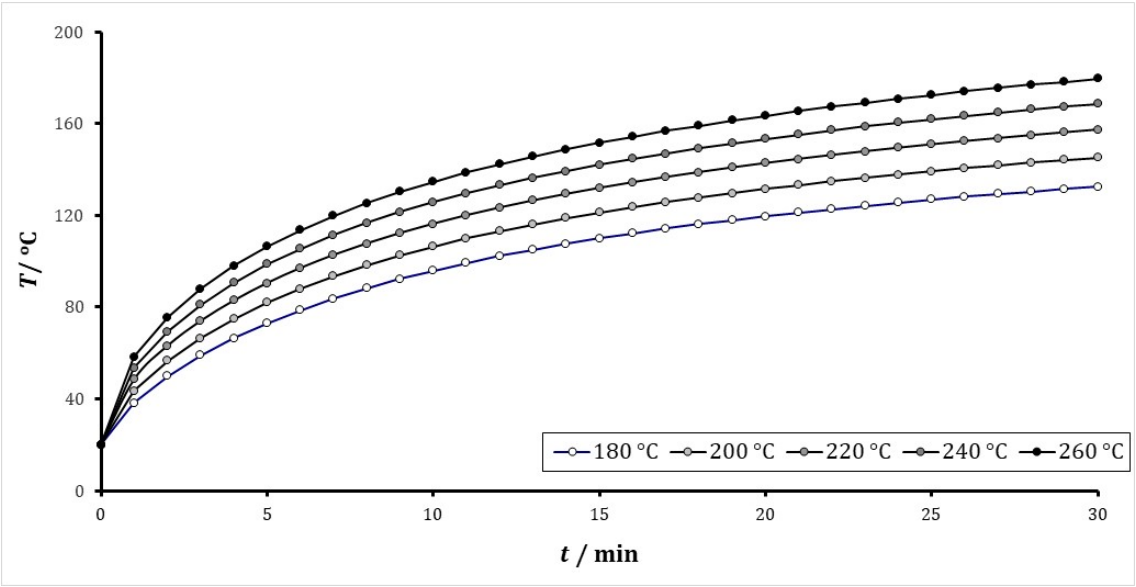

Fig. 4.3 Predicted temperature of the crust of bread process during the baking at different oven temperatures

It is worth to note that the bread temperature reaches 73.55 % of the heat balance at a temperature of 180 °C, while it reaches 69 % of the heat balance at an oven temperature of 260 °C, this could lead to using the lower temperature (180 °C to 220 °C) for a more efficient heat energy utilization.

4.2.2 Water Concentration Evaluation

The water transport depends on the material properties, the diffusivity coefficient, and the pressure gradient. Figure 4.4 shows that the external surface is drier than the core. The water concentration changes during the baking process. The increase in temperature causes the bread to reduce its water holding capacity and the water moves to the surface which is lost by evaporation. As a result, the water concentration gradient is developed within the bread. The temperature gradient gradually shifts towards the interior of the bread.

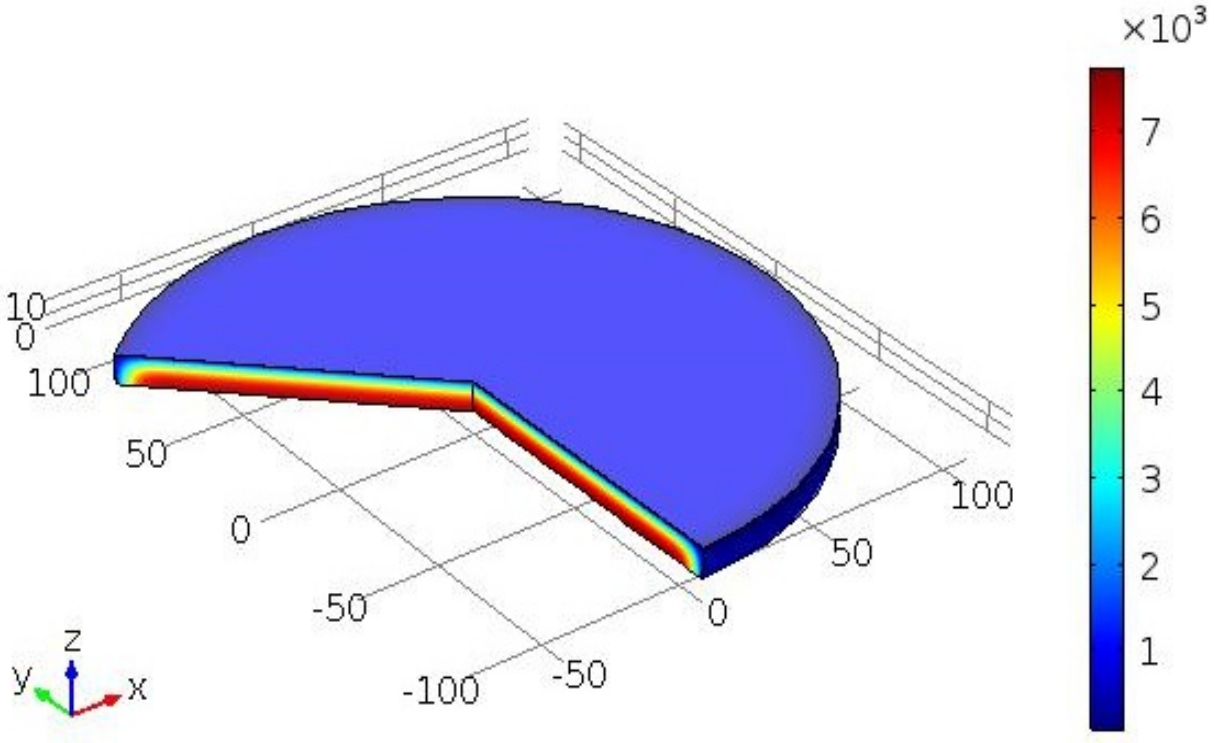

Fig. 4.4 The water concentration distribution (mol m^{-3}) in bread during the baking process at an oven temperature of 220 °C as the average temperature

Moisture content is an important parameter in baked bread that significantly affects shelf life. As baking time and temperature increases there is a reduction of moisture content. Figure 4.5 shows the predicted water concentration in bread during the baking process at an oven temperature of 220 °C as the average temperature. The results indicate that the water concentration decreases with increasing time. It decreases from 8 866.6 mol m^{-3} to 4 991.3 mol m^{-3} when the time increases from 0 to 30 min. Figure 4.6 demonstrates the predicted moisture content % during the baking process at the same oven temperature of 220 °C. The results show that the moisture content % decreases with increasing time. It decreases from 42 % to 23.6 % when the time increases from 0 min to 30 min.

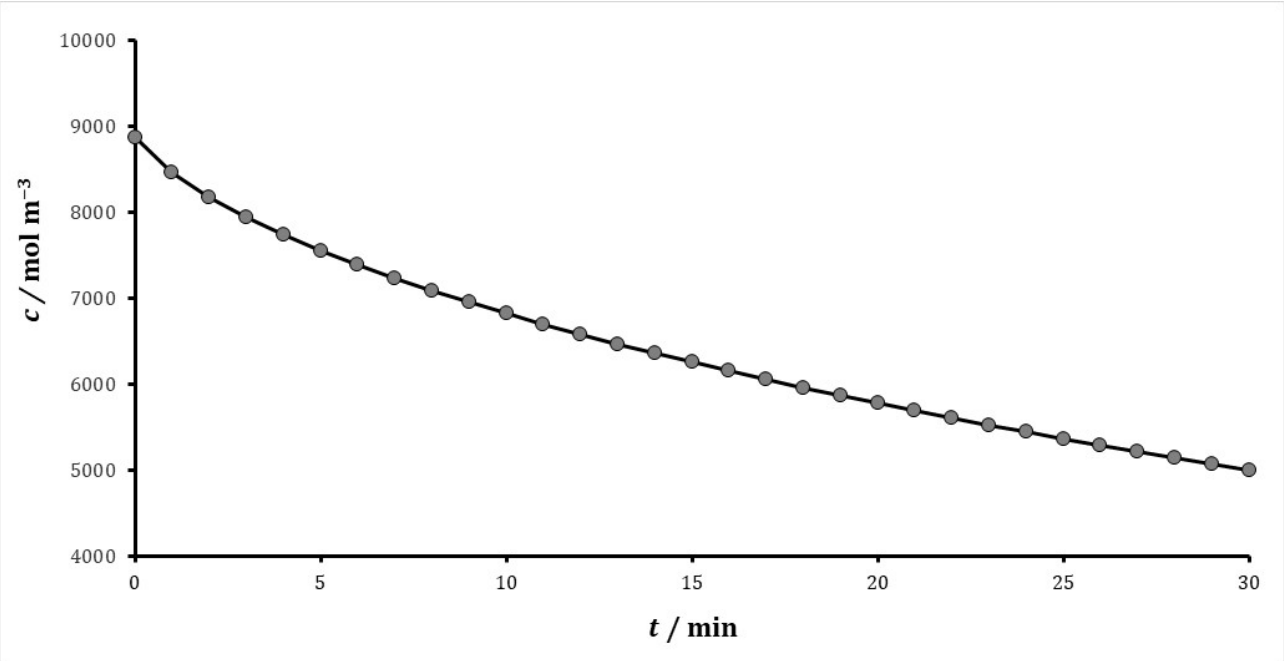

Fig. 4.5 The predicted water concentration in bread during the baking process at an oven temperature of 220 °C as the average temperature.

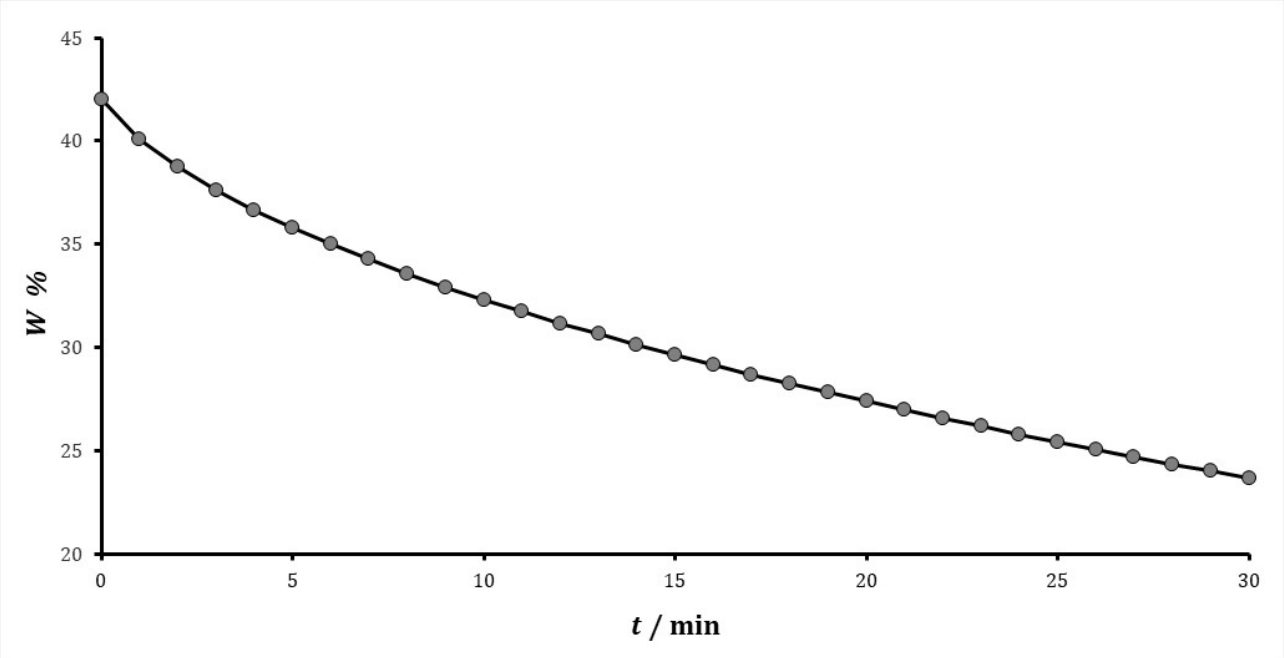

Fig. 4.6 The predicted moisture content % in bread during the baking process at an oven temperature of 220 °C as the average temperature

4.2.3 Cooking Yield

The cooking yield is a quantity that measures how much moisture remains in the bread after the cooking process.

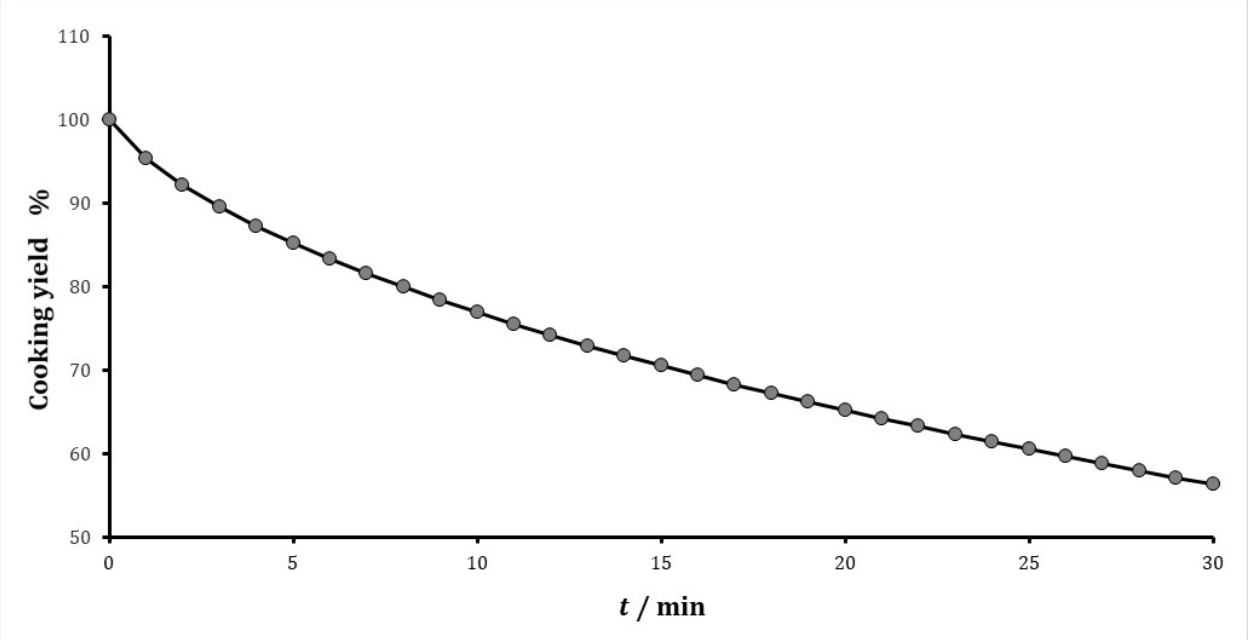

Fig. 4.7 The predicted cooking yield in bread during the baking process at an oven temperature of 220 °C as the average temperature.

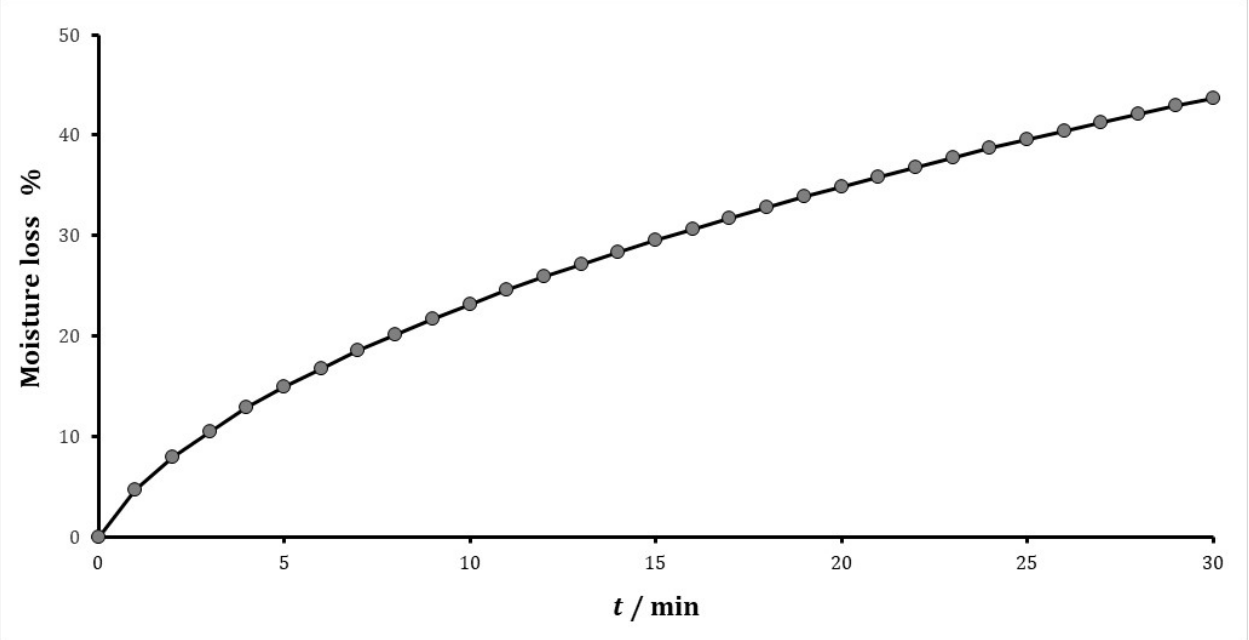

Fig. 4.8 The predicted moisture loss % in bread during the baking process at an oven temperature of 220 °C as the average temperature

Figure 4.7 shows the predicted cooking yield in bread during the baking process at an oven temperature of 220°C as the average temperature. The results indicate that the cooking yield decreases with increasing time. It decreases from 100 % to 56.2 % when the time increases from 0 min to 30 min. Figure 4.8 shows the predicted moisture loss % during the baking process at the same oven temperature of 220 °C.The results show that moisture loss % increases with increasing time. It increases from 0 % to 43.7 % when the time increases from 0 min to 30 min.

5 Mathematical Modeling for Simulation Heat, Water, and Vapor Diffusion Inside the Bread During Baking

The baking process is usually modeled as a simultaneous heat and mass transfer (SHMT) problem, although many theories were suggested for describing the internal mechanisms of transport. For instance, Sluimer, Krist-Spit [116] proposed theory for the evaporation–condensation to explain the rapid heating of porous dough during baking was integrated in a model of SHMT in dough and crumb, not involving the crust area [67]. When comparing experimental and simulated core temperature values good results were obtained, suggesting that the evaporation–condensation mechanism should be included in a model for bread baking. In this way, Thorvaldsson, Janestad [31] took into consideration the evaporation and condensation of water for modelling the drying of bread crumb and developing a model for heat, liquid water, and water vapor transfer including an empirical parameter named as the evaporation rate. Another theory to incorporate evaporation–condensation in a model for the "heating up" period of cake baking was taken by Lostie et al. [110]; this mechanism was included in the heat balance through an effective thermal conductivity.

The mechanisms of internal evaporation – condensation well explains the fact that heat transfer in bread during baking is much faster than the one described by conduction alone. It also supports the notice that at the center of bread during the early stage of baking there is an increase in the water content, rather than a monotonous decrease that has to be true if there is only liquid water diffusion and surface evaporation. Therefore, a multiphase flow model is the best model for bread baking process which consists of three partial differential equations for the simultaneous heat transfer, liquid water diffusion, and water vapor diffusion, respectively, together with two algebraic equations describing water evaporation and condensation in the gas cells. For the gas cells in the model saturated conditions can be accepted [31].

Mathematical modeling of bread baking remains a major challenge in food engineering. Until now, experimental drying and heating curves observed during the process cannot be reproducible by numerical simulation; especially the characteristic sigmoid trend of the temperature variation at the bread core. In addition, precise expressions for thermos physical properties of bread are still unavailable or available only for a narrow range of operative conditions, i.e. temperature below 100 °C.

The aim of this chapter is to develop model describes the mechanisms of simultaneous heat, water and vapour diffusion in a one-dimensional solid material that is heated with radiation and convection from the outside. Several critical values in the temperature and moisture profiles are also taken as the characteristic values of the process. The first critical value is the time when bread temperature reaches 100 °C. The second critical value is the time when the liquid water content at the center of bread reaches its peak. The third critical value is the level of the peaked liquid water content at the center.

5.1 Methodology

The object of this study was cylindrical Bread, the Bread was 2 cm thick and 22 cm in diameter. In this model, the dough is placed inside the oven which is maintained at temperature of 220 °C.

5.1.1 Mathematical Model

The model is based on a one-dimensional model, with some modification as described by Thorvaldsson, Janestad [31]. Considering that the system is symmetric, the model is governed by a set of three differential equations. One for heat transfer, one for water vapor diffusion and the third one for liquid water diffusion. The three equations in the system are connected with each other, a set of algebraic conditions which updates liquid water and water vapor with the help of tabled values for saturated vapor pressure content [70,31,117]. The equation for the heat transfer can be derived from the energy conservation equation by including a term which accounts for the latent heat in water evaporation. The temperature *T(x, t)* at the point *x* and in time *t* can be described as follows [118,31],

$$\frac{\partial T}{\partial t} = \frac{1}{\rho \cdot c_p}\frac{\partial}{\partial x}\left(k \cdot \frac{\partial T}{\partial x}\right) + \frac{\lambda}{c_p}\frac{\partial W}{\partial t} + \frac{\lambda \cdot W}{c_p \cdot \rho}\frac{\partial \rho}{\partial t}, \quad 0 < x < x_{L/2} \tag{5.1}$$

With boundary and initial conditions [118,119],

$$\begin{aligned} -k \cdot \left(\frac{\partial T}{\partial x}\right)_{x=0} = {} & h_{\text{rad}} \cdot (T_{\text{rs}} - T_{\text{srf}}) + h_{\text{cnv}} \cdot (T_{\text{ffs}} - T_{\text{srf}}) \\ & - \lambda\, \rho D_{(\text{H20,l})} \left(\frac{\partial w}{\partial x}\right)_{x=0} \end{aligned} \tag{5.2}$$

$$\left(\frac{\partial T}{\partial x}\right)_{x=x_{L/2}} = 0, \quad t > 0. \quad T(x,0) = T_0(x), \quad 0 < x < x_{L/2} \tag{5.3}$$

Where *T(x, t)* [K] is the temperature , *x* [m] is the space co-ordinate, ρ [kg m^{-3}] is the density which depends on the water content, c_p [J kg^{-1} K^{-1}] is the specific heat, *k* [W m^{-1} K^{-1}] is thermal conductivity, λ [kJ kg^{-1}] is the latent heat of evaporation of water, *W(x, t)* [kg (H_20) kg^{-1}(product)] is the liquid water content, T_{ffs} [K] the surrounding air temperature , T_{srf} [K] is the temperature of the surface of the bread, T_{rs} [K]is the temperature of the the radiation source , T_0 [K] is the initial temperature, $D_{(\text{H2O,l})}$ [m^2 s^{-1}] is liquid water diffusivity, h_{rad} [W m^{-2} K^{-1}] is the radiation heat transfer coefficient, and h_{cnv} [W m^{-2} K^{-1}] is the convective heat transfer coefficient. Other parameters and the formulas can be found in the paper by Thorvaldsson, Janestad [31].

Equations for the diffusion of liquid water and vapor water can be derived from Fick's Law. The equations are [120],

$$\frac{\partial V}{\partial t} = \frac{\partial}{\partial x}\left(D_{(\text{H20,g})}\frac{\partial V}{\partial x}\right), \quad 0 < x < x_{L/2}\,, \qquad t > 0 \tag{5.4}$$

$$\frac{\partial W}{\partial t} = \frac{\partial}{\partial x}\left(D_{(\text{H20,l})}\frac{\partial W}{\partial x}\right), \quad 0 < x < x_{L/2}\,, \qquad t > 0\,. \tag{5.5}$$

With the boundary and initial conditions:

$$\left(\frac{\partial V}{\partial x}\right)_{x=0} = k_{\mathrm{d(H20,g)}}\,(V(0,t) - V_{air}), \qquad \left(\frac{\partial V}{\partial x}\right)_{x=x_{L/2}} = 0\,, \quad t > 0\,. \tag{5.6}$$

$$V(x,0) = V_0(x), \quad 0 < x < x_{L/2} \tag{5.7}$$

$$\left(\frac{\partial W}{\partial x}\right)_{x=0} = k_{\mathrm{d(H20,l)}}\,(W(0,t) - W_{air}), \qquad \left(\frac{\partial W}{\partial x}\right)_{x=x_{L/2}} = 0\,, \quad t > 0\,. \tag{5.8}$$

$$W(x,0) = W_0(x), \quad 0 < x < x_{L/2} \tag{5.9}$$

where $V(x, t)$ [kg (H_20,g) kg^{-1}(product)] is water vapor content,$W(x, t)$ [kg (H_20,l) kg^{-1}(product)] is liquid water content, $k_{d(H2O,g)}$ [kg m^{-2} s^{-1}] is mass transfer coefficients of vapor at the surface and $k_{d(H2O,l)}$ [kg m^{-2} s^{-1}] is the mass transfer coefficients of water at the surface. $k_{d(H2O,g)}$ depends on the temperature content and $k_{d(H2O,l)}$ depends on water as well as temperature content, $D_{(H2O,l)}$ [m^2 s^{-1}] the diffusion coefficient for water which is a constant, $D_{(H2O,g)}$ [m^2 s^{-1}] is diffusion coefficient for vapor which depends on the temperature content, V_{air} [kg (H_20,g) kg^{-1}(product)] is the vapor content of the oven air, W_{air} [kg (H_20,l) kg^{-1}(product)] is the water content of the oven air, V_0 [kg (H_20,g) kg^{-1}(product)] is the initial content of vapor, and W_0 [kg (H_20,l) kg^{-1}(product)] is the initial content of water.

The above equations are supplemented by an algebraic equation describing the relationship between water vapour content V and liquid water content W. Saturation condition is assumed within the gas cells of bread. A saturated steam table can be used for this purpose. The physical parameters in (5.1) to (5.9) are not constants. They depend on the local temperature $T(x, t)$ and moisture content $W(x, t)$ as shown in Table 5.1.

Table 5.1 shows the material parameters and the diffusion coefficient for the matlab model. Taking an average each of the following thermal properties: conductivity, specific heat, and density; using the data in Table 3.2. Convection heat transfer coefficient, h_{Cnv} from (3.23), radiation heat transfer coefficient, h_{rad} from (3.31), Diffusion coefficient for water and initial water content of the oven air were taken from Table 3.14. Diffusion coefficient for vapour, mass transfer coefficient for vapour, mass transfer coefficient for water and Evaporation rate were taken from Thorvaldsson, Janestad [31] .

The implementation of the model is carried out through the following procedure:

- Temperature is calculated from the heat transfer (5.1) with the help of conditions in (5.2) and (5.3).
- Saturated water vapor is calculated from the equation as described by Powathil [70],

$$V = \frac{PMC}{RT\rho} \tag{5.10}$$

  where V [kg (H_20,g) kg^{-1}(product)] is the saturated water vapor, P [Pa] is the pressure, R [J mol^{-1} K^{-1}] is the universal gas constant, M [kg mol^{-1}] is the molar mass, T [k] is the temperature, ρ [kg m^{-3}] is the mass density, and C is a constant (about0.75) [70].
- Vapor and water contents of the dough are then updated using this saturated vapor with the help of following algebraic equations.

if (Water content + Vapor Content) < Saturated Vapor Content
Updated Vapor = (Water content + Vapor Content) (5.11)
Updated Water = 0

if (Water content + Vapor Content) ≥ Saturated Vapor Content
Updated Vapor = Saturated Vapor (5.12)
Updated Water = (Water content + Vapor Content) −Saturated Vapor

- Vapor content is calculated from the diffusion (5.4) with the help of the conditions (5.6) and (5.7).
- By adjusting the water vapour content V again, according to saturation condition, this step is to decide the amount of condensation of water after the water vapour diffusion.
- Then water content is calculated from the diffusion (5.5) with the help of (5.8) and (5.9).
- This entire procedure is repeated for each time step.

Table 5.1 The material parameters and the diffusion coefficient for the Matlab model

Symbol	**Value**	**Temperature (T) and water content (W) dependence**
Thermal conductivity, k [W m^{-1} K^{-1}]	0.1133	–
Density, ρ [kg m^{-3}]	380	170 + (380 × W)
Specific heat, c_p [J kg^{-1} K^{-1}]	1941	–
Convection heat transfer coefficient, h_{cnv} [W m^{-2} K^{-1}]	8.687	–
heat transfer coefficient, h_{rad} [W m^{-2} K^{-1}]	15.42	–
Emissivity, ε	0.9	–
Diffusion coefficient for water, $D_{(H2O,l)}$ [m^2 s^{-1}]	9.58 ×(10) $^{-9}$	–
Initial water content of the oven air W_{air} [kg (H_20,l) kg^{-1}(product)]	0.0354	–
Diffusion coefficient for vapour, $D_{(H2O,g)}$ [m^2 s^{-1}]	8 × (10) $^{-7}$	9 × (10) $^{-12}$ × T^2
Mass transfer coefficient for vapour, $k_{d(H2O,g)}$ [kg m^{-2} s^{-1}]	120	3.2 × (10)^9 T^{-3}
Mass transfer coefficient for water, $k_{d(H2O,l)}$ [kg m^{-2} s^{-1}]	0.01	(1.4 × (10) $^{-3}$ × T) + (0.27 × W) – (4.0 × (10) $^{-4}$ × T × W) – (0.77 × W^2)

5.1.2 Numerical Methods

The numerical method used for the differentiation was an unconditionally stable finite difference method, implicit Euler [121]. The equations were then connected by the partial water vapour pressure

according to the calculation algorithm described earlier. The source code was written in Matlab. The step sizes in space and time were 1.25 mm and 15 s, respectively.

When the time interval is less than 15 seconds, say at $\Delta t = 10s$ and $\Delta t = 5s$, numerical computation gives divergent results for temperature and moisture. When the time interval is large, these higher values of moisture contents does not have a great influence on the system of governing equations since for the next time step, the increase in moisture values matches with the increase in temperature with respect to the large time interval. It means that when the time increment is longer, the temperature is getting higher in each step and hence the moisture values has to be higher.

5.1.3 Discretization of Governing Equation

Equations for heat transfer and diffusion of water and water vapor were taken from Powathil [70].

Heat Transfer Equation

Equation for heat transfer is discretized as described by Powathil [70],

$$\frac{\partial T}{\partial t} = \frac{1}{\rho c_p}\frac{\partial}{\partial x}\left(k\frac{\partial T}{\partial x}\right) + \frac{\lambda}{c_p}\frac{\partial W}{\partial t} + \frac{\lambda W}{\rho c_p}\frac{\partial \rho}{\partial t}, \tag{5.13}$$

Since

$$\frac{\partial W}{\partial t} = \frac{\partial}{\partial x}\left(D_{(\mathrm{H20,l})}\frac{\partial W}{\partial x}\right) \tag{5.14}$$

For simplicity, this heat transfer equation can be rewritten by ignoring the last term since it doesn't make a significant contribution to the total heat transfer (which is verified using simulations) and thus the governing equation for heat transfer becomes [31],

$$\frac{\partial T}{\partial t} = \frac{1}{\rho c_p}\frac{\partial}{\partial x}\left(k\frac{\partial T}{\partial x}\right) + \frac{\lambda}{c_p}\frac{\partial}{\partial x}\left(D_{(\mathrm{H20,l})}\frac{\partial W}{\partial x}\right) \tag{5.15}$$

Taking k and $D_{(\mathrm{H20,l})}$ outside the derivative since they are constants (by using the chain rule) and then discretizing,

$$\begin{aligned}\frac{T_{i,j+1} - T_{i,j}}{\Delta \mathrm{t}} = \\ = \frac{k}{\rho c_p}\left((1-\theta)\left(\frac{T_{i-1,j+1} - 2T_{i,j+1} + T_{i+1,j+1}}{(\Delta x)^2}\right) + (\theta)\left(\frac{T_{i-1,j} - 2T_{i,j} + T_{i+1,j}}{(\Delta x)^2}\right)\right) \\ + \frac{\lambda\, D_{(\mathrm{H20,l})}}{c_p}\left(\frac{W_{i-1,j} - 2W_{i,j} + W_{i+1,j}}{(\Delta x)^2}\right)\end{aligned} \tag{5.16}$$

Equivalently,

$$\begin{aligned}-\alpha_1 T_{i-1,j+1} + (1+2\alpha_1)T_{i,j+1} - \alpha_1 T_{i+1,j+1} = \alpha_2 T_{i-1,j} + (1-2\alpha_2)T_{i,j} \\ + \alpha_2 T_{i+1,j} + \alpha_3\left(W_{i-1,j} - 2W_{i,j} + W_{i+1,j}\right)\end{aligned} \tag{5.17}$$

where

$$\alpha_1 = \frac{k\,\Delta t}{\rho c_p (\Delta x)^2}(1-\theta), \alpha_2 = \frac{k\Delta t}{\rho c_p (\Delta x)^2}(\theta),\ \alpha_3 = \frac{\lambda\, D_{(\mathrm{H20,l})}\,\Delta t}{c_p (\Delta x)^2} \tag{5.18}$$

and the boundary conditions at $i = 0$ and $i = N$ are,

$$\begin{aligned} -k\left(\frac{T_{1,j} - T_{-1,j}}{2\Delta x}\right) = \\ = h_{\mathrm{rad}}\left(T_{\mathrm{rs}} - T_{0,\mathrm{j}}\right) + h_{\mathrm{cnv}}\left(T_{\mathrm{ffs}} - T_{0,\mathrm{j}}\right) - \\ -\lambda\ \rho\ D_{(\mathrm{H20,l})}\ k_{\mathrm{d(H20,l)}}\left(W_{0,\mathrm{j}} - W_{\mathrm{air}}\right) \end{aligned} \tag{5.19}$$

$$\frac{T_{N+1,j} - T_{N-1,j}}{2\Delta x} = 0 \tag{5.20}$$

the boundary conditions for water diffusion are,

$$\frac{W_{1,j} - W_{-1,j}}{2\Delta x} = k_{\mathrm{d(H20,l)}}\left(W_{0,j} - W_{\mathrm{air}}\right) \tag{5.21}$$

$$\frac{W_{N+1,j} - W_{N-1,j}}{2\Delta x} = 0 \tag{5.22}$$

or it can be written as,

$$\begin{aligned} T_{-1,j} = T_{1,j} - \left(\frac{2\Delta x(h_{\mathrm{rad}} + h_{\mathrm{cnv}})}{k}\right)T_{0,j} + \frac{2\Delta x h_{\mathrm{rad}}}{k}T_{\mathrm{rad}} + \frac{h_{\mathrm{cnv}}}{k}T_{\mathrm{ffs}} \\ -2\Delta\, x\, \lambda\, \rho\, D_{(\mathrm{H20,l})}\, k_{\mathrm{d(H20,l)}}\left(W_{0,\mathrm{j}} - W_{\mathrm{air}}\right) \end{aligned} \tag{5.23}$$

$$T_{N+1,j} = T_{N-1,j} \tag{5.24}$$

$$W_{-1,j} = W_{1,j} - 2\Delta\, x\ \ k_{\mathrm{d(H20,l)}}\left(W_{0,\mathrm{j}} - W_{\mathrm{air}}\right) \tag{5.25}$$

$$W_{N+1,j} = W_{N-1,j} \tag{5.26}$$

From (5.15) it can be seen that for calculating the T at $(j+1)^{\mathrm{th}}$ time level it requires other two $(j+1)^{\mathrm{th}}$ level unknown values of T and known values at $(j)^{\mathrm{th}}$ level. That is, even though initial data $T_{\mathrm{i},0}$ $i = 0, 1, 2 \ldots$. M are known, it is not possible to get the values of the unknown at the $(j+1)^{\mathrm{th}}$ level with a single explicit step (using (5.15) only once) but by using the equation for $i = 0, 1, 2 \ldots N$ and solving linear system thus formed for the unknowns with the help of boundary conditions of heat transfer equation and diffusion equation. At boundary, (5.15) becomes,

$$\begin{aligned} -\alpha_1 T_{-1,j+1} + (1+2\alpha_1)T_{0,j+1} - \alpha_1 T_{1,j+1==\alpha_2 T_{-1,j}} + (1-2\alpha_2)T_{0,j} \\ +\alpha_2 T_{1,j} + \alpha_3\left(W_{-1,j} - 2W_{0,j} + W_{1,j}\right) \end{aligned} \tag{5.27}$$

$$\begin{aligned} -\alpha_1 T_{N-1,j+1} + (1+2\alpha_1)T_{N,j+1} - \alpha_1 T_{N+1,j+1} = \alpha_2 T_{N-1,j} \\ +(1-2\alpha_2)T_{N,j} + \alpha_2 T_{N+1,j} \\ +\alpha_3\left(W_{N-1,j} - 2W_{N,j} + W_{N+1,j}\right) \end{aligned} \tag{5.28}$$

here the ghost points $T_{-1,j}, T_{-1,j+1}, T_{N+1,j}, T_{N+1,j+1}, W_{-1,j}$ and $W_{N+1,j}$ are replaced and the following linear system is obtained,

$$AX = B$$

where

$$A = \begin{pmatrix} 1+2\alpha_1\left(1+\frac{2\Delta x(h_{\text{rad}}+h_{\text{cnv}})}{k}\right) & -2\alpha_1 & 0 & - & - & 0 & 0 & 0 \\ -\alpha_1 & 1+2\alpha_1 & -\alpha_1 & - & - & 0 & 0 & 0 \\ - & - & - & - & - & - & - & - \\ 0 & 0 & 0 & - & - & -\alpha_1 & 1+2\alpha_1 & -\alpha_1 \\ 0 & 0 & 0 & - & - & 0 & -2\alpha_1 & 1+2\alpha_1 \end{pmatrix} \tag{5.29}$$

where

$$B = \begin{pmatrix} \alpha_2 T_{-1,j} + (1-2\alpha_2)T_{0,j} + \alpha_2 T_{1,j} + \alpha_3\left(W_{-1,j} - 2W_{0,j} + W_{1,j}\right) + C \\ \alpha_2 T_{0,j} + (1-2\alpha_2)T_{1,j} + \alpha_2 T_{2,j} + \alpha_3\left(W_{0,j} - 2W_{1,j} + W_{2,j}\right) \\ \dots \\ \alpha_2 T_{N-2,j} + (1-2\alpha_2)T_{N-1,j} + \alpha_2 T_{N,j} + \alpha_3\left(W_{N-2,j} - 2W_{N-1,j} + W_{N,j}\right) \\ \alpha_2 T_{N-1,j} + (1-2\alpha_2)T_{N,j} + \alpha_2 T_{N-1,j} + \alpha_3\left(W_{N-1,j} - 2W_{N,j} + W_{N-1,j}\right) \end{pmatrix} \tag{5.30}$$

$$X = \begin{pmatrix} T_{0,j+1} \\ T_{1,j+1} \\ \dots \\ T_{N-1,j+1} \\ T_{N,j+1} \end{pmatrix} \tag{5.31}$$

and

$$C = \alpha_1\left(\frac{2\Delta x h_{\text{rad}}}{k}T_{\text{rs}} + \frac{2\Delta x h_{\text{cnv}}}{k}T_{\text{ffs}}\right) - 2\Delta x\lambda\,\rho\, D_{(\text{H20,l})}\, k_{\text{d(H20,l)}}\left(W_{0,\text{j}} - W_{\text{air}}\right) \tag{5.32}$$

the unknown values of temperature at discrete points are obtained by solving this linear system. This is repeated for each time interval till it reaches the final time.

Diffusion Equation for Water Vapor

The diffusion equation for vapor is discretized in the following way as described by Powathil [70],

$$\frac{V_{i,j+1} - V_{i,j}}{\Delta t} = \frac{\left(D_{(\text{H20,g})}\frac{\partial V}{\partial x}\right)_{i+1,j} - \left(D_{(\text{H20,g})}\frac{\partial V}{\partial x}\right)_{i,j}}{\Delta x} \tag{5.33}$$

$$= \frac{(D_{(\text{H20,g})})_{i+1,j}V_{i+1,j} - \left(D_{(\text{H20,g})}\right)_{i+1,j} + ((D_{(\text{H20,g})})_{i,j})V_{i,j} + (D_{(\text{H20,g})})_{i,j}V_{i-1,j}}{(\Delta x)^2} \tag{5.34}$$

If we use θ method it can be written as,

$$\frac{V_{i,j+1} - V_{i,j}}{\Delta t} = \tag{5.35}$$

$$= (\theta)\left(\frac{\left(D_{(H20,g)}\right)_{i+1,j}V_{i+1,j} - \left(\left(D_{(H20,g)}\right)_{i+1,j} + \left(D_{(H20,g)}\right)_{i,j}\right)V_{i,j} + \left(D_{(H20,g)}\right)_{i,j}V_{i-1,j}}{(\Delta x)^2}\right) +$$

$$+(1-\theta)\left(\frac{\left(D_{(H20,g)}\right)_{i+1,j+1}V_{i+1,j+1}-\left(\left(D_{(H20,g)}\right)_{i+1,j+1}+\left(D_{(H20,g)}\right)_{i,j+1}\right)V_{i,j+1}+\left(D_{(H20,g)}\right)_{i,j}V_{i-1,j+1}}{(\Delta x)^2}\right)$$

or it can be written as,

$$\begin{aligned}
&-\alpha_1\left(D_{(H20,g)}\right)_{i,j+1}V_{i-1,j+1}\\
&+\left(1+\alpha_1\left(\left(D_{(H20,g)}\right)_{i+1,j+1}+\left(D_{(H20,g)}\right)_{i,j+1}\right)\right)V_{i,j+1}\\
&-\alpha_1\left(D_{(H20,g)}\right)_{i+1,j+1}V_{i+1,j+1}\\
&=\alpha_2\left(D_{(H20,g)}\right)_{i,j}V_{i-1,j}\\
&+\left(1-\alpha_2\left(\left(D_{(H20,g)}\right)_{i+1,j}+\left(D_{(H20,g)}\right)_{i,j}\right)\right)V_{i,j}\\
&+\alpha_2\left(D_{(H20,g)}\right)_{i+1,j}V_{i+1,j}
\end{aligned} \tag{5.36}$$

where

$$\alpha_1=\frac{\Delta t}{(\Delta x)^2}(1-\theta),\ and\ \ \alpha_2=\frac{\Delta t}{(\Delta x)^2}(\theta) \tag{5.37}$$

The boundary conditions are

$$\frac{V_{1,j}-V_{-1,j}}{2\Delta x}=\ k_{d(H20,g)}(V_{0,j}-V_{air}) \tag{5.38}$$

$$\frac{V_{N+1,j}-V_{N-1,j}}{2\Delta x}=0 \tag{5.39}$$

Then at each time interval a linear system $AX = B$ is formulated by varying i = 0, 1, 2,... N and with the help of the boundary conditions like it is mentioned in the case of heat transfer equation. This is solved for the unknown value of the vapor at each time interval. Here,

$$A=\begin{pmatrix}
1+\alpha_1\beta & -\alpha_1\xi_0 & 0 & - & - & 0 & 0 & 0\\
-\alpha_1\beta_1 & (1+\alpha_1\xi_1) & -\alpha_1\beta_2 & - & - & 0 & 0 & 0\\
- & - & - & - & - & - & - & -\\
0 & 0 & 0 & - & - & -\alpha_{N-1} & (1+\alpha_1\xi_{N-1}) & -\alpha_1\beta_N\\
0 & 0 & 0 & - & - & 0 & -\alpha_1\xi_N & (1+\alpha_1\xi_N)
\end{pmatrix} \tag{5.40}$$

where

$$\beta=\left(\left(D_{(\mathrm{H20,g})}\right)_{1,j+1}+\left(D_{(\mathrm{H20,g})}\right)_{0,j+1}(1+2\Delta x\ k_{\mathrm{d(H20,g)}})\right) \tag{5.41}$$

$$\beta_i=\left(D_{(\mathrm{H20,g})}\right)_{i,j+1} \tag{5.42}$$

$$\xi_i=\left(\left(D_{(\mathrm{H20,g})}\right)_{i,j+1}+\left(D_{(\mathrm{H20,g})}\right)_{i+1,j+1}\right) \tag{5.43}$$

$$B = \begin{pmatrix} \alpha_2\left(D_{(H20,g)}\right)_{0,j} V_{-1,j} + (1-\alpha_2\eta_0)V_{0,j} + \alpha_2\left(D_{(H20,g)}\right)_{1,j} V_{1,j} + 2\alpha_1\left(D_{(H20,g)}\right)_{0,j+1} \Delta x k_{d(H20,l)} V_{air} \\ \alpha_2\left(D_{(H20,g)}\right)_{1,j} V_{0,j} + (1-\alpha_2\eta_1)V_{1,j} + \alpha_2\left(D_{(H20,g)}\right)_{2,j} V_{2,j} \\ \dots \\ \alpha_2\left(D_{(H20,g)}\right)_{N-1,j} V_{N-2,j} + (1-\alpha_2\eta_{N-1})V_{N-1,j} + \alpha_2\left(D_{(H20,g)}\right)_{N,j} V_{N,j} \\ \alpha_2\left(D_{(H20,g)}\right)_{N,j} V_{N-1,j} + (1-\alpha_2\eta_N)V_{N,j} + \alpha_2\left(D_{(H20,g)}\right)_{N,j} V_{N-1,j} \end{pmatrix} \tag{5.44}$$

where

$$\eta_0 = \left(\left(D_{(\mathrm{H20,g})}\right)_{i,j} + \left(D_{(\mathrm{H20,g})}\right)_{i+1,j}\right) \tag{5.45}$$

and

$$X = \begin{pmatrix} V_{0,j+1} \\ V_{1,j+1} \\ \dots. \\ V_{N-1,j+1} \\ V_{N,j+1} \end{pmatrix} \tag{5.46}$$

Diffusion Equation for Liquid Water

The liquid water diffusion equation is discretized as follows as described by Powathil [70] (Since $D_{(\mathrm{H20,l})}$ is a constant, it is pulled outside the derivative by using the chain rule),

$$\begin{aligned} \frac{W_{i,j+1} - W_{i,j}}{\Delta t} = \\ = D_{(\mathrm{H20,l})}\left((1-\theta)\left(\frac{W_{i-1,j+1} - 2W_{i,j+1} + W_{i+1,j+1}}{(\Delta x)^2}\right)\right) + \\ + \theta\left(\frac{W_{i-1,j} - 2W_{i,j} + W_{i+1,j}}{(\Delta x)^2}\right) \end{aligned} \tag{5.47}$$

or

$$\begin{aligned} -\alpha_1 W_{i-1,j+1} + (1+2\alpha_1)W_{i,j+1} - \alpha_1 W_{i+1,j+1} = \\ = \alpha_2 W_{i-1,j} + (1-2\alpha_2)W_{i,j} + \alpha_2 W_{i+1,j} \end{aligned} \tag{5.48}$$

where,

$$\alpha_1 = \frac{D_{(\mathrm{H20,l})}\Delta t}{(\Delta x)^2}(1-\theta), and \;\; \alpha_2 = \frac{D_{(\mathrm{H20,l})}\Delta t}{(\Delta x)^2}(\theta) \tag{5.49}$$

The boundary conditions are,

$$\frac{W_{1,j} - W_{-1,j}}{2\Delta x} = k_{d(H20,l)}\left(W_{0,j} - W_{air}\right) \tag{5.50}$$

$$\frac{W_{N+1,j} - W_{N-1,j}}{2\Delta x} = 0 \tag{5.51}$$

The corresponding linear system is *AX=B,* where,

$$A = \begin{pmatrix} 1+\alpha_1\left(2+2\Delta x k_{d(H20,l)}\right) & -2\alpha_1 & 0 & - & - & 0 & 0 & 0 \\ -\alpha_1 & (1+2\alpha_1) & -\alpha_1 & - & - & 0 & 0 & 0 \\ - & - & - & - & - & - & - & - \\ 0 & 0 & 0 & - & - & -\alpha_1 & (1+2\alpha_1) & -\alpha_1 \\ 0 & 0 & 0 & - & - & 0 & -2\alpha_1 & (1+2\alpha_1) \end{pmatrix} \quad (5.52)$$

$$B = \begin{pmatrix} \alpha_2 W_{-1,j} + (1-2\alpha_2)W_{0,j} + \alpha_2 W_{1,j} + 2\alpha_1 \Delta x k_{d(H20,l)} W_{air} \\ \alpha_2 W_{0,j} + (1-2\alpha_2)W_{1,j} + \alpha_2 W_{2,j} \\ \dots \\ \alpha_2 W_{N-2,j} + (1-2\alpha_2)W_{N-1,j} + \alpha_2 W_{N,j} \\ \alpha_2 W_{N-1,j} + (1-2\alpha_2)W_{N,j} + \alpha_2 W_{N-1,j} \end{pmatrix} \quad (5.53)$$

$$X = \begin{pmatrix} W_{0,j+1} \\ W_{1,j+1} \\ \dots . \\ W_{N-1,j+1} \\ W_{N,j+1} \end{pmatrix} \quad (5.54)$$

and,

$$W_{-1,j} = W_{1,j} - 2\Delta x \, k_{d(H20,l)}(W_{0,j} - W_{air}) \quad (5.55)$$

The linear system is solved for each time interval for the liquid water.

5.2 Results and Discussions

In Figures 5.1 to 5.3 it can be seen that the simulated water content at the surface decreases rapidly when the temperature increases. The simulated water content at halfway to the center at first increases a little and then starts to decrease and the simulated temperature remains on a plateau while the water content starts to decrease. In the center, the water content increases in the beginning and then it slowly starts to decrease.

When the bread sample is placed in the oven, the surface temperature rises quickly, while the temperature rise in the center is slower. As the temperature increases, the partial water vapour pressure in the pores inside the bread increases. This means that the partial water vapour pressure close to the surface becomes higher than in the center. The water vapour therefore starts moving towards the center and towards the surface to reduce the pressure difference. These results are in agreement with those obtained by Thorvaldsson, Skjöldebrand [58].

In the center, where the temperature is lower, however, the water vapour condenses. In the oven where the temperature is high, the partial water vapour pressure is far from saturation. The water vapour from the surface diffuses into the air and the surface starts to dry out. Underneath the surface where liquid water still exists, water is evaporated to saturate the partial water vapour pressure. The water vapour diffuses towards the surface or towards the center and more water is evaporated until there is no liquid water left. A drying zone is developed which slowly increases in size [31].

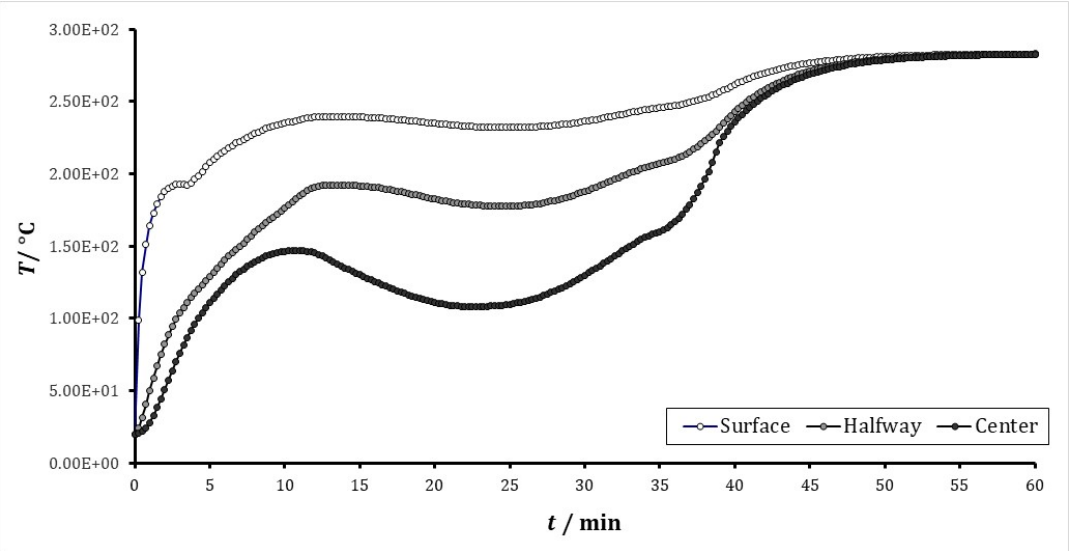

Fig. 5.1 The simulated temperatures versus time

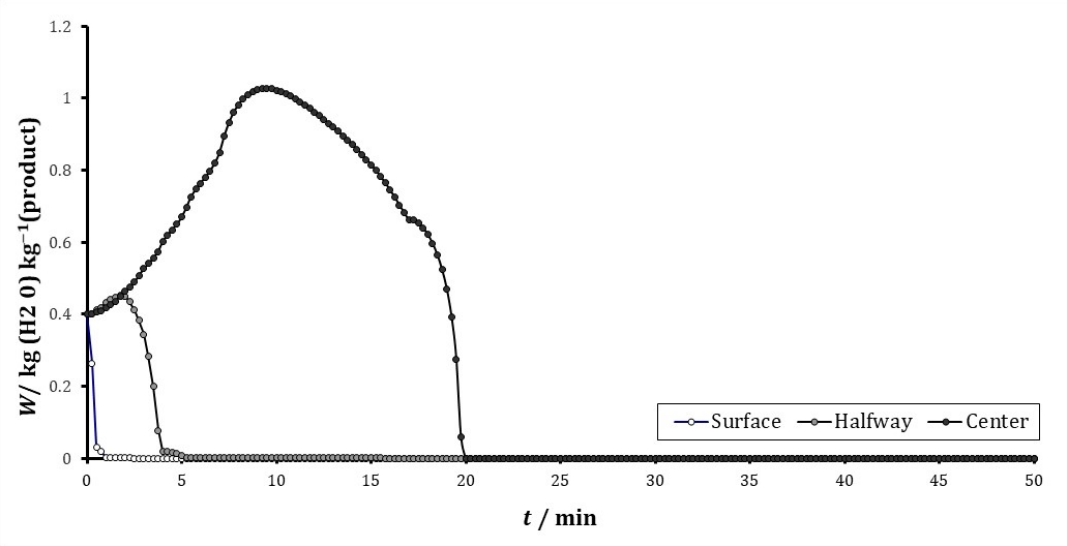

Fig. 5.2 The simulated liquid water content versus time

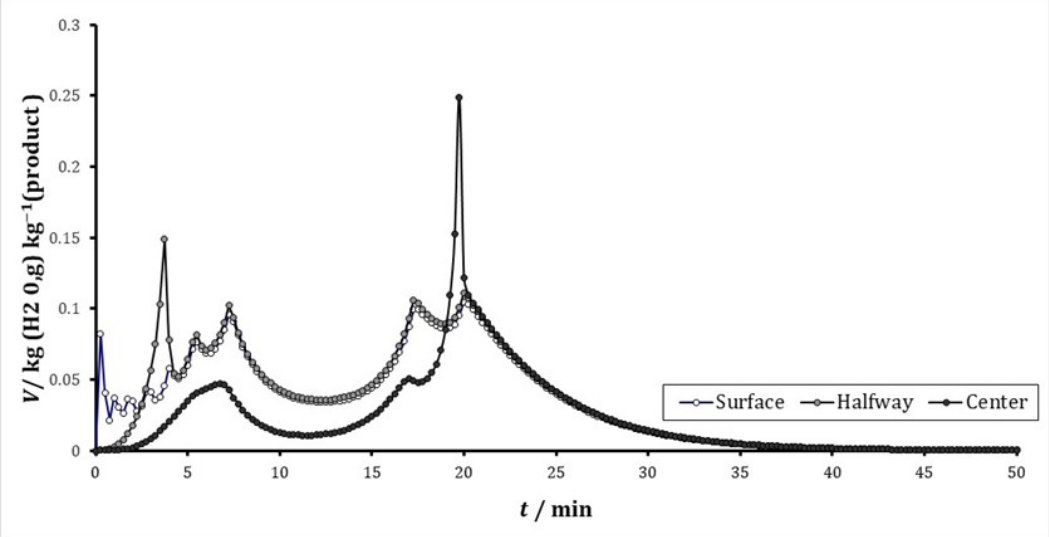

Fig. 5.3 The simulated water vapor content versus time.

It is worth to note that in the center and towards the center where the water vapour condenses, the liquid water content increases. This means that a liquid water content gradient is built up. The liquid water therefore starts moving in the opposite direction of the water vapour, i.e. towards the surface. This transport, however, is much slower than the vapour transport [120].

In order to study the behavior of the temperature, liquid water and water vapor and with respect to the time interval, the profiles are drawn with respect to time. Several critical values in the temperature and moisture profiles are also taken as the characteristic values of the process. The first critical value is the time when bread temperature reaches 100 °C. During baking, crumb converts to crust at this temperature where all liquid water evaporates, see Fig. 5.4. The second critical value is the time when the liquid water content at the center of bread reaches its peak, see Fig. 5.5. The third critical value is the level of the peaked liquid water content at the center (Fig. 5.6). This value, although higher than the initial moisture content of the dough, should be reasonably restrained due to the small diffusivity of water vapour in bread.

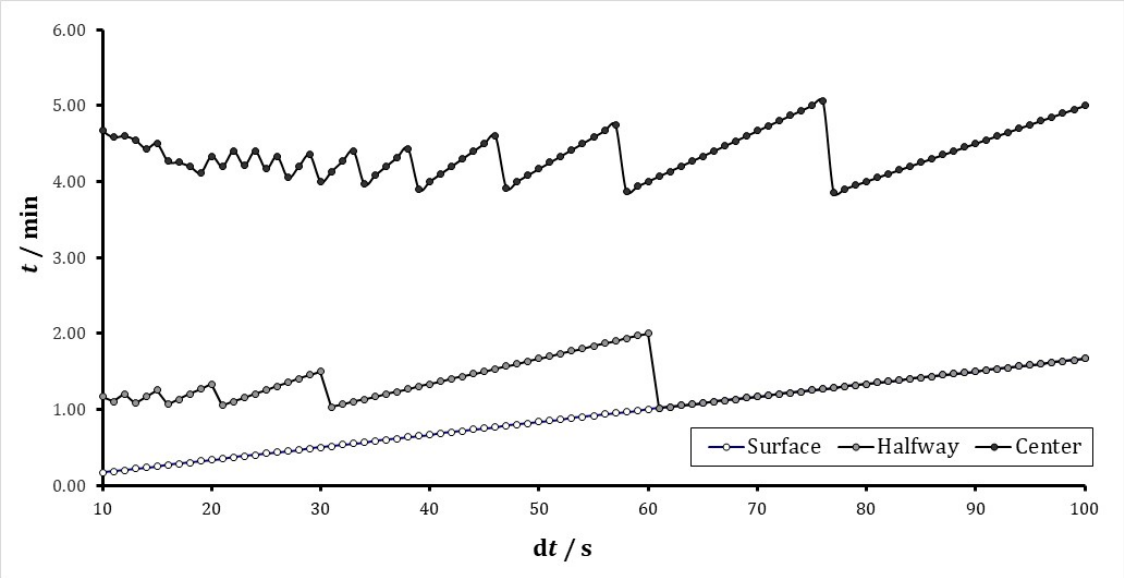

Fig. 5.4 The time when bread temperature reaches 100 °C

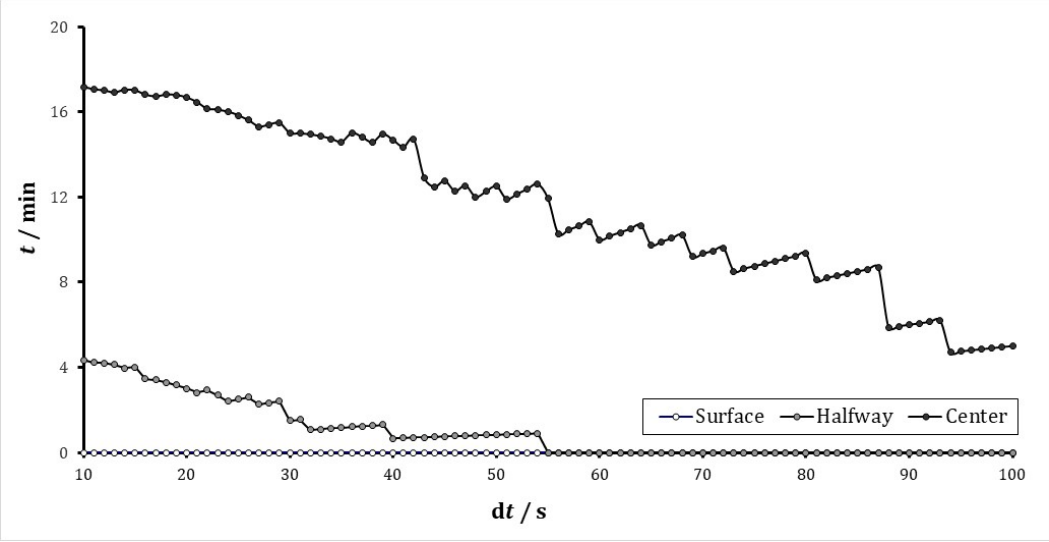

Fig. 5.5 The time when the liquid water content reaches its peak

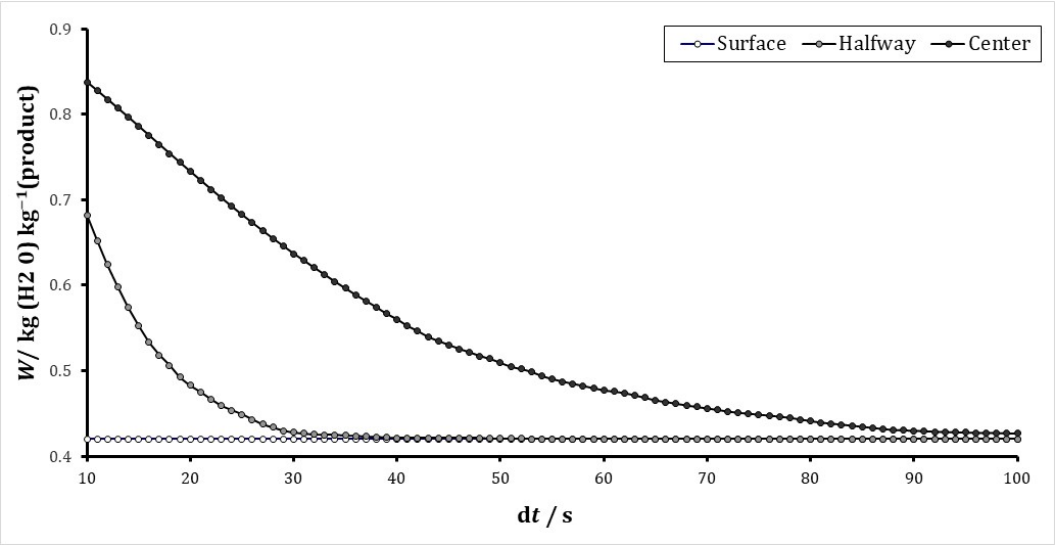

Fig. 5.6 The level of the peaked liquid water content

The numerical solution was sensitive to the value of time step Δt. Both small Δt and large Δt yielded useless results. Figures 5.4 to 5.6 show the sensitivity of the numerical solution to Δt in the range of 10 s –100 s by which satisfactory results were produced. These results were in agreement with those obtained by Zhou [117].

6 Energy and Exergy Analysis of Continuous Baking Process in Direct Heating Oven

The increased attention that the world's energy resources are limited has caused scientists to take a closer look at the energy conversion devices and to develop new techniques to better utilize the existing limited resources. Energy cannot be created or destroyed from the point view of the first law of thermodynamics which manages the quantity of energy, on the other hand, the second law of thermodynamics manages the quality of energy which is subject to disintegration during a process as a result of the entropy generation.

Exergy is characterized as the greatest work which can be made by a system as it comes to the full equilibrium with a reference environment. Exergy analysis is a method for assessing systems and processes [122,3]. Energy analysis is based on the first law of thermodynamics while exergy is based on the first and second laws. Exergy is destroyed during the irreversibilities.

Exergy analysis is a powerful tool for evaluating, developing and improving a thermal system, particularly when this analysis is part of an exergoeconomic analysis. However, exergy analysis not being very familiar among energy practitioners [123].

The common fossil fuel used in industrial, commercial and domestic applications is natural gas. Many efforts made to control natural gas emissions, even though its emissions per unit fuel energy are lower than those for oil and coal.

As natural gas consumption increases, fluctuating costs and market competition often force manufacturers to enhance natural gas efficiency and reduce fuel consumption.

For most gas-fired furnaces and boilers, one possible answer to environmental and economic concerns is to use the regenerative burner technology. The regenerative technology is not a new one. However, the application of some new techniques to the conventional regenerators and burners can bring the thermodynamic benefits. It needs to be investigated whether or not a regenerative burner system is more efficient to combustion performance, and whether or not it is more beneficial to energy efficiency improvement on natural gas-fired furnaces, such as heating furnaces.

The aim of this chapter is to identify and discuss the efficiency improvement after the implementation of a new burner system on a heating furnace. The prime objective of the study is to apply exergy analysis to a specific industrial application.

6.1 Methodology

The bread is produced as 140 gram per loaf. The main production stages of the process are:

- *Mixing:* raw ingredients are transferred from large storage silos into dough mixers according to the required recipe. The resulting dough is mixed intensely for a few minutes. Under these conditions the yeast can begin to grow and the dough will start to become elastic;
- *Primary fermentation:* the dough is allowed to rest in a trough for a few minutes;
- Dividing: the large dough mass is tipped into a divider which produces dough pieces of the correct weight for the product being made;

- *Molding:* the dough pieces are then processed through a molding machine to achieve the appropriate shape for baking;
- *Final fermentation:* the bread achieving approximately 90 % of its final size. This expansion is the result of the yeast growing and producing CO_2;
- *Baking:* the bread is then backed for a few second, depending on the specific requirements of the product.

A single continuous running conveyor belt oven was used as an example. The oven contains of one direct-heated baking chamber (constructed mainly of medium – duty straight fireclay brick of 30% alumina content and super-duty straight and side arches fireclay brick of 42 % alumina content for the inner walls and arch) while the outer walls were built using traditional red brick. The inner brick construction is covered with flat thermal insulated steel sheet iron covers. The oven has a steel frame and steel angle bars work as guides for the conveyor belts chains. Steel conveyor chains with dimensions of 450 x 75 cm.

Manual operation furnace has undergone only minor improvements that cannot affect to the significant changes in operating efficiency. After some research, a decision was made to replace the inefficient conventional gas burner in the baking bread furnace operation in order to improve the baking performance. This is to preheat combustion air by reclaiming heat from the flue exhaust.

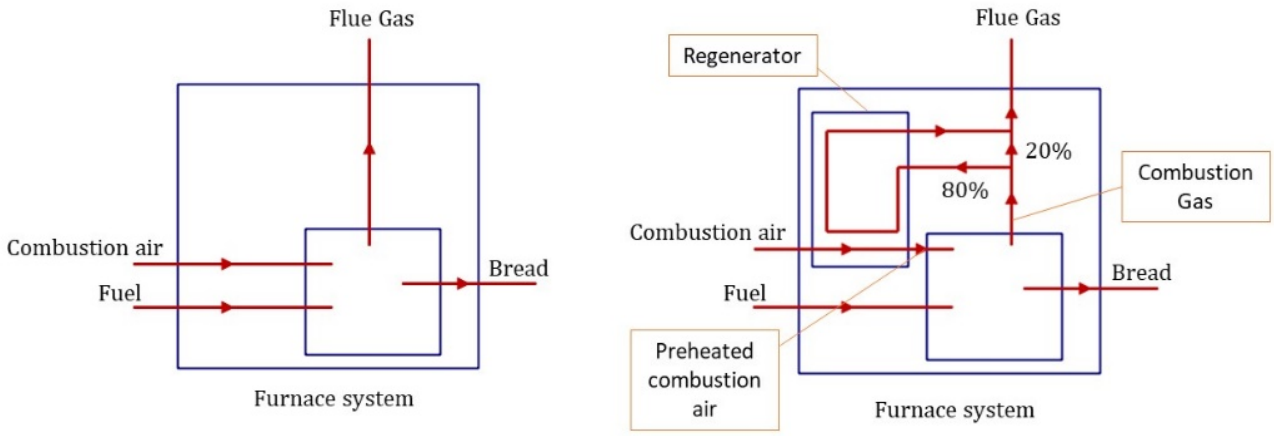

Fig. 6.1 Oven operation before and after upgrading

Figure 6.1 illustrates the change before and after upgrading. Discharge from the oven is bread. One rectangular frame represents the combustion chamber. The largest frame represents the furnace system as a whole, which consists of the chamber, the stack and the regenerator.

6.1.1 Analysis of the Process

The information of process and production was obtained from the operation control system, facilities administration personnel, and archived documents.

To permit a reasonable comparison, this study examines the energy and exergy consumption involved in 700 kg (5000 loaves) production before and after the upgrade. Fuel consumption corresponds to the daily log of natural gas meter readings, 5000 loaves require on average 32.4 m^3 fuel before the upgrade and 23.1 m^3 fuel after the upgrade. Natural gas pressure was 115 k Pa and has been increased to 170 k Pa while new burners are installed, and its density value is approximately 0.74 kg m^{-3}.

Combustion air is supplied by a supply fan and taken directly from indoor air at the plant. To balance the plant indoor air pressure, the plant pressurization is controlled by a group of air handling units. The quantity of combustion air and the quantity of stack flue gas are computed from the quantity of fuel consumed. Before upgrades, the plant recorded the temperature of the flue gas for the oven as 660 K. After upgrades, the furnace monitoring system displays a mean temperature of Combustion gas at 680 K and also records flue gas temperature at 420 K while flue gas exits regenerator. In this study, "combustion gas" is used for the gas exits furnace chamber and enters regenerator. Figures 6.2 and 6.3 illustrate the process before and after upgrading project.

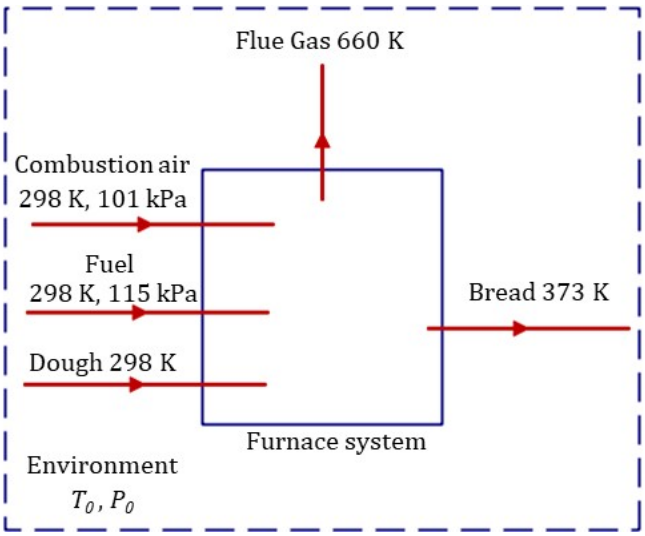

Fig. 6.2 The process before upgrades

The big rectangular frame represents the furnace system, which consists of a combustion chamber, stack, and regenerator (after upgrades). The small rectangular frame presents the combustion chamber where high temperature combustion takes place. The dashed rectangular frame denotes the boundary of the combined system, which includes furnace system and reference environment, which is assumed to be 25 °C and 1.01×10^5 Pa (1 atm).

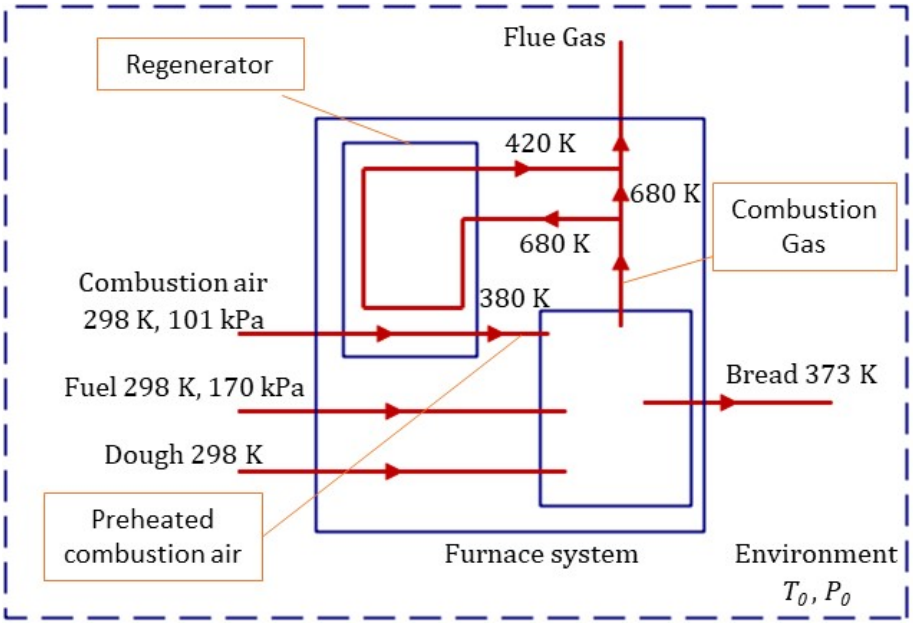

Fig. 6.3 The process after upgrades

It is worth noting that after upgrades, the regenerator is a part of furnace system but is examined as an individual device as well one energy/exergy input to regenerator is the energy/exergy of combustion gas entering regenerator, and one energy/exergy output is the energy/exergy of flue gas exiting regenerator and exhausted through stack. Another energy/exergy input to regenerator is the combustion air, which flows through regenerator and another energy/exergy output is the preheated combustion air.

6.1.2 Thermodynamic Analysis of Furnace

Energy and exergy balances and efficiencies are obtained for the furnace system, following the approach described by Moran et al. [124]. The reference-environment temperature T_0 and pressure P_0 are assumed to be equal to 25 °C and 1 atm, respectively.

Assumptions

The following assumptions are made:

- The systems assessed operates at steady state and has no work interactions.
- The fuel and flue gas products behave as ideal gas mixtures.
- Flue gas products exit the furnace through the stack.
- Electricity consumption for motors, monitoring, and control devices is neglected because it is small compared to the fuel energy.
- The fuel supplied by the natural gas vendor includes nitrogen (N_2), carbon dioxide (CO_2), hydrogen sulfide (H_2S) and water vapor (H_2O), the volumes of N_2, CO_2, H_2S and H_2O are neglected because they are small.
- The kinetic and potential energy effects are negligible.

Chemical Equation

The chemical equation for the complete combustion of methane is:

$$CH_4 + 2\,O_2 \rightarrow CO_2 + 2H_2O \tag{6.1}$$

Considering combustion air which supplies O_2 is taken from the environment, the above equation becomes:

$$CH_4 + 2\,(O_2 + 3.76\,N_2) \rightarrow CO_2 + 7.52\,N_2 + 2H_2O \tag{6.2}$$

On a molar basis, the air–fuel ratio is

$$(AFR)_{\text{theo}} = \frac{2}{1}\,x\,4.76 = 9.52 \tag{6.3}$$

In actual furnace operation, *AFR* is always higher than $(AFR)_{\text{theo}}$. Before upgrades, *AFR* ratio was controlled by furnace operators observing the flame color. After upgrades, regenerative burner's PLC control system adjusts the actual air-fuel ratio mainly based on furnace temperature. The actual chemical equation becomes

$$CH_4 + n\,(O_2 + 3.76\,N_2) \rightarrow CO_2 + (n-2)\,O_2 + 3.76n\,N_2 + 2\,H_2O \qquad (6.4)$$

Natural gas supplied is not pure methane (CH_4). The natural gas composition is shown in Table 6.1. The molar enthalpy and Gibbs function of formation at the reference environment of fuel natural gas are calculated in the following table.

Table 6.1 Natural gas composition

Substance	**Chemical Form**	y_i	$\bar{h}^{o}_{f\,(fuel)}$ / kJ kmol^{-1}	$\bar{g}^{o}_{f\,(fuel)}$ / kJ kmol^{-1}
Methane	CH_4	0.90	–67.365	–50.790
Ethane	C_2H_6	0.046 3	–3.921	–32.890
Propane	C_3H_8	0.039 1	–4.061	–23.490
Butane	C_4H_{10}	0.009 8	–1.236	–15.710
Pentane	C_5H_{12}	0.000 8	–117.00 0	–8.200
Natural Gas		1.0	–76.700	–48.313

To introduce natural gas composition to (6.4).

$$\begin{gathered}(0.9\,CH_4 + 0.046\,3\,C_2H_6 + 0.039\,1\,C_3H_8 + 0.009\,8\,C_4H_{10} + \\ +0.000\,8\,C_5H_{12}) + n\,(O_2 + 3.76\,N_2) \rightarrow \\ \rightarrow 1.15\,CO_2 + (n-2.225)O_2 + (3.76n)N_2 + 2.15\,H_2O\end{gathered} \qquad (6.5)$$

In the following discussions, n_1 and n_2 are defined as coefficients in (6.5) for before upgrades and after upgrades, respectively.

Before upgrades, stack testing (on a wet basis) on the furnace was conducted by the plant, 5 % O_2 in volume of emission was found in the flue gas exhaust. According to (6.5)

$$\frac{(n_1 - 2.225)}{[1.15 + (n_1 - 2.225) + 3.76\,n_1 + 2.15]} = 5\% \qquad (6.6)$$

Thus, n_1 = 2.99 makes (6.5) balanced. Thus, before upgrading project, chemical equation is:

$$\begin{gathered}1(\text{Fuel}) + 2.99\,O_2 + 11.24\,N_2 \rightarrow \\ \rightarrow 1.15\,CO_2 + 0.765\,O_2 + 11.24\,N_2 + 2.15\,H_2O\end{gathered} \qquad (6.7)$$

Then, ratio $(AFR)_1$ = (2.99/ 1) x 4.76 = 14.232.

After upgrades, the regenerative burner's emission analysis is based on lab testing for this type of burner. The testing was carried out in the manufacturer's lab, Bloom Engineering. 1.74 % O_2 is found in flue gas. From (6.5), it gives:

$$\frac{(n_2 - 2.225)}{[1.15 + (n_2 - 2.225) + 3.76\,n_2 + 2.15]} = 1.74\,\% \qquad (6.8)$$

So n_2 = 2.45 and the (6.5) is balanced. Thus, after upgrading project, chemical equation is:

$$1(\text{Fuel}) + 2.45\ O_2 + 9.21\ N_2 \rightarrow \rightarrow 1.15\ CO_2 + 0.225\ O_2 + 9.21\ N_2 + 2.15\ H_2O \quad (6.9)$$

Then, ratio $(AFR)_2$ = (2.45/1) x 4.76 = 11.662.

Energy Input to Furnace System

The chemical reaction (fuel combustion) generates the majority of energy input. It must be noted that another part of energy input is the energy associated with combustion air (and with preheated combustion air after upgrades). The two parts are calculated separately as the following.

Energy Balance of Combustion:

Since fuel and air enter the combustion chamber separately, Fig. 6.4 illustrates the combustion for the following calculation.

The lower heating value (*LHV*), H_i [kJ kmol^{-1}], is used here for calculating energy input of combustion.

$$H_i = \sum_P n_e\,(h_f^o)_e - \sum_R n_i\,(h_f^o)_i \quad (6.10)$$

where:

$$\sum_P n_e\,(h_f^o)_e = n_{CO_2}\,(\bar{h}_f^o)_{CO_2} + n_{O_2}\,(\bar{h}_f^o)_{O_2} + n_{N_2}\,(\bar{h}_f^o)_{N_2} + n_{H_2O}\,(\bar{h}_f^o)_{H_2O} \quad (6.11)$$

$$\sum_R n_i\,(h_f^o)_i = n_{fuel}\,(\bar{h}_f^o)_{fuel} + n_{O_2}\,(\bar{h}_f^o)_{O_2} + n_{N_2}\,(\bar{h}_f^o)_{N_2} = (\bar{h}_f^o)_{fuel} \quad (6.12)$$

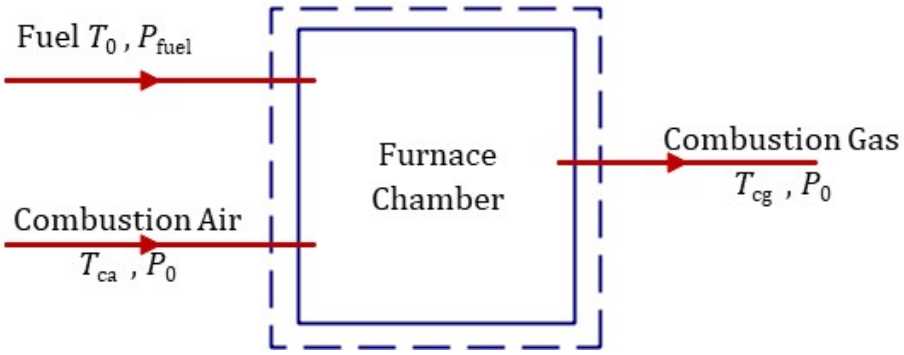

Fig. 6.4 Schematic of energy calculation of fuel combustion

The values of enthalpy of formation of the component at the reference environment are on basis of per kmole fuel. Energy input of combustion from natural source fuel can be expressed as:

$$E_{fuel} = E_{source} = n_{fuel}\,H_i \quad (6.13)$$

n_{fuel} denotes total moles of fuel consumed. With enthalpy of formation values from Moran et al. [124] calculation results are tabulated in Table 6.2.

Table 6.2 Calculation of energy input to the furnace chamber

Items	Before upgrades	After upgrades
$\sum_{\mathrm{P}} n_e\ (h_{\mathrm{f}}^{\mathrm{o}})_{\mathrm{e}}$ [MJ kmol^{-1}]	−972.5	−972.5
$\sum_{\mathrm{R}} n_{\mathrm{i}}\ (h_{\mathrm{f}}^{\mathrm{o}})_{\mathrm{i}}$ [MJ kmol^{-1}]	−76.7	−76.7
H_i [kJ kmol^{-1}]	−895.7	−895.7
n_{fuel} [kmol]	+1.33	+0.95
E_{fuel} (E_{source}) [MJ]	−1 191.4	−851

Energy Associated with Preheated Combustion air:

Another source of energy input to the system is the combustion air, and preheated combustion air (after upgrades). The energy associated with combustion air $E_{\mathrm{ca}} = 0$ as air taken directly from the environment. The energy associated with preheated combustion air, E_{pa} , is equal to the heat recovered in the regenerator, Q_{rec} . Refer to Fig. 6.5:

$$E_{\mathrm{pa}} = Q_{\mathrm{rec}} = n_{\mathrm{fuel}} \left[n_{\mathrm{O_2}} \left(\bar{h}_T - \bar{h}_0 \right)_{\mathrm{O_2}} + n_{\mathrm{N_2}} \left(\bar{h}_T - \bar{h}_0 \right)_{\mathrm{N_2}} \right] \tag{6.14}$$

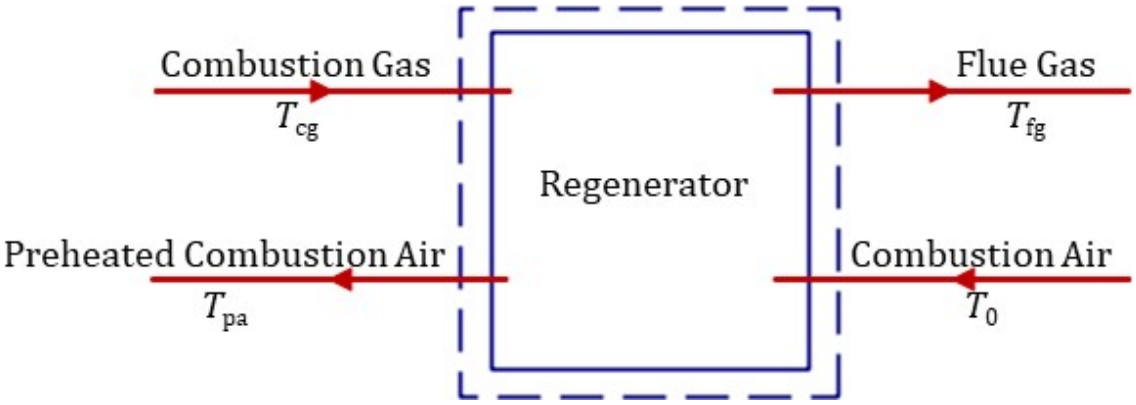

Fig. 6.5 Schematic of energy calculation of preheated combustion air

The values of enthalpy of the component are on basis of per kmole fuel. Energy balance equations:

Before upgrades

$$E_{\mathrm{input}} = E_{\mathrm{fuel}} + E_{\mathrm{dough}} + E_{\mathrm{ca}} \tag{6.15}$$

After upgrades,

$$E_{\mathrm{input}} = E_{\mathrm{fuel}} + E_{\mathrm{dough}} + (E_{\mathrm{ca}} + Q_{\mathrm{rec}}) \tag{6.16}$$

With enthalpy values, $\bar{h}_T$ and $\bar{h}_0$ from Moran et al. [124] calculation results are tabulated in Table 6.3.

Table 6.3 Energy Input to Furnace Chamber

Items	Before upgrades	After upgrades
T_{ca} [K]	298	298
T_{pa} [K]		380
E_{ca} [MJ]	0	0
$E_{pa} = Q_{rec}$, [MJ]		26.5
E_{source} [MJ]	1 191.4	851
E_{dough}[MJ]	0	0
$E_{input} = E_{source} + E_{dough} + (E_{ca} + Q_{rec})$, [MJ]	1 191.4	877.5

The total energy input to furnace chamber also can be calculated via $\bar{h}_p$ and $\bar{h}_R$, enthalpies of the combustion product and reactant per mole of fuel, the change of the two enthalpies presents the heat liberated from combustion. Figures 6.6 and 6.7 shown before and after upgrades.

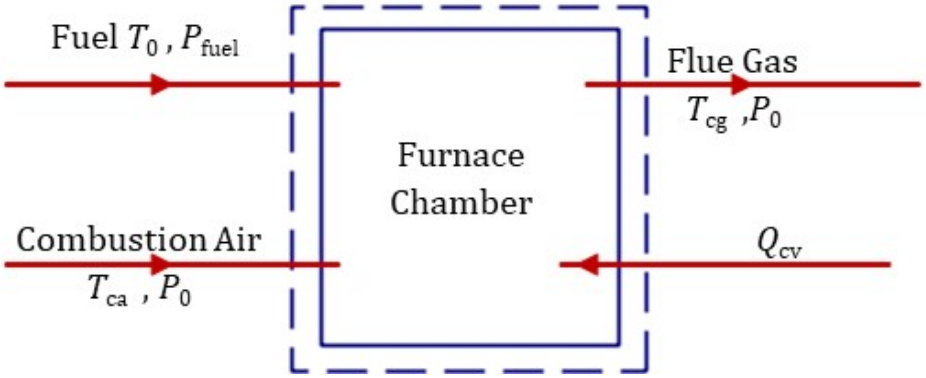

Fig. 6.6 Schematic of alternative energy input calculation before the upgrade.

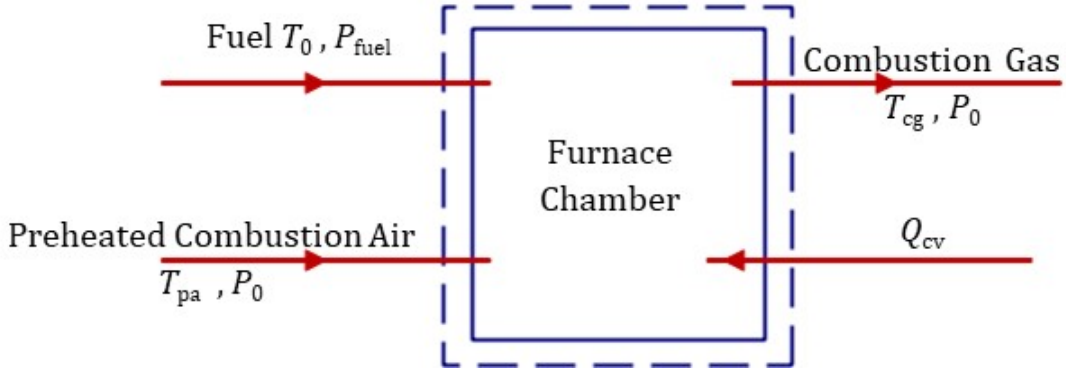

Fig. 6.7 Schematic of alternative energy input calculation after upgrade

Before upgrades

$$E_{input} = E_{fuel} + E_{ca} \tag{6.17}$$

Followed the combustion system's energy balance equations in Moran et al. [124],

$$E_{fuel} + E_{ca} = E_{fg} - Q_{CV} \tag{6.18}$$

After upgrades,

$$E_{\text{input}} = E_{\text{fuel}} + E_{\text{pa}} = E_{\text{cg}} - Q_{\text{CV}} \tag{6.19}$$

where

$$Q_{\text{CV}} = n_{\text{fuel}}(\bar{h}_{\text{p}} - \bar{h}_{\text{R}}) \tag{6.20}$$

$$\bar{h}_{\text{p}} - \bar{h}_{\text{R}} = \sum_{\text{p}} n_{\text{e}}\left(h_{\text{f}}^{0} + [h(T_{\text{p}}) - h(T_0)]\right)_{\text{e}} - \sum_{\text{R}} n_{\text{i}}\left(h_{\text{f}}^{0} + [h(T_{\text{R}}) - h(T_0)]\right)_{\text{i}} \tag{6.21}$$

Then for:

Before upgrades

$$E_{\text{fuel}} = E_{\text{input}} - E_{\text{ca}} \tag{6.22}$$

After upgrades,

$$E_{\text{fuel}} = E_{\text{input}} - E_{\text{pa}} \tag{6.23}$$

All terms are defined as same as in the previous section, all molar entropy values are based on per mole fuel and available in Moran et al. [124], and E_{fg} *(*E_{cg}*)* need to be referred in next section, the calculation results then are tabulated in Table 6.4.

Table 6.4 Alternative calculation of energy input to furnace chamber

Symbol	Before upgrades	After upgrades
$\bar{h}_{\text{p}}$ [MJ kmol^{-1}]	–798.0	–817.3
$\bar{h}_{\text{R}}$ [MJ kmol^{-1}]	–76.7	–48.8
$(\bar{h}_{\text{p}} - \bar{h}_{\text{R}})$ [MJ kmol^{-1}]	–721.3	–768.6
n_{fuel} [kmol]	1.33	0.95
Q_{cv} [MJ]	–959.4	–730.1
$E_{\text{fg}}(E_{\text{cg}})$ [MJ]	232	147.4
$E_{\text{input}} = E_{\text{fg}} - Q_{\text{cv}}$ [MJ]	1 191.4	877.5
$\bar{e}_{\text{input}}$ [MJ kmol^{-1}]	895.8	923.7
E_{ca} [MJ]	0	0
E_{pa} [MJ]		26.5
$E_{\text{fuel}} = E_{\text{input}} - E_{\text{ca}}$ (E_{pa}) [MJ]	1191.4	851.0

The results E_{fuel} and E_{input} conform to the calculation results in Table 6.3.

Energy Output from Furnace System:

Energy output from furnace chamber consists of three parts, energy associated with Baking bread, with stack flue gas (or combustion gas) exiting furnace chamber, and with heat loss transferring to furnace surroundings. These three parts of energy output are calculated separately as follows.

Energy for baking bread:

To permit a reasonable comparison, energy and exergy analyses are carried out for 5000 loaves (700 kg). the baking process is to heat the dough at 373 K to evaporate moisture and convert fragile dough to stable bread. The energy (heat) transferred to bread in the baking process is:

$$E_{\text{bak}} = m\, c_p\, (T_{\text{f}} - T_{\text{i}}) \tag{6.24}$$

where c_p = 1470 [J kg^{-1} K^{-1}] for bread is taken from Zhou, Therdthai [106], and T_{f} and T_{i} denote final and initial temperatures, respectively, of bread baking.

For reasonable comparison before and after upgrades, the same quantity of bread is considered. Thus, after upgrades, the same amount of heat required for the same quantity of production.

Energy Associated with flue gas:

The energy associated with flue gas (and combustion gas after upgrades) can be calculated by the sum of enthalpy of each component in the mixture of flue gas, refer to Figures 6.8 and 6.9.

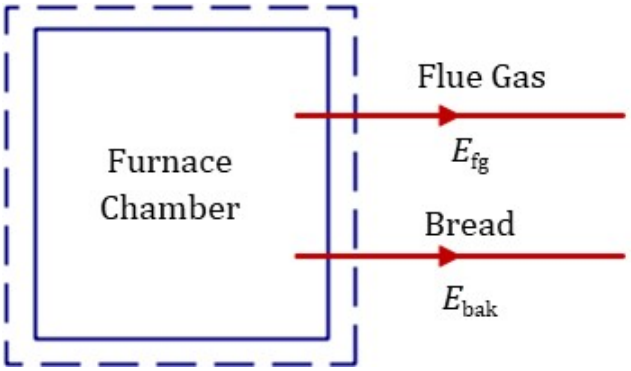

Fig. 6.8 Schematic of energy calculation of flue gas (before upgrades).

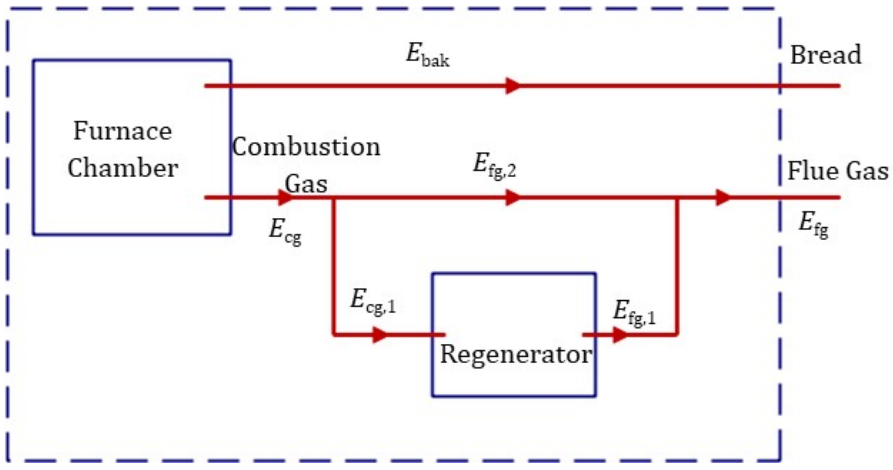

Fig. 6.9 Schematic of energy calculation of combustion gas and flue gas (after upgrades).

$$E_{\mathrm{fg}}(E_{\mathrm{cg}}) = n_{\mathrm{fuel}} \sum n_i (\bar{h}_T - \bar{h}_0)_{\mathrm{i}}$$
$$= n_{\mathrm{fuel}} \left[n_{\mathrm{CO_2}} (\bar{h}_T - \bar{h}_0)_{\mathrm{CO_2}} + n_{\mathrm{O_2}} (\bar{h}_T - \bar{h}_0)_{\mathrm{O_2}} + n_{\mathrm{N_2}} (\bar{h}_T - \bar{h}_0)_{\mathrm{N_2}} + n_{\mathrm{H_2O}} (\bar{h}_T - \bar{h}_0)_{\mathrm{H_2O}} \right] \quad (6.25)$$

The enthalpies of the component are on basis of per kmole of fuel. After upgrades, the temperature of stack flue gas, T_{fg}, can be calculated by the enthalpy of the components of flue gas. Refer to Fig. 6.10, $E_{\mathrm{fg}} = E_{\mathrm{fg,1}} + E_{\mathrm{fg,2}}$ from the energy balance equation, it is found $\Delta E_{\mathrm{fg,1}} = \Delta E_{\mathrm{fg,2}}$. Being more specific, to a particular component in the flue gas, such as CO_2, then it is found.

$$(\Delta E_{\mathrm{fg,1}})_{\mathrm{CO_2}} = (\Delta E_{\mathrm{fg,2}})_{\mathrm{CO_2}} \quad (6.26)$$

$$80\ \%\ n_{(\mathrm{fuel})} (\bar{h}_{\mathrm{fg,1}} - \bar{h}_{\mathrm{fg}})_{\mathrm{CO_2}} = 20\ \%\ n_{(\mathrm{fuel})} (\bar{h}_{\mathrm{fg}} - \bar{h}_{\mathrm{fg,2}})_{\mathrm{CO_2}} \quad (6.27)$$

$$(\bar{h}_{\mathrm{fg}})_{\mathrm{CO_2}} = (\bar{h}_{\mathrm{fg,2}} + 4\bar{h}_{\mathrm{fg,1}})/5 \quad (6.28)$$

The enthalpies of the component are on basis of per kmole fuel. Extract temperatures and enthalpy values from previous, it is found $(\bar{h}_{\mathrm{fg}})_{\mathrm{CO_2}} = 16592.4$ [kJ kmol^{-1}] fuel From Moran et al. [124], $T_{\mathrm{fg}} = 480$ K is found. The result can be validated by calculating enthalpy of other components in flue gas, such as, $(\bar{h}_{\mathrm{fg}})_{\mathrm{O_2}} = 13956$ [kJ kmol^{-1}], $(\bar{h}_{\mathrm{fg}})_{\mathrm{N_2}} = 13778.2$ [kJ kmol^{-1}], $(\bar{h}_{\mathrm{fg}})_{H_2O} = 15902.8$ [kJ kmol^{-1}], and all the final temperatures conform to 480 K. The energy loss (heat rejection through flue gas duct to environment) is not considered since the loss can be merged to waste energy with mixed flue gas directly exiting to environment.

Summarizing data for flue gas and combustion gas from the furnace chamber are given in Table 6.5.

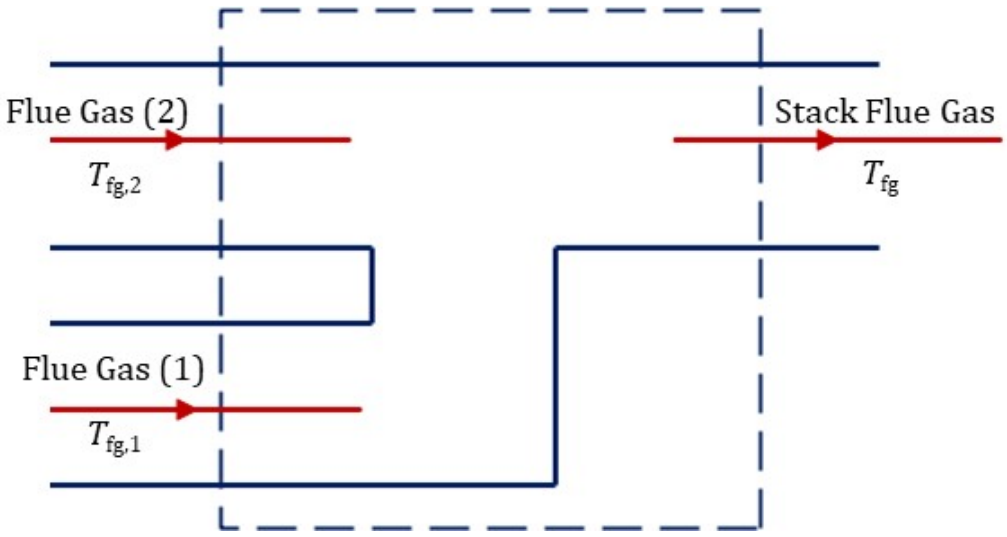

Fig. 6.10 A Schematic of mixing flue gas

Table 6.5 Energy calculation of flue gas and combustion gas

	Before upgrades	After upgrades		
T_{fg} [K]	660.0	$T_{fg,1=420}$	$T_{fg,2=680}$	$T_{fg=480}$
$\sum n_i(\bar{h}_T - \bar{h}_0)_i$ [MJ kmol^{-1}]	174.4	48.0	155.1	60.2
E_{fg} [MJ]	232.0	36.5	29.5	66
T_{cg} [K]		680.0		
E_{cg} [MJ]		147.4		
$E_{cg,1}$ [MJ]		117.9		
E_{bak} [MJ]	77.2	77.2		

Energy loss from Furnace Chamber:

The relationship between energy loss (heat loss) and energy balance can be shown in Fig. 6.11.

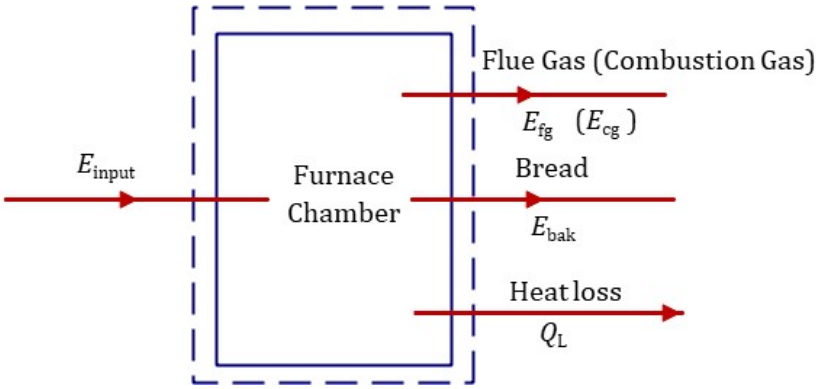

Fig. 6.11 Schematic of heat loss from the furnace

$$Q_L = E_{input} - E_{transfer} = E_{input} - E_{bak} - E_{fg} \quad (6.29)$$

Energy loss in the furnace can be found in Table 6.6.

Table 6.6 Calculation of energy loss from the furnace chamber

Items	Before upgrades	After upgrades
E_{input} [MJ]	1 191.4	877.5
$E_{fg}(E_{cg})$ [MJ]	232.0	147.4
E_{bak} [MJ]	77.2	77.2
Q_L [MJ]	882.2	653.0

Energy Calculation in Regenerator:

Referring to the following figure, the energy balance equation in the regenerating process can be expressed as

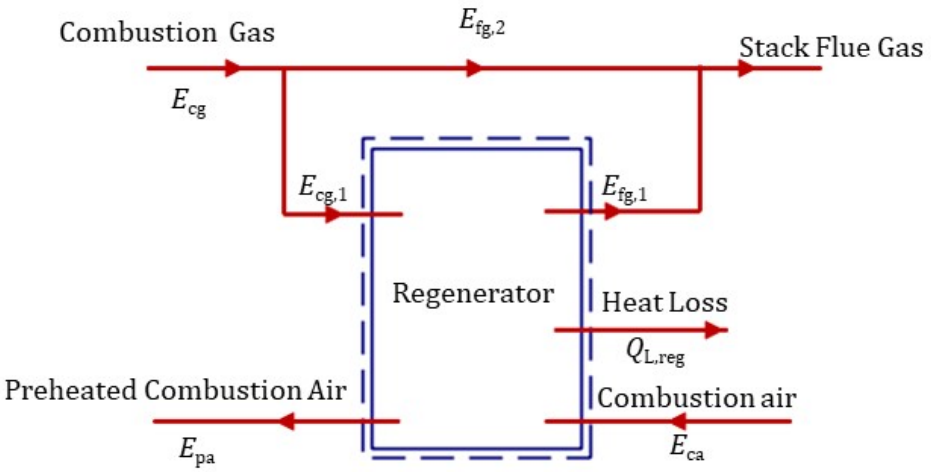

Fig. 6.12 Schematic of energy balance in the regenerator.

$$E_{\text{input}} = E_{\text{output}} \tag{6.30}$$

where

$$E_{\text{input}} = E_{\text{cg,1}} + E_{\text{ca}} \tag{6. 31}$$

$$E_{\text{output}} = E_{\text{pa}} + E_{\text{fg,1}} + Q_{\text{L,reg}} \tag{6. 32}$$

$E_{\text{cg,1}} = 0.8\ E_{\text{cg}}$ while E_{cg} knew in Table 6.5 then $Q_{\text{L,reg}}$ can be calculated.

$$Q_{\text{L,reg}} = \left(E_{\text{cg,1}} + E_{\text{ca}} \right) - (E_{\text{pa}} + E_{\text{fg,1}}) \tag{6. 33}$$

where $E_{\text{ca}} = 0$, and the results are tabulated in Table 6.7.

Table 6.7 Energy balance calculation for regenerator

Items	In regenerator
$E_{\text{cg,1}}$ [MJ]	117.9
E_{ca} [MJ]	0
E_{pa} [MJ]	26.5
$E_{\text{fg,1}}$ [MJ]	36.5
$Q_{\text{L,reg}}$ [MJ]	54.9

Exergy Input to Furnace System

Exergy is calculated in this section through study of a combined system consisting of a furnace system and an environment. The object of the calculation is to express the maximum theoretical work obtainable from the combined system as the furnace system comes into thermal and mechanical equilibrium with the environment.

Refer to the following figure and recall (6.7) and (6.9) as follows,

Before upgrades

$$1(\text{Fuel}) + 2.99\,O_2 + 11.24N_2 \rightarrow \\ \rightarrow 1.15CO_2 + 0.765O_2 + 11.24\,N_2 + 2.15\,H_2O \tag{6.7}$$

After upgrades,

$$1(\text{Fuel}) + 2.45\,O_2 + 9.21N_2 \rightarrow 1.15CO_2 + 0.225O_2 + 9.21\,N_2 + 2.15\,H_2O \tag{6.9}$$

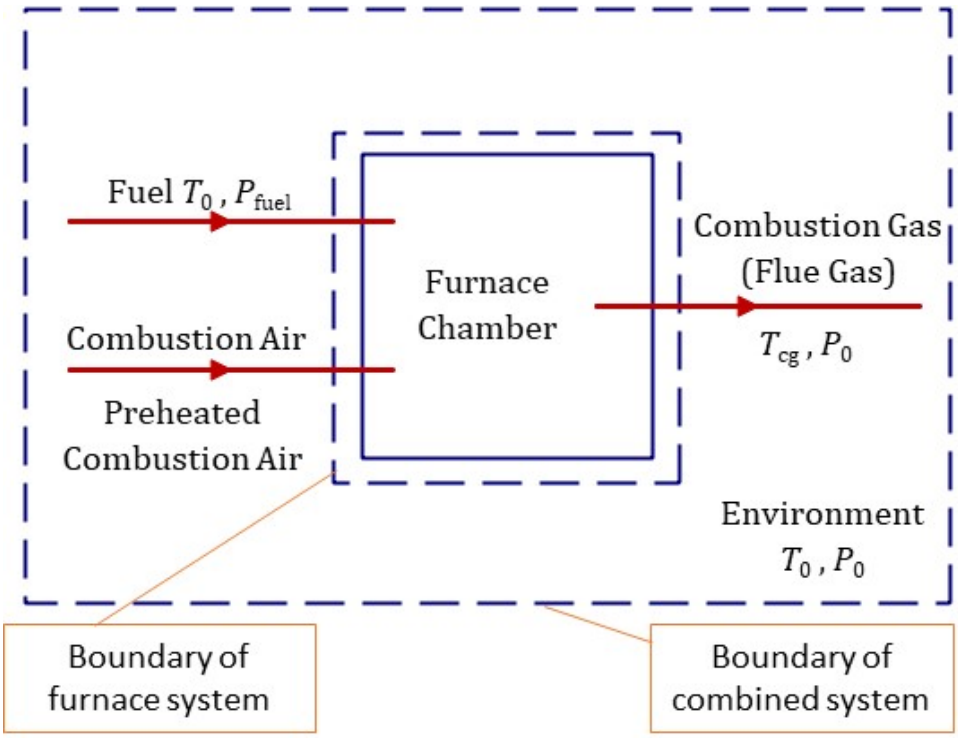

Fig. 6.13 Schematic of exergy calculation of fuel combustion.

Exergy input to furnace chamber is expressed by:

$$E_{\text{input}} = E_{\text{fuel}} + E_{\text{dough}} + (E_{\text{ca}} + E_{\text{rec}}) \tag{6.34}$$

$E_{\text{ca}} = 0$, due to combustion air taken at temperature of reference environment.

E_{dough} is considered zero since the raw material are used at the temperature of reference environment and assume that no chemical reaction involved in the baking process.

Input Exergy Associated with Combustion Reaction:

Exergy associated with fuel, E_{fuel}, is the sum of two contributions, thermomechanical exergy ($E_{\text{fuel}}^{\text{PH}}$) and chemical exergy ($E_{\text{fuel}}^{\text{CH}}$), i.e.

$$E_{\text{fuel}} = E_{\text{fuel}}^{\text{CH}} + E_{\text{fuel}}^{\text{PH}} \tag{6. 35}$$

$$E_{\text{fuel}}^{\text{PH}} = n_{\text{fuel}}\,\bar{e}_{\text{fuel}}^{\text{PH}} \tag{6. 36}$$

$\bar{e}_{\text{fuel}}^{\text{PH}}$, Molar thermomechanical exergy is obtained from the following equation

$$\bar{e}_{\text{fuel}}^{\text{PH}} = (\bar{h} - \bar{h}_0) - T_0(\bar{s} - \bar{s}_0) + \bar{R}T_0 \, ln(\frac{P_{\text{fuel}}}{P_0}) \tag{6.37}$$

$$E_{\text{fuel}}^{\text{CH}} = n_{\text{fuel}} \, \bar{e}_{\text{fuel}}^{\text{CH}} \tag{6. 38}$$

$\bar{e}_{\text{fuel}}^{\text{CH}}$, molar chemical exergy is obtained from following equation:

$$\bar{e}_{\text{fuel}}^{\text{CH}} = (\bar{g}_{\text{f(fuel)}}^{0} + n_{\text{O}_2} \, \bar{g}_{\text{f(O}_2\text{)}}^{0}) - (n_{\text{CO}_2} \, \bar{g}_{\text{f(CO}_2\text{)}}^{0} + n_{\text{H}_2\text{O}} \, \bar{g}_{\text{f(H}_2\text{O)}}^{0} + \bar{R}T_0 \ln(\frac{(y_{\text{O}_2}^{\text{e}})^{n_{\text{O}_2}}}{(y_{\text{CO}_2}^{\text{e}})^{n_{\text{CO}_2}} \, (y_{\text{H}_2\text{O}}^{\text{e}})^{n_{\text{H}_2\text{O}}}}) \tag{6.39}$$

$\bar{g}_{\text{f(fuel)}}^{0}$ = – 48,313[kJ kmol^{-1}], $\bar{g}_{\text{f(O}_2\text{)}}^{0}$=0 , $\bar{g}_{\text{f(CO}_2\text{)}}^{0}$ = -394,380 [kJ kmol^{-1}], and

$\bar{g}_{\text{f(H}_2\text{O)}}^{0}$ = – 228,590 [kJ kmol^{-1}]

y_i^e denotes molar fraction of *i* component of reactants and products in reference environment.

y_i^e and n_i are listed in Table 6.8.

Table 6.8 Air composition of Reference Environment and combustion Gas

Component	y_i^e	n_i	
		Before Upgrades	**After Upgrades**
O_2	0.21	2.99	2.45
CO_2	0.000 3	1.15	1.15
H_2O_{gas}	0.030 3	2.15	2.15

Some major terms in Tables 6.9 and 6.10 are tabulated.

Table 6.9 Calculation of fuel exergy

Items	**Before upgrades**	**After upgrades**
P_{fuel} [10^5 Pa]	1.15	1.70
P_0 [10^5 Pa]	1.01	1.01
$\bar{e}_{\text{fuel}}^{\text{PH}}$ [MJ kmol^{-1}]	0.32	1.30
$E_{\text{fuel}}^{\text{PH}} = n_{\text{fuel}} \, \bar{e}_{\text{fuel}}^{\text{PH}}$ [MJ]	0.42	1.20
T_0=T_{ca} [K]	298	298
T_{pa} [K]		380
$\bar{e}_{\text{fuel}}^{\text{CH}}$ [MJ kmol^{-1}]	926.9	929.0
$E_{\text{fuel}}^{\text{CH}} = n_{\text{fuel}} \, \bar{e}_{\text{fuel}}^{\text{CH}}$ [MJ]	1232.7	882.5
$E_{\text{fuel}} = E_{\text{fuel}}^{\text{CH}} + E_{\text{fuel}}^{\text{PH}}$ [MJ]	1233.2	883.7
$\bar{e}_{\text{fuel}}^{\text{CH}} + \bar{e}_{\text{fuel}}^{\text{PH}}$ [MJ kmol^{-1}]	927.2	930.2

Input Exergy Associated with Combustion air:

Before upgrades,

no combustion air was preheated,

$$E_{\mathrm{ca}} = 0, \text{and} \quad E_{\mathrm{rec}} = 0 \tag{6. 40}$$

After upgrades,

E_{ca} = 0, however, exergy associated with preheated combustion air is:

$$E_{\mathrm{pa}} = E_{\mathrm{rec}} = n_{\mathrm{fuel}}\, \bar{e}_{\mathrm{pa}} \tag{6. 41}$$

$\bar{e}_{\mathrm{pa}}$ denotes unit exergy of preheated combustion air on basis of per kmole of fuel,

$$\bar{e}_{\mathrm{pa}} = n_{\mathrm{O_2}}\left[\left(\bar{h} - \bar{h}_0\right) - T_0\,(\bar{s} - \bar{s}_0)\right]_{\mathrm{O_2}} + n_{\mathrm{N_2}}\left[\left(\bar{h} - \bar{h}_0\right) - T_0\,(\bar{s} - \bar{s}_0)\right]_{\mathrm{N_2}} \tag{6.42}$$

Calculation results are tabulated in Table 6.10.

Table 6.10 Summary of exergy input

Items	**Before upgrades**	**After upgrades**
T_{ca}[K]	298	298
T_{pa} [K]		380
E_{ca} [MJ]	0	0
E_{pa} [MJ]		3.1
E_{rec} [MJ]		3.1
E_{dough} [MJ]	0	0
E_{fuel} [MJ]	1233.2	883.7
$E_{\mathrm{input}} = E_{\mathrm{fuel}} + E_{\mathrm{dough}} + [E_{\mathrm{ca}} + E_{\mathrm{rec}}]$ [MJ]	1233.2	886.8

Exergy Output from Furnace System:

Exergy outputs consist of three parts, which are exergy change of Baking bread ($\Delta E_{\mathrm{bread}}$), exergy associated with flue gas (E_{fg}) and with heat loss (E_{L}), these three parts of exergy output are calculated as follows:

Exergy Change of Bread in Baking Process:

Exergy change of bread baking from 298 K to 373 K can be expressed as the sum of changes of thermomechanical and chemical contributions, i.e.

$$\Delta E_{\mathrm{bread}} = \Delta E_{\mathrm{bread}}^{\mathrm{PH}} + \Delta E_{\mathrm{bread}}^{\mathrm{CH}} \tag{6. 43}$$

$\Delta E_{\mathrm{bread}}^{\mathrm{PH}}$ denotes thermomechanical exergy change accompanying heat transfer to bread in the baking process, it can be shown as follows:

$$\Delta E_{\mathrm{bread}}^{\mathrm{PH}} = m\left(\left(\bar{h} - \bar{h}_0\right) - T_0(\bar{s} - \bar{s}_0)\right)_{\mathrm{bread}} \tag{6. 44}$$

where the values of enthalpy of the component are on basis of per kilogram bread. To breakdown the equation, the $\Delta E_{\text{bread}}^{\text{PH}}$ accompanying heat transfer to bread

$$\Delta E_{\text{bread}}^{\text{PH}} = \text{m}\,(c_p\,(T_{\text{f}} - T_{\text{i}})\; -\; T_0\,c_p\;\ln(\frac{T_{\text{f}}}{T_{\text{i}}})) \tag{6.45}$$

Assume chemical exergy change of bread $\Delta E_{\text{bread}}^{\text{CH}}$= 0 in the whole baking process. Since the same production of bread is taken account for before and after upgrading, the same exergy value is used for analysis after upgrades.

Output exergy associated with flue gas:

Exergy of flue gas is the sum of two contributions, thermomechanical exergy, and chemical exergy, i.e.

$$E_{\text{fg}} = E_{\text{fg}}^{\text{CH}} + E_{\text{fg}}^{\text{PH}} \tag{6.46}$$

where

$$E_{\text{fg}}^{\text{PH}} = n_{\text{fuel}}\,\bar{e}_{\text{fg}}^{\text{PH}}$$

$\bar{e}_{\text{fg}}^{\text{PH}}$, denotes unit thermomechanical exergy on per mole of fuel basis, it can be expressed as:

$$\bar{e}_{\text{fg}}^{\text{PH}} = \sum n_i\left[(\bar{h} - \bar{h}_0) - T_0(\bar{s} - \bar{s}_0)\right]_i \tag{6.47}$$

$$E_{\text{fg}}^{\text{ch}} = n_{\text{fuel}}\,\bar{e}_{\text{fg}}^{\text{ch}}$$

$\bar{e}_{\text{fg}}^{\text{ch}}$, denotes unit chemical exergy on per mole of fuel basis, it can be expressed as:

$$\bar{e}_{\text{fg}}^{\text{ch}} = \bar{R}T_0 \sum_i n_i\,\ln\left(\frac{y_i}{y_i^e}\right) \tag{6.48}$$

where y_i and y_i^e denote the molar fraction of component i (CO_2, O_2, N_2, and H_2O) in flue gas and in the reference environment, respectively. y_i^e , y_i and n_i are listed in the following table

Table 6.11 Air combustion of reference environment and combustion gas

Component		**Before Upgrades**		**After Upgrades**	
	y_i^e	y_i	n_i	y_i	n_i
CO_2	0.000 3	0.075	1.15	0.09	1.15
O_2	0.21	0.05	0.765	0.018	0.225
N_2	0.76	0.734 4	11.24	0.72	9.21
H_2O	0.030 3	0.14	2.15	0.169	2.15

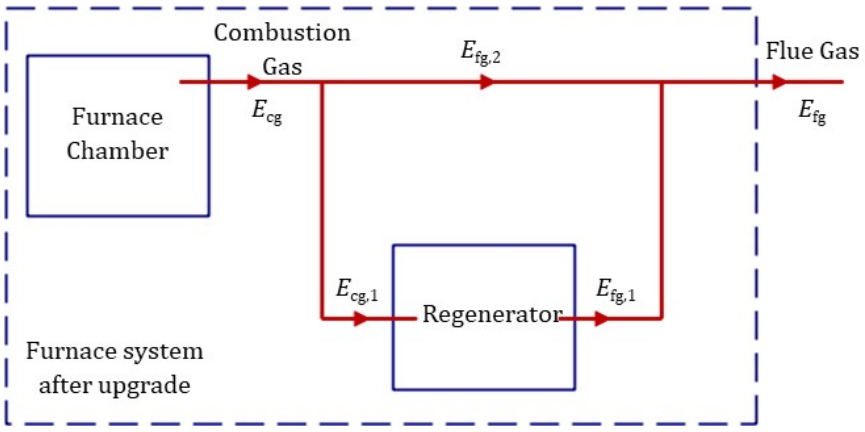

Fig. 6.14 Schematic of exergy of flue gas and combustion gas

Refer to the above figure, some major calculated results in (6.46), (6.47) and (6.48) are listed in Table 6.12.

Table 6.12 Exergy calculation for stack flue gas and combustion gas

Items	Before upgrades	After upgrades
Stack Flue Gas		
T_{fg} [K]	660	480
$\bar{e}_{fg}^{PH}$ [MJ kmol^{-1}]	60.9	16.0
$\bar{e}_{fg}^{CH}$ [MJ kmol^{-1}]	20.2	22.8
$E_{fg} = n_{fuel}(\bar{e}_{fg}^{PH} + \bar{e}_{fg}^{CH})$ [MJ]	107.8	36.8
Internal flows		
$\bar{e}_{cg}^{PH}$ [MJ kmol^{-1}]		56.0
$\bar{e}_{cg}^{CH}$ [MJ kmol^{-1}]		22.8
$E_{cg} = n_{fuel}(\bar{e}_{cg}^{PH} + \bar{e}_{cg}^{CH})$ [MJ]		74.8
$E_{cg,1}$ [MJ]		59.8
$E_{fg,1}$ [MJ]		23.3
$E_{fg,2}$ [MJ]		15.0

All specific enthalpy and entropy values of each component in flue gas can be found in Moran et al. [124].

Exergy Loss and Exergy Destruction

Exergy Loss and Destruction in Furnace Chamber

The exergy loss from the furnace chamber to the environment can be expressed as follows,

$$E_L = Q_L(1 - T_0/T_L) \tag{6.49}$$

T_L = 420 K is taken in this study. Then, taking data from Table 6.6, the exergy loss accompanying heat loss from the furnace chamber is found

Before upgrades

$$E_{L,1} = 882.2(1 - (298 / 420)) = 256.3 \text{ MJ} \quad (6.50)$$

After upgrades,

$$E_{L,2} = 653\,(1 - (298 / 420)) = 189.7 \text{ MJ} \quad (6.51)$$

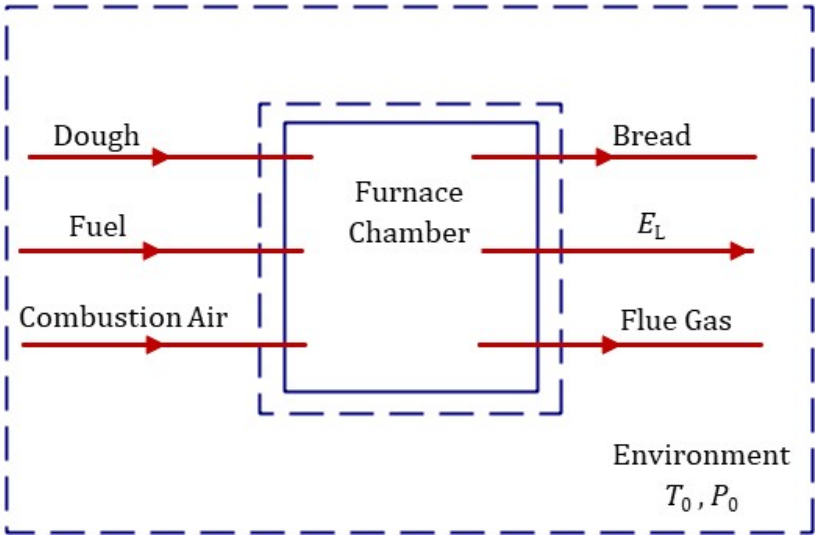

Fig. 6.15 Schematic of exergy loss from the furnace chamber to the environment

Exergy destruction can be found from the exergy balance equation:

$$E_D = E_{input} - E_{transfer} - E_L \quad (6.52)$$

Being more specific, in the furnace chamber, exergy destruction is:

Before upgrades

$$E_{D,1} = E_{input} - (\Delta E_{bread} + E_{fg}) - E_L = \\ = 1\,233.2 - (8.3 + 107.8) - 256.3 = 860.7 \text{ MJ} \quad (6.53)$$

After upgrades,

$$E_{D,2} = E_{input} - (\Delta E_{bread} + E_{cg}) - E_L = \\ = 886.8 - (8.3 + 74.8) - 189.7 = 614.1 \text{ MJ} \quad (6.54)$$

Exergy loss and Destruction in Regenerator:

Refer to the following figure for exergy flows in regenerator,

Exergy loss accompanying heat transfer to environment can be expressed as

$$E_L = Q_{L,reg}\,(1 - (T_0 / T_{L,reg})) \quad (6.55)$$

Where $T_{L,reg}$ = 325 K is taken for regenerator. Then exergy loss in the regenerator is found

$$E_{\mathrm{L}} = 54.9(1 - (298 / 325)) = 4.6 \text{ MJ} \tag{6.56}$$

From the exergy balance equation in regenerator and Fig. 6.16, exergy destruction can be expressed as

$$\begin{aligned} E_{\mathrm{D,reg}} &= E_{\mathrm{input}} - E_{\mathrm{transfer}} - E_{\mathrm{L}} = \\ &= \left(E_{\mathrm{ca}} + E_{\mathrm{cg,1}}\right) - \left(E_{\mathrm{pa}} + E_{\mathrm{fg,1}}\right) - E_{\mathrm{L}} = \\ &= (0 + 59.8) - (3.1 + 23.3) - 4.6 = 28.9 \text{ MJ} \end{aligned} \tag{6.57}$$

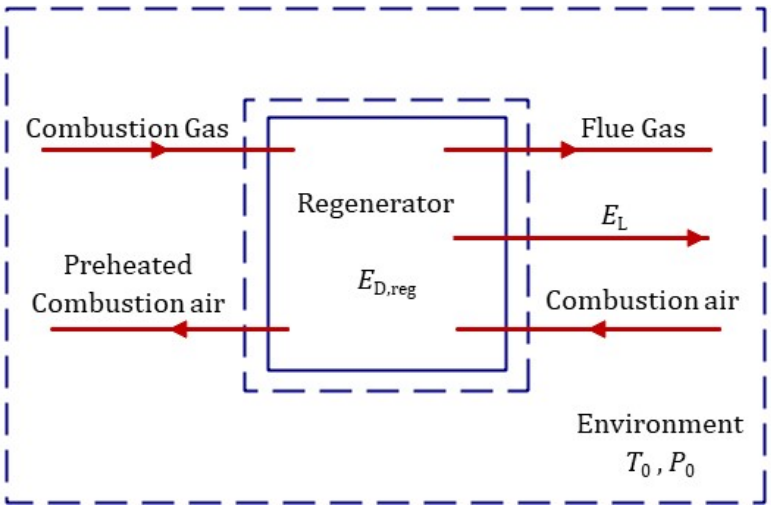

Fig. 6.16 Schematic of exergy loss from the regenerator to environment.

Exergy loss and Destruction in Mixing flue gas

Like many heat exchange process, mixing flue gas from the regenerator and bypass flue gas results in exergy destruction. Exergy loss accompanying heat loss through flue duct to the environment is not considered since the flue gas exits to the environment directly. Refer to the following figure, the exergy flows and destruction are found,

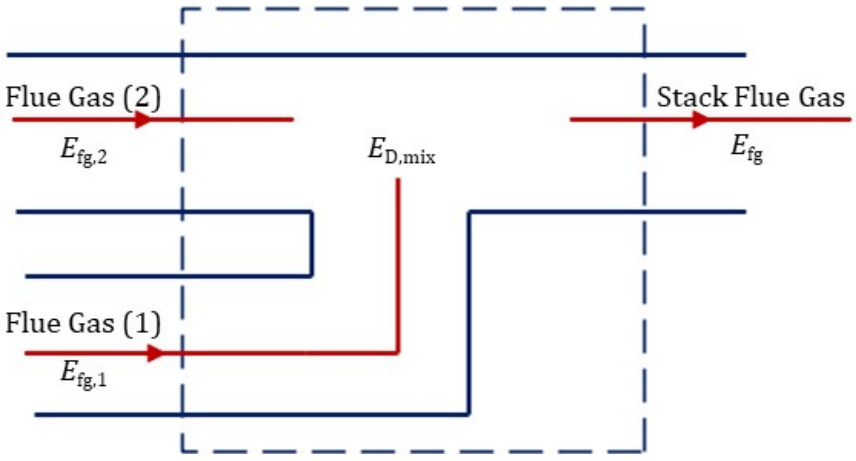

Fig. 6.17 Schematic of exergy flows of mixing flue gas.

$$E_{\mathrm{D,mix}} = E_{\mathrm{fg,1}} + E_{\mathrm{fg,2}} - E_{\mathrm{fg}} \tag{6.58}$$

$$E_{\mathrm{D,mix}} = 23.3 + 15 - 36.8 = 1.4 \text{ MJ} \tag{6.59}$$

Energy and Exergy Efficiency

Energy efficiency (η) of baking bread is measured as the ratio of product energy output to source energy input. Exergy efficiency (ε) of Baking bread is measured as the ratio of product exergy output to source exergy input with consideration of exergy destructed in process. Source input energy (exergy) is associated with fuel only. Equations are:

$$\eta = \Delta E_{bread}/E_{fuel} \tag{6.60}$$

$$\varepsilon = \Delta E_{bread}/E_{fuel} \tag{6. 61}$$

6.2 Results and Discussions

6.2.1 Energy and Exergy Balances for Furnace

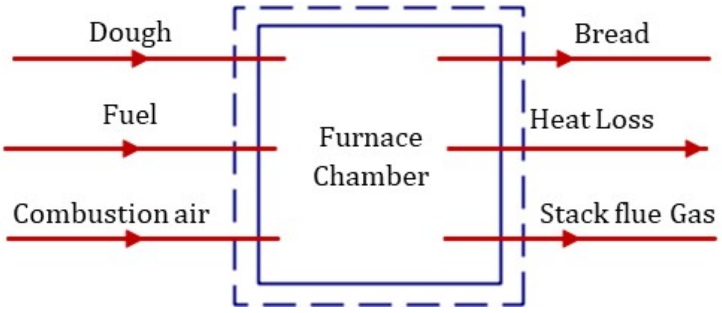

Fig. 6.18 Energy flows of furnace system before upgrades

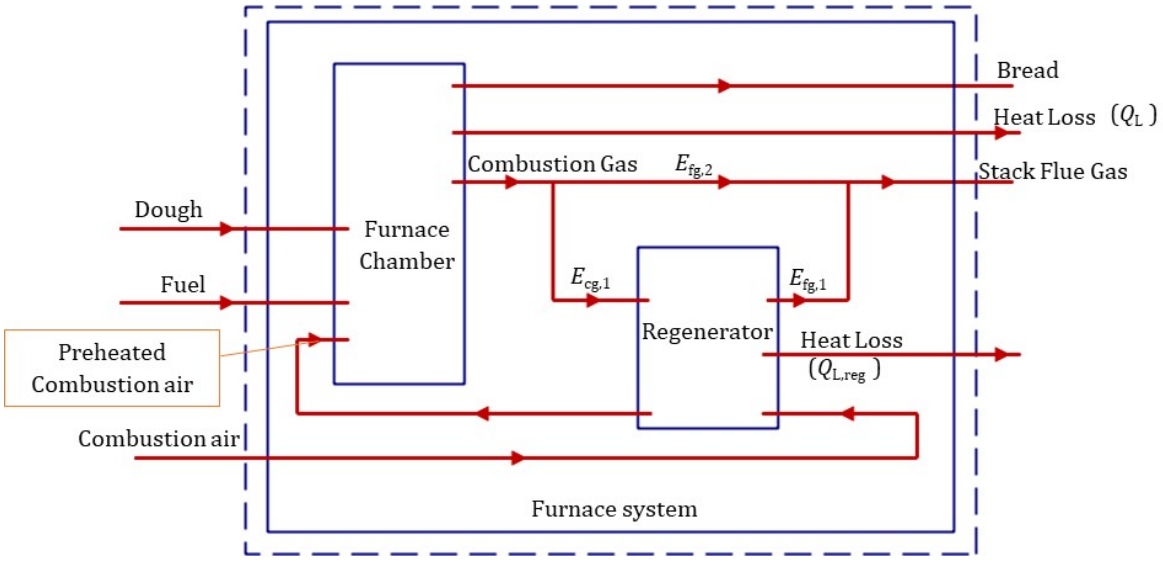

Fig. 6.19 Energy flows of furnace system after upgrades

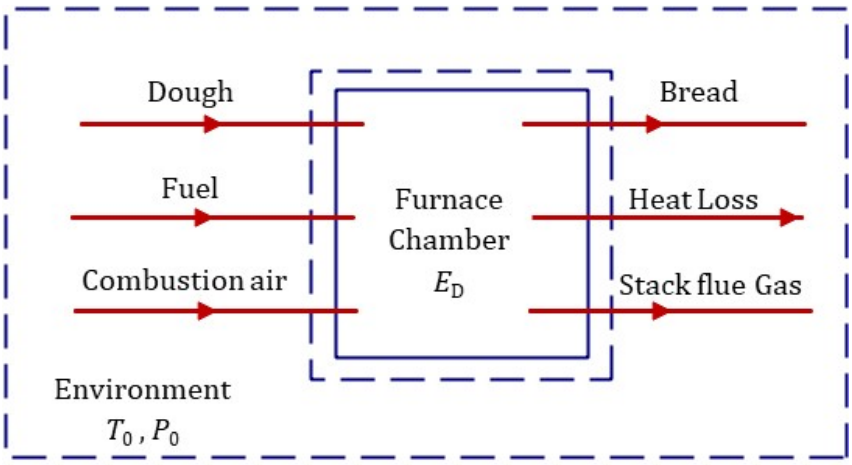

Fig. 6.20 Exergy flows of furnace system before upgrades

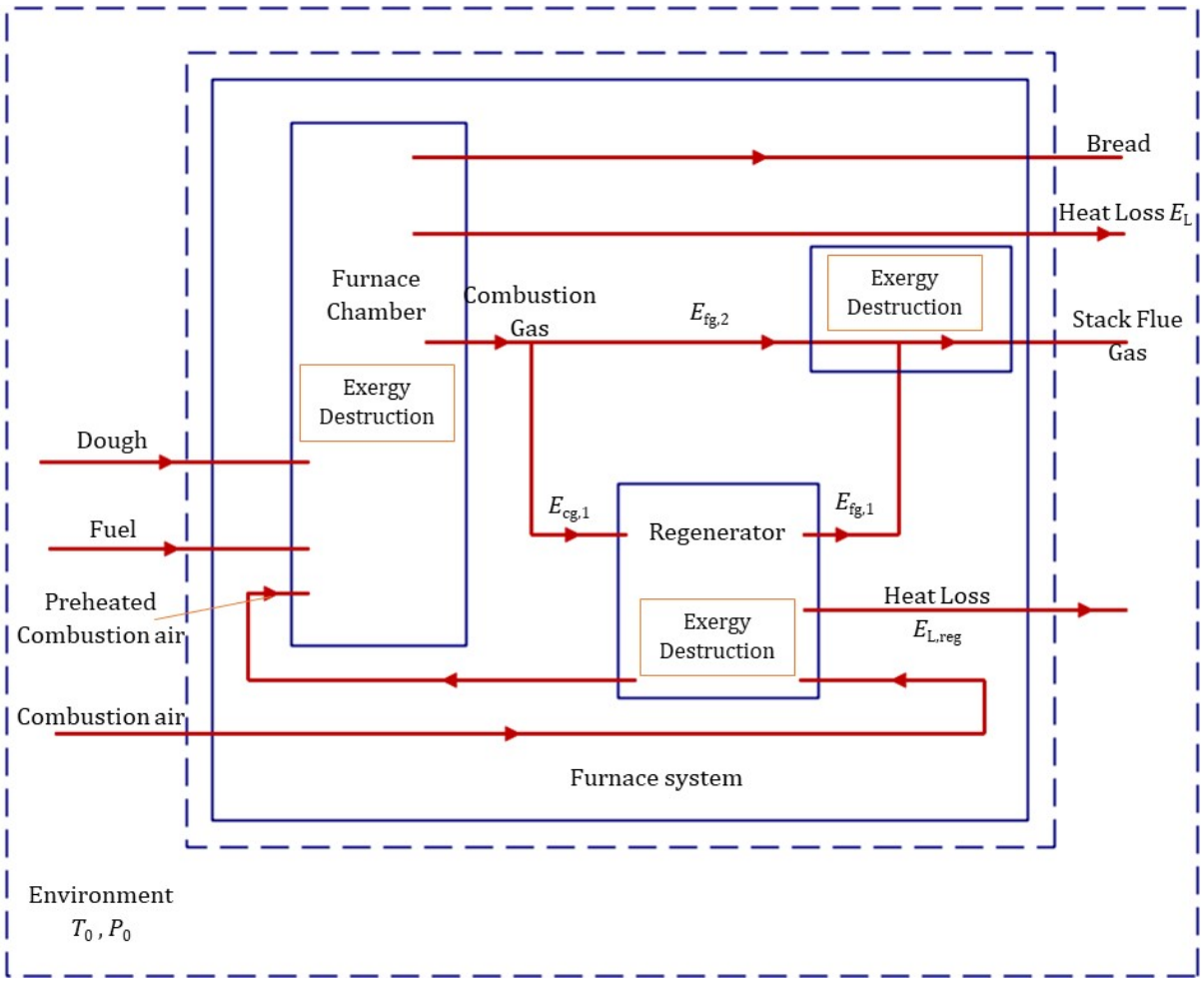

Fig. 6.21 Exergy flows of furnace system after upgrades.

Tables 6.13 and 6.14 present energy and exergy balances respectively of the furnace system for before and after upgrades.

From Tables 6.13 and 6.15, the overall system energy efficiency increases from 6.5% to 9% due to less source energy input (from 1 191.4 kJ to 851 MJ) when the same production is maintained, i.e. 77.2 MJ energy consumed for baking before and after upgrades. Energy saving 340.4 MJ (= 1191.4 – 851) from less energy source consumption mainly relies on better performed gas burner and regenerator. Refer to

calculation Table 6.4 ($\bar{h}_{\mathrm{p}} - \bar{h}_{\mathrm{R}}$), the unit heat transfer from combustion based on per mole of fuel, is greatly improved, from 721.3 (MJ kmol^{-1}) to 768.6 (MJ kmol^{-1}) due to better performed gas burner which gives higher temperature of POC (680 K vs. 660 K) and better A / F rate (11.662 vs. 14.232 4), also due to regenerating system which gives higher temperature of reactant air (380 K vs.298K).

After upgrades, heat rejection 7.8 % (66 MJ) to the environment from stack flue gas, is significantly less than before upgrades. The reduction decreases thermal impact to the environment and after upgrades, the energy loss (653 MJ) to the environment from the furnace chamber is slightly reduced from previous loss (882.2 MJ). It is benefited from the new monitor and control system which better operates pressure balance of combustion gas.

Before upgrades, total unused energy in system is 93.5% (232 + 882.2 = 1 114.2 MJ); after upgrades, total unused energy in system reduced to 91 % (66 + 653 + 54.9 = 773.8 MJ). The overall system performance is improved.

Exergy comparison is observed from Tables 6.14 and 6.15. Overall system exergy efficiency increases from 0.68 % to 0.94 % due to less exergy input (1 233.2 kJ vs. 883.7 MJ) and additional input (3.1 MJ with preheated combustion air) while the same production is maintained, i.e. 8.3 MJ exergy consumed for baking. Source exergy supplied to process after upgrades is less than before 1 233.2 MJ, a total of 349.4MJ (=1 233.2 – 883.7).

Table 6.13 Energy balance before and after upgrades

Quantity	**Energy flow**			
	Before Upgrades		**After Upgrades**	
	MJ/ 5000 loaves	**% of input**	**MJ/ 5000 loaves**	**% of input**
Energy input				
Fuel (natural gas)	1 191.4	100	851	100
Combustion air	0		0	
Bread	0		0	
Total	**1 191.4**	**100**	**851**	**100**
Energy output				
Flue gas	232	19.5	66	7.8
Baking Bread	77.2	6.5	77.2	9
Energy loss from furnace	882.2	74	653	76.7
Energy loss from regenerator			54.9	6.5
Total	**1191.4**	**100**	**851**	**100**

Table 6.14 Exergy balance before and after upgrades

Quantity	Exergy flow			
	Before Upgrades		After Upgrades	
	MJ/ 5000 loaves	% of input	MJ/ 5000 loaves	% of input
Exergy input				
Fuel natural gas	1 233.2	100	883.7	100
Thermomechanical contribution	0.42	0.03	1.2	0.14
Chemical contribution	1 232.7	99.97	882.5	99.86
Combustion air	0		0	
Dough	0		0	
Total	**1 233.2**	**100**	**883.7**	**100**
Exergy output				
Flue gas	107.8	8.7	36.8	4.2
Baking Bread	8.3	0.7	8.3	0.9
Exergy loss from furnace	256.3	20.8	189.7	21.5
Exergy loss from regenerator			4.6	0.5
Total	**372.4**	**30.2**	**239.4**	**27.1**
Exergy destruction				
Furnace	860.7	69.8	614.1	69.4
Regenerator			28.9	3.3
Flue gas mixing			1.4	0.2
Total	**860.7**	**69.8**	**644.4**	**72.9**

Table 6.15 Furnace energy and exergy efficiencies comparison

Efficiency	Before Upgrades %	After Upgrades %	Improvement %
Energy	6.5	9	38.5
Exergy	0.68	0.94	38.2

As seen in Table 6.9, molar fuel thermomechanical exergy is increased from 0.32 (MJ kmol^{-1}) to 1.3 (MJ kmol^{-1}). It resulted from gas pressure increased from 115 kPa to 170 kPa. However thermomechanical exergy contribution of natural gas is a small portion comparing to chemical contribution when the temperature of natural gas is the same as the environment, so the thermomechanical exergy contribution is sometimes ignored when calculating natural gas exergy. Overall chemical exergy consumption reduced from 1232.7 MJ to 882.5 MJ. Molar chemical exergy of fuel is improved approximate 0.23 %, from 926.9 (MJ kmol^{-1}) to 929 (MJ kmol^{-1}).

Waste exergy from stack flue gas is decreased from 107.8 MJ to 36.8 MJ because of the regenerating process. The reduction of waste exergy emission decreased the environmental impact. Meanwhile, 4.2 % waste exergy of flue gas still shows the availability of the flow.

After upgrades, 803.7 MJ (=189.7 +614.1) exergy loss and destruction from furnace chamber appears less than before 1.117×10^3 MJ (=256.3 + 860.7). It shows the furnace performance is improved.

The process inside the furnace chamber destroys more than 60 % of exergy input before and after upgrades. The largest exergy waste in the system is the destruction in the processes of combustion, heat transfer and baking due to the nature of the furnace operation. Overall unutilized exergy reduced from 1.2×10^3 (=107.8+ 256.3 + 860.7) to 875.4 MJ (=36.8 +189.7 + 4.6+ 614.1 + 28.9 +1.4) while retaining the same production.

6.2.2 Energy and Exergy Balances for Regenerator

As seen in Table 6.16, exergy efficiency is 5.2 % and the energy efficiency is 22.5 %. Even though 46.5 % energy loss (heat rejection) from regenerator seems to be a large portion, the 7.6 % exergy loss indicates less availability associated with the loss. In other word 7.6 % exergy loss indicates that one should spend less effort on focusing on recovering 7.6 % exergy loss (or 46.5 % energy loss) because the availability of the loss is limited.

The flue gas exergy is 39 % exergy input to the unit. This reminds to recover the availability. 48.2 % of exergy destruction shows the irreversibility of heat transfer in the regenerator.

Table 6.16 Energy and exergy flows for regenerator

Quantity	Energy		Exergy	
	MJ/ 5000 loaves	% of input	MJ/ 5000 loaves	% of input
Input				
Combustion air	0		0	
Combustion gas	117.9	100	59.8	100
Total	**117.9**	**100**	**59.8**	**100**
Output				
Flue gas (1)	36.5	31	23.3	39
Preheated combustion air	26.5	22.5	3.1	5.2
Loss from regenerator	54.9	46.5	4.6	7.6
Total	**117.9**	**100**	**31**	**51.7**
Exergy destruction			**28.8**	**48.2**

6.2.3 Comparison of Before Upgrade and after Upgrade

Before Upgrades

Before upgrades, based on Table 6.13, energy input before upgrades 1 191.4 MJ is normalized as 100 %; so based on Table 6.14, exergy input before upgrades 1 233.2 MJ is normalized as 103.5 %. The discrepancy between 100 and 103 shows the difference in energy and exergy of fuel when adopting two methods. The other values of energy and exergy are also normalized as shown in Table 6.17.

Table 6.17 Normalization of energy and exergy for before upgrades

Quantity	Energy		Exergy	
	MJ/ 5000 loaves	**% of input**	**MJ/ 5000 loaves**	**% of input**
Input				
Natural gas	1 191.4	100	1 233.2	103.5
Combustion air	0		0	
Dough	0		0	
Total	**1 191.4**	**100**	**1 233.2**	**103.5**
Output				
Stack flue gas	233	19.5	107.8	9
Baking Bread	77.2	6.5	8.3	0.7
loss from furnace	882.2	74	256.2	21.5
Total	**1 191.4**	**100**	**372.4**	**31.2**
Exergy destruction in furnace			**860.7**	**72.3**

In the system, without control of exhaust flue gas, 19.5% energy associated with flue gas exhausted to the environment. In view of exergy, actually 9 % exergy associated with the emitted flue gas. In view of energy, 6.5 % was transferred to the product. The rest were released to plant and atmosphere through enclosure and stack, i.e. 93.5% (= 100 – 6.5) energy was wasted, and 0.7 % exergy transferred to product shows 30.5 % (= 103.5 – 0.7 – 72.3) exergy was wasted. Both low efficiencies of 6.5 % and 0.7 % show potential benefit to upgrading those facilities. This was subjective of the upgrading project.

After Upgrades

Based on Table 6.13, energy input before upgrades 119 1.4 MJ again is normalized as 100 %; refer to Table 6.18, input energy after upgrades 851 MJ is normalized as 71.4 %; source natural gas exergy input after upgrades 883.7 MJ is normalized as 63 %.

Table 6.18 shows 28.6 % (=100 – 71.4) energy saving than before upgrades when maintaining same production, 6.5 % energy on baking, and compare to previous source exergy input, 74.2 % source exergy input shows 29.3 % (=103.5 % – 74.2%) exergy saving as comparing to 100 % energy input before upgrades.

Energy loss (54.8 %) from furnace chamber to environment reminds a possibility of utilizing heat loss from the furnace, however exergy value 15.9 % shows less availability of the loss. This again examples the benefit of using exergy value.

Table 6.18 Normalization of energy and exergy for after upgrades

Quantity	Energy		Exergy	
	MJ/ 5000 loaves	**% of input**	**MJ/ 5000 loaves**	**% of input**
Input				
Fuel natural gas	851	71.4	883.7	74.2
Combustion air	0		0	
Dough	0		0	
Total	851	71.4	883.7	74.2
Output				
Flue gas	65 979.838 9	5.5	36.8	3.1
Baking Bread	77.2	6.5	8.3	0.7
Loss from furnace	653	54.8	189.7	15.9
Loss from regenerator	54.9	4.6	4.6	0.4
Total	**851**	**71.4**	**239.4**	**20.1**
Exergy destruction				
Furnace			614.1	51.5
Regenerator			28.9	2.4
Flue gas mixing			1.4	0.12
Total			**644.4**	**54.1**

6.2.4 Energy and Exergy Analysis

The values of energy and exergy are normalized here. Energy input (1191.4 MJ) before upgrades is normalized as 100 % in energy analysis when energy input (851 MJ) after upgrades is normalized as 71.4 %; exergy input (1233.2 MJ) before upgrades is also normalized as 100 % in exergy analysis when exergy input (883.7 MJ) after upgrades is normalized as 71.7 %. Both of traditional energy method and current exergy method are used to evaluate changes of efficiencies of furnace and regenerator.

Energy Analysis

Table 6.19 shows energy saving 28.6 % (=100 – 71.4) achieved when maintaining 6.5 % energy for the baking process. As shown in Table 6.4, after upgrades, the new burner offers higher unit energy input (923.7 MJ $kmol^{-1}$) than before (895.8 MJ $kmol^{-1}$). This results from higher pressure of fuel supply (1.7 x 10^5 Pa vs. 1.15 x 10^5 Pa) and better performances of the system, such as higher combustion temperature, etc.

Table 6.19 Normalization of energy balances for before and after upgrades

Quantity	Energy flow			
	Before Upgrades		After Upgrades	
	MJ/ 5000 loaves	% of input	MJ/ 5000 loaves	% of input
Energy input				
Fuel (natural gas)	1191.4	100	851	71.4
Combustion air	0		0	
Dough	0		0	
Total	**1 191.4**	**100**	**851**	**71.4**
Energy output				
Flue gas	232	19.5	66	5.5
Baking Bread	77.2	6.5	77.2	6.5
Energy loss from furnace	882.2	74	653	54.8
Energy loss from regenerator			54.9	4.6
Total	**1 191.4**	**100**	**851**	**71.4**

After upgrades, 19.2 % reduction of energy loss from furnace chamber (54.8 %) is found less than before (74 %). 2.2 % (26.5 MJ) energy transferred to combustion air reduced total energy input and fuel consumption.

Exergy Analysis

28.3 % exergy saving (=100 – 71.7) is achieved when maintaining 0.7% exergy for production. Thermomechanical exergy contribution increased from 0.03 % to 0.1 % shows the benefit of higher gas pressure. This also can be referred to in Table 6.9 unit thermomechanical exergy contribution are relatively small (0.32 MJ kmol^{-1} and 1.3 MJ kmol^{-1}, for before and after upgrades respectively) when compared to chemical exergy contribution (926.9 MJ kmol^{-1}and 929 MJ kmol^{-1}, for before and after upgrades respectively). The improvement of unit chemical exergy (926.9 MJ kmol^{-1} fuel vs. 929 MJ kmol^{-1}) is attained from better performance of gas burner, which consumes less oxygen, i.e. increasing logarithm part in chemical exergy calculation equation: $\bar{R}T_0 \ln(\frac{(y^e_{O2})^{n_{O2}}}{(y^e_{CO2})^{n_{CO2}}\,(y^e_{H2O})^{n_{H2O}}})$ in (6.39).

Waste exergy of flue gas at stack is greatly reduced from 8.7 % to 3 % and Exergy loss from furnace slightly reduced from 20.8 % to 15.3 %.

0.3 % exergy is transferred to combustion air reduces total exergy input. This small number shows chemical exergy of preheated combustion air is zero because it is not related to the temperature of preheated air. Unused exergy is reduced from 99.3 % (=100 – 0.7) to 71 % (=71.7 – 0.7).

Table 6.20 Normalization of exergy balances before and after upgrades

Quantity	Exergy flow			
	Before Upgrades		After Upgrades	
	MJ/ 5000 loaves	%	MJ/ 5000 loaves	%
Exergy input				
Fuel natural gas	1 233.2	100	883.7	71.7
Thermomechanical contribution	0.42	0.03	1.2	0.1
Chemical contribution	1 232.7	99.97	882.5	71.6
Combustion air	0		0	
Dough	0		0	
Total	**1 233.2**	**100**	**883.7**	**71.7**
Exergy output				
Flue gas	107.8	8.7	36.8	3
Baking Bread	8.3	0.7	8.3	0.7
Exergy loss from furnace	256.3	20.8	189.7	15.3
Exergy loss from regenerator			4.6	0.4
Total	**372.4**	**30.2**	**239.4**	**19.4**
Exergy destruction				
Furnace	860.7	69.8	614.1	49.8
Regenerator			28.9	2.3
Flue gas mixing			1.4	0.2
Total	**860.7**	**69.8**	**644.4**	**52.3**

7 Conclusions and Recommendations

7.1 Conclusions

This thesis has demonstrated the capability of modelling and simulation techniques for the optimization of an industrial bread baking process and improve the efficiency after the implementation of a new burner system on the baking oven. Techniques used in this study included computational fluid dynamic model using COMSOL Multiphysics and mathematical model using MATLAB.

The bread baking oven, and dough/bread within it, are successfully modeled and simulated. The bread baking process is proven to involve the physics of radiation, convection, and mass transfer (with respect to both the dough/bread and oven).

Computational fluid dynamic (CFD) modeling for the baking process was developed successively according to heat balance and mass balances in order to study the bread temperature and water content at different oven temperatures. The most important results obtained can be summarized as follows:

The model shows that, the predicted bread temperature increases with increasing oven temperature, where, the oven temperature increases from 180 °C to 260 °C, and the temperature of the crust of bread increases from 132.4 °C to 179.5 °C.

The model shows that, the temperature increases with increasing time, where, it increases from 20 °C to 132.4 °C when the time increases from 0 min to 30 min at an oven temperature of 180 °C. On the other hand, the temperature increases from 20 °C to 179.5 °C at an oven temperature of 260°C.

The surface of the bread is at a much higher temperature than the inside part of the bread sample, and a large temperature gradient is developed in the region close to the surface, using the lower temperature (180 °C to 220 °C) more effectively in utilization of heat energy.

The model shows that the, water concentration decreases with increasing time. It decreases from 8866.6 mole/m^3 to 4 991.3 mole/m^3 when the time increases from 0 min to 30 min at an oven temperature of 220 °C. The model shows that the moisture content % decreases with increasing time. It decreases from 42 % to 23.6 % when the time increases from 0 min to 30 min at an oven temperature of 220 °C. The model shows that, the cooking yield decreases with increasing time. It decreases from 100 % to 56.2 % when the time increases from 0 min to 30 min, and the moisture loss % increases with increasing time. It increases from 0 % to 43.7 % when the time increases from 0 min to 30 min.

The mathematical model well describes the mechanisms of simultaneous heat, water, and vapour diffusion in one-dimensional solid material that is heated with radiation and convection from the outside. The simulated water content at the surface decreases rapidly when the temperature increases. The simulated water content at halfway to the center at first increases a little and then starts to decrease, the simulated temperature remains on a plateau while the water content starts to decrease. In the center, the water content increases in the beginning and then slowly starts to decrease.

The mathematical model was highly sensitive to the time step and satisfactory results were only yielded over a range of time steps, between 15 s and 100s. Smaller time steps produced an erroneous and diverged result, while a bigger time step rendered a useless result.

System efficiency are calculated based on the energy and exergy methodology. Exergy is a more practical tool compared to the conventional energy method when examining the thermal performance of the same baking oven and the same regenerator. Implementing regenerative technology results in enhanced system performance indicated by an exergy efficiency improvement. The regenerative burner system improves efficiency and achieves fuel saving. The most important results obtained can be summarized as follows:

The overall system energy efficiency increases from 6.5 % to 9.0 % and the system exergy efficiency increases from 0.68 % to 0.94 %, when the same production is maintained. 28.3 % exergy saving and 28.6 % energy saving of fuel consumption are mainly obtained from the regenerative burner system with the same production.

Before upgrades, the total unused energy in the system is 93.5 %; after upgrades, the total unused energy in the system is reduced to 91 %; current 650.9 MJ exergy loss and destruction from the furnace chamber is less than before 1117 MJ. These show the overall furnace system performance is improved.

In the regenerator, exergy efficiency (5.2 %) is lower than energy efficiency (22.5 %) when two different methods are used to study the same system. Exergy destruction in the regenerator is 48.2 % of the total exergy input to the regenerator. Miscellaneous exergy loss in the regenerator is less than 7.6 % which indicates the availability of the loss is limited even though 46.5 % of the total energy associated with the loss.

7.2 Recommendations for Further Studies

The following recommendations follow from this study:

- Evaluate the effects of varying baking temperature and time on the quality of bread.
- More effective refractories and insulation materials to maximize the efficiency.
- The exergy methodology should be extended to analyze a wider range of industrial and engineering problems, and more regenerative technologies should be considered in similar applications.
- To recover heat from the flue gas and preheat the dough is recommended, as it directly reduces waste while saving fuel when the device design is economically possible.

References

[1] Ureta MM, Goñi SM, Salvadori VO, Olivera DF (2017) Energy requirements during sponge cake baking: Experimental and simulated approach. Appl Therm Eng 115:637-643. https://doi.org/10.1016/j.applthermaleng.2016.12.078

[2] Decock P, Cappelle S (2005) Bread technology and sourdough technology. Trends Food Sci Technol 16 (1-3):113-120. https://doi.org/10.1016/j.tifs.2004.04.012

[3] Szargut J, Morris DR, Steward FR (1987) Exergy analysis of thermal, chemical, and metallurgical processes. United States. https://www.osti.gov/biblio/6157620

[4] Corsini A, Bonacina F, De Propris L, Feudo S, Marchegiani A (2015) Multivariate Key Performance Indicator of Baking Process. Energy Procedia 82:554-561. https://doi.org/10.1016/j.egypro.2015.11.869

[5] Dryden IGC (1982) Refractory and insulating materials. In: The Efficient Use of Energy (Second Edition). Butterworth-Heinemann, Elsevier, pp 394-412. https://doi.org/10.1016/B978-0-408-01250-8.50026-X

[6] Le-bail A, Dessev T, Jury V, Zuniga R, Park T, Pitroff M (2010) Energy demand for selected bread making processes: Conventional versus part baked frozen technologies. J Food Eng 96 (4):510-519. https://doi.org/10.1016/j.jfoodeng.2009.08.039

[7] Paton J, Khatir Z, Thompson H, Kapur N, Toropov V (2013) Thermal energy management in the bread baking industry using a system modelling approach. Appl Therm Eng 53 (2):340-347. https://doi.org/10.1016/j.applthermaleng.2012.03.036

[8] Therkelsen P, Masanet E, Worrell E (2014) Energy efficiency opportunities in the U.S. commercial baking industry. J Food Eng 130:14-22. https://doi.org/10.1016/j.jfoodeng.2014.01.004

[9] Paton JB (2013) Energy utilisation in commercial bread baking. University of Leeds

[10] Mondal A, Datta AK (2008) Bread baking – A review. J Food Eng 86 (4):465-474. https://doi.org/10.1016/j.jfoodeng.2007.11.014

[11] Bakalis S, Knoerzer K, Fryer PJ (2015) Modeling food processing operations. Woodhead Publishing. https://doi.org/10.1016/C2013-0-16519-1

[12] Kulp K (1988) Wheat: chemistry and technology, vol 2. U.K

[13] Eliasson A-C, Larsson K (1993) Cereals in breadmaking: a molecular colloidal approach. vol 664.6. Routledge, New York. https://doi.org/10.1201/9781315139005

[14] Fellows PJ (2009) Food processing technology: principles and practice. Woodhead Publishing

[15] RD R (1983) Furnace operations. Third edition edn. Gulf publishing company, Houston, United States. https://www.osti.gov/biblio/6644164

[16] Cauvain SP (2017) Baking problems solved. Woodhead Publishing

[17] Díaz-Ovalle CO, Martínez-Zamora R, González-Alatorre G, Rosales-Marines L, Lesso-Arroyo R (2017) An approach to reduce the pre-heating time in a convection oven via CFD simulation. Food Bioprod Process 102:98-106. https://doi.org/10.1016/j.fbp.2016.12.009

[18] Purlis E, Salvadori VO (2009) Bread baking as a moving boundary problem. Part 2: Model validation and numerical simulation. J Food Eng 91 (3):434-442. https://doi.org/10.1016/j.jfoodeng.2008.09.038

[19] Mousa E, Ibrahim R, Shuey W, Maneval R (1979) Influence of wheat classes, flour extractions, and baking methods on Egyptian Balady bread. Cereal Chemistry

[20] Hallab A, Khatchadourian H, Jabr I (1974) nutritive value and organoleptic properties of white Arabic bread supplemented with soybean and chickpea. Cereal Chem

[21] Gadalla M, Mansour M, Mahdy E, El-Mahallawy F Energy-efficient ovens for unpolluted balady bread. In: Energy Conversion Engineering Conference, 1996. IECEC 96., Proceedings of the 31st Intersociety, 1996. IEEE, pp 1997-2002. https://doi.org/10.1109/IECEC.1996.553425

[22] Eladly I, Bahnasawy A, Ali S, Khater E (2016) Bread baking process energy requirements as affected by oven belt speed and type of breads. Misr J Ag Eng 33 (4)

[23] Wesley IJ, Larsen N, Osborne BG, Skerritt JH (1998) Non-invasive Monitoring of Dough Mixing by Near Infrared Spectroscopy. J Cereal Sci 27 (1):61-69. https://doi.org/10.1006/jcrs.1997.0151

[24] Kilborn R (1981) Device senses changes in dough consistency during dough mixing part1: with Tweedy mixer. Bakers J:16-19

[25] Larsen N, Greenwood D (1991) Water addition and the physical properties of mechanical dough development doughs and breads. J Cereal Sci 13 (2):195-205. https://doi.org/10.1016/S0733-5210(09)80036-2

[26] Swortfiguer M (1968) Dough absorption and moisture retention in bread. The Bakers Digest 42:42-44, 67

[27] Walker SB (2013) Physicochemical Transformations in Low-Moisture Dough During Baking. Dissertation, University of Guelph, Guelph, Ontario, Canada. http://hdl.handle.net/10214/6656

[28] Grenier A, Monteau J-Y, Le Bail A, Hayert M (2002) Effect of external conditions on the rate of post-baking chilling of bread. J Food Eng 55 (1):19-24. https://doi.org/10.1016/S0260-8774(01)00224-2

[29] Farinu A (2006) Heat and mass transfer analogy under turbulent conditions of frying. Dissertation, University of Saskatchewan. http://hdl.handle.net/10388/etd-10302006-230414

[30] Ayalew A (2009) Transient heat transfer analysis of injera baking pan (" Mitad") by finite element method. Dissertation, University of Addis Ababa.

[31] Thorvaldsson K, Janestad H (1999) A model for simultaneous heat, water and vapour diffusion. J Food Eng 40 (3):167-172. https://doi.org/10.1016/S0260-8774(99)00052-7

[32] Favre-Marinet M, Tardu S (2013) Convective Heat Transfer: Solved Problems. Wiley, USA

[33] Rao SS (2017) The finite element method in engineering. Butterworth-heinemann

[34] Wu Y, Irudayaraj J (1996) Analysis of heat, mass and pressure transfer in starch based food systems. J Food Eng 29 (3):399-414. https://doi.org/10.1016/0260-8774(96)00008-8

[35] Irudayaraj JM, Jun S (2008) Food processing operations modeling: design and analysis. CRC press

[36] Choi Y (1986) Effects of temperature and composition on the therma properties of food. Food engineering and process applications

[37] Gupta T (2001) Individual heat transfer modes during contact baking of Indian unleavened flat bread (chapati) in a continuous oven. J Food Eng 47 (4):313-319. https://doi.org/10.1016/S0260-8774(00)00135-7

[38] Kaletunç G (2007) Prediction of specific heat of cereal flours: A quantitative empirical correlation. J Food Eng 82 (4):589-594. https://doi.org/10.1016/j.jfoodeng.2007.03.028

[39] Valentas KJ, Rotstein E, Singh RP (1997) Handbook of food engineering practice. CRC press

[40] Krokida M, Michailidis P, Maroulis Z, Saravacos G (2002) Literature data of thermal conductivity of foodstuffs. Int J Food Prop 5 (1):63-111. https://doi.org/10.1081/JFP-120015594

[41] Sabapathy ND (2005) Heat and mass transfer during cooking of chickpea: measurements and computational simulation. Dissertation, University of Saskatchewan, Saskatoon, SK, Canada. http://hdl.handle.net/10388/etd-03022005-153357

[42] Boukouvalas CJ, Krokida M, Maroulis Z, Marinos-Kouris D (2006) Density and porosity: literature data compilation for foodstuffs. Int J Food Prop 9 (4):715-746. https://doi.org/10.1080/10942910600575690

[43] Midden T (1995) Impingement air baking for snack foods. Cereal foods world (USA)

[44] Unklesbay N, Unklesbay K, Nahaisi M, Krause G (1982) Thermal conductivity of white bread during convective heat processing. J Food Sci 47 (1):249-253. https://doi.org/10.1111/j.1365-2621.1982.tb11071.x

[45] Monteau J-Y (2008) Estimation of thermal conductivity of sandwich bread using an inverse method. J Food Eng 85 (1):132-140. https://doi.org/10.1016/j.jfoodeng.2007.04.034

[46] Wong S-Y, Zhou W, Hua J (2007) CFD modeling of an industrial continuous bread-baking process involving U-movement. J Food Eng 78 (3):888-896. https://doi.org/10.1016/j.jfoodeng.2005.11.033

[47] Bergman TL, Incropera FP, DeWitt DP, Lavine AS (2011) Fundamentals of heat and mass transfer. Wiley, USA

[48] Ramos J (1990) Basic Heat Transfer. Elsevier

[49] Rohsenow WM, Hartnett JP, Cho YI (1998) Handbook of heat transfer, vol 3. McGraw-Hill New York

[50] Zhang J, Datta AK (2006) Mathematical modeling of bread baking process. J Food Eng 75 (1):78-89. https://doi.org/10.1016/j.jfoodeng.2005.03.058

[51] Therdthai N, Zhou W, Adamczak T (2003) Two-dimensional CFD modelling and simulation of an industrial continuous bread baking oven. J Food Eng 60 (2):211-217. https://doi.org/10.1016/S0260-8774(03)00043-8

[52] Hamdami N, Monteau J-Y, Le Bail A (2004) Heat and mass transfer in par-baked bread during freezing. Food Res Int 37 (5):477-488. https://doi.org/10.1016/j.foodres.2004.02.011

[53] Zanoni B, Peri C, Bruno D (1995) Modelling of starch gelatinization kinetics of bread crumb during baking. LWT Food Sci Technol 28 (3):314-318. https://doi.org/10.1016/S0023-6438(95)94458-3

[54] Šeruga B, Budžaki S, Ugarčić-Hardi Ž (2007) Individual Heat Transfer Modes During Baking of "Mlinci" Dough. Agriculturae Conspectus Scientificus (ACS) 72 (3):257-263

[55] Doty S, Turner WC (2004) Energy management handbook. Crc Press

[56] Chhanwal N, Anishaparvin A, Indrani D, Raghavarao K, Anandharamakrishnan C (2010) Computational fluid dynamics (CFD) modeling of an electrical heating oven for bread-baking process. J Food Eng 100 (3):452-460. https://doi.org/10.1016/j.jfoodeng.2010.04.030

[57] Tong C, Lund D (1993) Microwave heating of baked dough products with simultaneous heat and moisture transfer. J Food Eng 19 (4):319-339. https://doi.org/10.1016/0260-8774(93)90023-D

[58] Thorvaldsson K, Skjöldebrand C (1998) Water diffusion in bread during baking. LWT Food Sci Technol 31 (7-8):658-663. https://doi.org/10.1006/fstl.1998.0427

[59] Zanoni B, Pierucci S, Peri C (1994) Study of the bread baking process — II. Mathematical modelling. J Food Eng 23 (3):321-336. https://doi.org/10.1016/0260-8774(94)90057-4

[60] Sablani S, Marcotte M, Baik O, Castaigne F (1998) Modeling of simultaneous heat and water transport in the baking process. LWT Food Sci Technol 31 (3):201-209. https://doi.org/10.1006/fstl.1997.0360

[61] Baik O, Grabowski S, Trigui M, Marcotte M, Castaigne F (1999) Heat transfer coefficients on cakes baked in a tunnel type industrial oven. J Food Sci 64 (4):688-694. https://doi.org/10.1111/j.1365-2621.1999.tb15111.x

[62] Geankoplis CJ (2003) Transport processes and separation process principles:(includes unit operations). University of Minnesota

[63] Anandharamakrishnan C (2013) Computational fluid dynamics applications in food processing. Springer, New York. https://doi.org/10.1007/978-1-4614-7990-1_1

[64] Perez-Correa J, Zaror C (1993) Recent advances in process control and their potential applications to food processing. Food Control 4 (4):202-209. https://doi.org/10.1016/0956-7135(93)90250-R

[65] Yanniotis S, Stoforos N (2014) Modelling Food Processing Operations with Computational Fluid Dynamics: A Review. Scientia Agriculturae Bohemica. https://doi.org/10.7160/sab.2014.450101

[66] Zanoni B, Peri C, Pierucci S (1993) A study of the bread-baking process. I: A phenomenological model. J Food Eng 19 (4):389-398. https://doi.org/10.1016/0260-8774(93)90027-H

[67] Vries Ud, Sluimer P, Bloksma A (1988) A quantitative model for heat transport in dough and crumb during baking. Cereal Science and technology:174-188

[68] Stenby Andresen M (2013) Experimentally supported mathematical modeling of continuous baking processes. Dissertation, Technical University of Denmark. https://core.ac.uk/download/pdf/19118352.pdf

[69] Feyissa AH (2011) Robust Modelling of Heat and Mass Transfer in Processing of Solid Foods. Dissertation, Technical University of Denmark. http://orbit.dtu.dk/files/5796903/Phdthesis_Aberham%20Hailu%20Feyissa_2011_finalver.pdf

[70] Powathil GG (2004) A heat and mass transfer model for bread baking: an investigation using numerical schemes. Dissertation, National University of Singapore. https://cronfa.swan.ac.uk/Record/cronfa18365

[71] Mathioulakis E, Karathanos V, Belessiotis VG (1998) Simulation of air movement in a dryer by computational fluid dynamics: application for the drying of fruits. J Food Eng 36 (2):183-200. https://doi.org/10.1016/S0260-8774(98)00026-0

[72] Chhanwal N, Tank A, Raghavarao K, Anandharamakrishnan C (2012) Computational fluid dynamics (CFD) modeling for bread baking process—a review. Food Bioprocess Technol 5 (4):1157-1172. http://dx.doi.org/10.1007/s11947-012-0804-y

[73] Nicolas V, Salagnac P, Glouannec P, Jury V, Boillereaux L, Ploteau JP (2010) Modeling Heat and Mass Transfer in Bread during Baking. Comsol Conference.

[74] Young DF, Munson BR, Okiishi TH, Huebsch WW (2010) A brief introduction to fluid mechanics. John Wiley & Sons, USA

[75] Fuhrmann E, Sockel H, Steinrück P (1984) Improvement of continuous baking oven's efficiency. J Wind Eng Ind Aerodyn 16 (2-3):201-212. https://doi.org/10.1016/0167-6105(84)90007-2

[76] Verboven P, Datta AK, Anh NT, Scheerlinck N, Nicolaï BM (2003) Computation of airflow effects on heat and mass transfer in a microwave oven. J Food Eng 59 (2-3):181-190. https://doi.org/10.1016/S0260-8774(02)00456-9

[77] Chhanwal N, Indrani D, Raghavarao KSMS, Anandharamakrishnan C (2011) Computational fluid dynamics modeling of bread baking process. Food Res Int. https://doi.org/10.1016/j.foodres.2011.02.037

[78] Khatir Z, Paton J, Thompson H, Kapur N, Toropov V, Lawes M, Kirk D (2012) Computational fluid dynamics (CFD) investigation of air flow and temperature distribution in a small scale bread-baking oven. Appl Energy 89 (1):89-96. https://doi.org/10.1016/j.apenergy.2011.02.002

[79] Zienkiewicz OC, Taylor RL (2005) The finite element method for solid and structural mechanics. Elsevier

[80] Versteeg HK, Malalasekera W (2007) An introduction to computational fluid dynamics: the finite volume method. Pearson Education

[81] Adamic RM (2012) CFD and Heat Transfer Models of Baking Bread in a Tunnel Oven. Dissertation, University of Cleveland State. https://engagedscholarship.csuohio.edu/etdarchive/3

[82] Multiphysics C, Module CMHT (2014) COMSOL multiphysics user's guide. Version: COMSOL Multiphysics 3

[83] Tabatabaian M (2015) COMSOL5 for Engineers. Stylus Publishing, LLC

[84] Bejan A (2016) Advanced engineering thermodynamics. Wiley, USA. https://doi.org/10.1002/9781119245964

[85] Sun D-W (2012) Thermal food processing: new technologies and quality issues. CRC Press

[86] Kotas TJ (2013) The exergy method of thermal plant analysis. Elsevier

[87] Etele J, Rosen MA (2001) Sensitivity of exergy efficiencies of aerospace engines to reference environment selection. Exergy, An International Journal 1 (2):91-99. https://doi.org/10.1016/S1164-0235(01)00014-0

[88] Çamdali Ü, Tunc M, Dikec F (2001) A thermodynamic analysis of a steel production step carried out in the ladle furnace. Appl Therm Eng 21 (6):643-655. https://doi.org/10.1016/S1359-4311(00)00076-4

[89] Verkhivker G, Yantovski E (2001) Zero-emissions gas-fired cogeneration of power and hydrogen. Int J Hydrogen Energy 26 (10):1109-1113. https://doi.org/10.1016/S0360-3199(01)00048-9

[90] Struchtrup H, Rosen MA (2002) How much work is lost in an irreversible turbine? Exergy, an international journal 2 (3):152-158. https://doi.org/10.1016/S1164-0235(02)00068-7

[91] Ratts EB, Brown JS (2000) An experimental analysis of cycling in an automotive air conditioning system. Appl Therm Eng 20 (11):1039-1058. https://doi.org/10.1016/S1359-4311(99)00080-0

[92] Stegou-Sagia A, Paignigiannis N (2003) Exergy losses in refrigerating systems. A study for performance comparisons in compressor and condenser. Int J Energy Res 27 (12):1067-1078. https://doi.org/10.1002/er.936

[93] Ghaddar N, Ghali K, Najm A (2003) Use of desiccant dehumidification to improve energy utilization in air-conditioning systems in Beirut. Int J Energy Res 27 (15):1317-1338. https://doi.org/10.1002/er.945

[94] Zheng D, Ji P, Qi J (2001) Maximum excess Gibbs function of working pairs and absorption cycle performance. Int J Refrig 24 (8):834-840. https://doi.org/10.1016/S0140-7007(00)00049-9

[95] Qureshi BA, Zubair SM (2003) Application of exergy analysis to various psychrometric processes. Int J Energy Res 27 (12):1079-1094. https://doi.org/10.1002/er.933

[96] Dincer I, Rosen M (1999) The intimate connection between exergy and the environment. In: Thermodynamic optimization of complex energy systems. Springer, Dordrecht, pp 221-230. https://doi.org/10.1007/978-94-011-4685-2_15

[97] Cownden R, Nahon M, Rosen MA (2001) Exergy analysis of a fuel cell power system for transportation applications. Exergy, An International Journal 1 (2):112-121. https://doi.org/10.1016/S1164-0235(01)00017-6

[98] Aprea C, de Rossi F, Greco A, Renno C (2003) Refrigeration plant exergetic analysis varying the compressor capacity. Int J Energy Res 27 (7):653-669. https://doi.org/10.1002/er.903

[99] Bayrak M, Midilli A, Nurveren K (2003) Energy and exergy analyses of sugar production stages. Int J Energy Res 27 (11):989-1001. https://doi.org/10.1002/er.916

[100] Jentsch A (2010) A novel exergy-based concept of thermodynamic quality and its application to energy system evaluation and process analysis. Dissertation, Technical University of Berlin. http://dx.doi.org/10.14279/depositonce-2399

[101] Sorgenfrei M (2016) Analysis of IGCC-based plants with carbon capture for an efficient and flexible electric power generation. Dissertation, Technical University of Berlin. http://dx.doi.org/10.14279/depositonce-5073

[102] Rosen MA, Dincer I (1997) On exergy and environmental impact. Int J Energy Res 21 (7):643-654. https://doi.org/10.1002/(SICI)1099-114X(19970610)21:7<643::AID-ER284>3.0.CO;2-I

[103] Rosen MA, Dincer I (2001) Exergy as the confluence of energy, environment and sustainable development. Exergy, an International journal 1 (1):3-13. https://doi.org/10.1016/S1164-0235(01)00004-8

[104] Pyler EJ (1973) Baking science & technology. Sosland Pub Co

[105] Sahin S, Sumnu SG (2006) Water activity and sorption properties of foods Food properties Springer, New York.
https://doi.org/10.1007/0-387-30808-3_5

[106] Zhou W, Therdthai N (2007) Three-Dimensional CFD Modeling of a Continuous Industrial Baking Process. CRC Press

[107] Mirade P, Daudin J, Ducept F, Trystram G, Clément J (2004) Characterization and CFD modelling of air temperature and velocity profiles in an industrial biscuit baking tunnel oven. Food Res Int 37 (10):1031-1039.
https://doi.org/10.1016/j.foodres.2004.07.001

[108] Simpson R (2009) Engineering aspects of thermal food processing. CRC Press

[109] De Cindio B, Correra S (1995) Mathematical modelling of leavened cereal goods. J Food Eng 24 (3):379-403.
https://doi.org/10.1016/0260-8774(95)90052-D

[110] Lostie M, Peczalski R, Andrieu J, Laurent M (2002) Study of sponge cake batter baking process. II. Modeling and parameter estimation. J Food Eng 55 (4):349-357.
https://doi.org/10.1016/S0260-8774(02)00132-2

[111] Broyart B, Trystram G (2003) Modelling of heat and mass transfer phenomena and quality changes during continuous biscuit baking using both deductive and inductive (neural network) modelling principles. Food Bioprod Process 81 (4):316-326.
https://doi.org/10.1205/096030803322756402

[112] Bikard J, Coupez T, Della Valle G, Vergnes B (2008) Simulation of bread making process using a direct 3D numerical method at microscale: Analysis of foaming phase during proofing. J Food Eng 85 (2):259-267.
https://doi.org/10.1016/j.jfoodeng.2007.07.027

[113] Baldino N, Gabriele D, Lupi FR, de Cindio B, Cicerelli L (2014) Modeling of baking behavior of semi-sweet short dough biscuits. Innovative Food Sci Emerg Technol- 25:40-52.
https://doi.org/10.1016/j.ifset.2013.12.022

[114] Purlis E (2012) Baking process design based on modelling and simulation: towards optimization of bread baking. Food control 27 (1):45-52.
https://doi.org/10.1016/j.foodcont.2012.02.034

[115] Chen H, Marks BP, Murphy RY (1999) Modeling coupled heat and mass transfer for convection cooking of chicken patties. J Food Eng 42 (3):139-146.
https://doi.org/10.1016/S0260-8774(99)00111-9

[116] Sluimer P, Krist-Spit C (1987) Heat transport in dough during the baking of bread. National Agricultural Library

[117] Zhou W (2005) Application of FDM and FEM in solving the simultaneous heat and moisture transfer inside bread during baking. International Journal of Computational Fluid Dynamics 19 (1):73-77. https://doi.org/10.1080/10618560412331286337

[118] Holman J (1968) Heat Transfer McGraw-Hill Book Company, New York

[119] Balaban M, Pigott G (1988) Mathematical model of simultaneous heat and mass transfer in food with dimensional changes and variable transport parameters. J Food Sci 53 (3):935-939. https://doi.org/10.1111/j.1365-2621.1988.tb08990.x

[120] Hines AL, Maddox RN (1985) Mass transfer: fundamentals and applications, vol 434. Prentice-Hall Englewood Cliffs, NJ

[121] Butcher JC (1987) The numerical analysis of ordinary differential equations : Runge-Kutta and general linear methods. J. Wiley, Chichester. https://doi.org/10.1137/1031147

[122] Ibrahim D, Rosen MA (2007) Exergy: Energy, Environment, and Sustainable Development, vol 64. Elsevier

[123] Tsatsaronis G, Kelly SO, Morosuk TV (2006) Endogenous and exogenous exergy destruction in thermal systems. In: Advanced Energy Systems. ASME. https://doi.org/10.1115/IMECE2006-13675

[124] Moran MJ, Shapiro HN, Boettner DD, Bailey MB (2010) Fundamentals of engineering thermodynamics. John Wiley & Sons, USA